Click dimers to target HIV TAR RNA conformation

Sunil Kumar[1], Patrick Kellish[1], W. Edward Robinson, Jr.[2], Deyun Wang[3], Daniel H. Appella[3], Dev P. Arya[1]

[1]Laboratory of Medicinal Chemistry, Department of Chemistry, Clemson University, Clemson, SC 29634

[2]Department of Pathology & Laboratory Medicine, University of California at Irvine, Irvine, CA 92697

[3]Laboratory of Bioorganic Chemistry, NIDDK, NIH, DHHS, Bethesda, MD 20892

Supporting Information

Appendices

1. Chemical structure of neomycin dimers ……..…….....S1
2. Characterization of neomycin dimers …….....S2
3. UV-thermal denaturation profiles …….....S3
4. Ethidium bromide displacement assay …….....S4
5. FRET-mediated competition binding assay …….....S5
6. Ethidium bromide displacement titration to determine the binding constants…….S6

1. Chemical structure of neomycin dimers (S1).

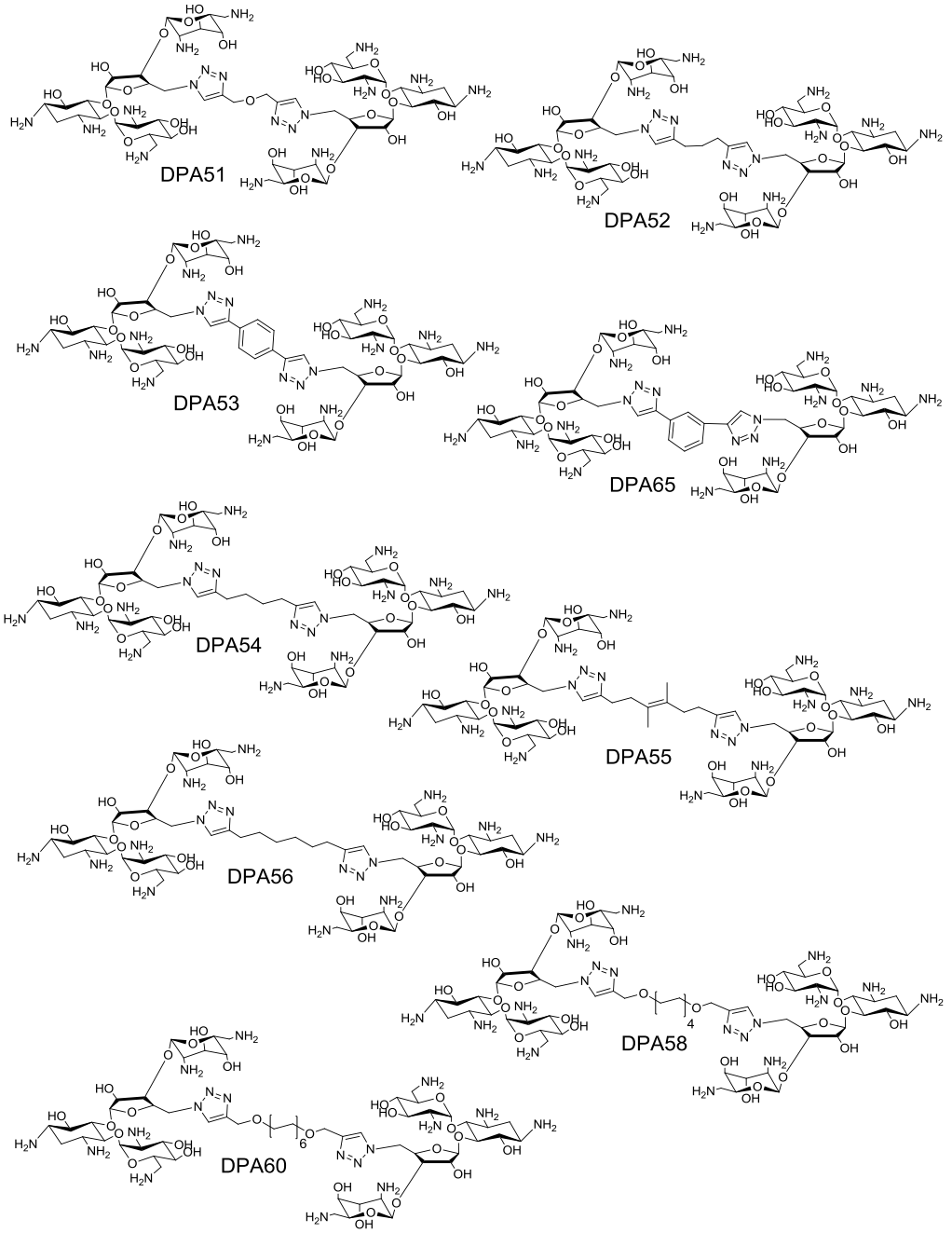

Scheme 1. Chemical structure of neoneo dimers. All the amine groups in neomycin dimers are in salt form (+HCl).

2. Characterization of neomycin dimers (S2).

N-Boc DPA51.

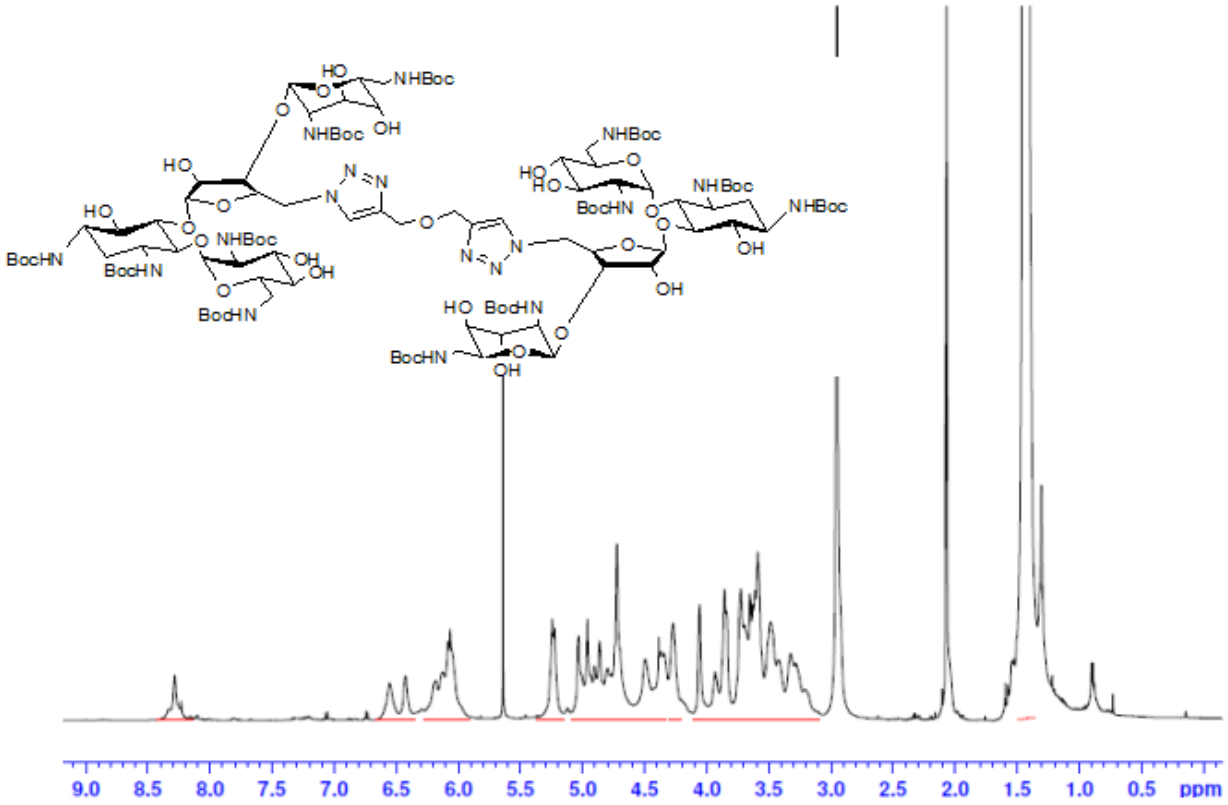

Figure S2.1. ^{1}H-NMR of N-Boc DPA51.

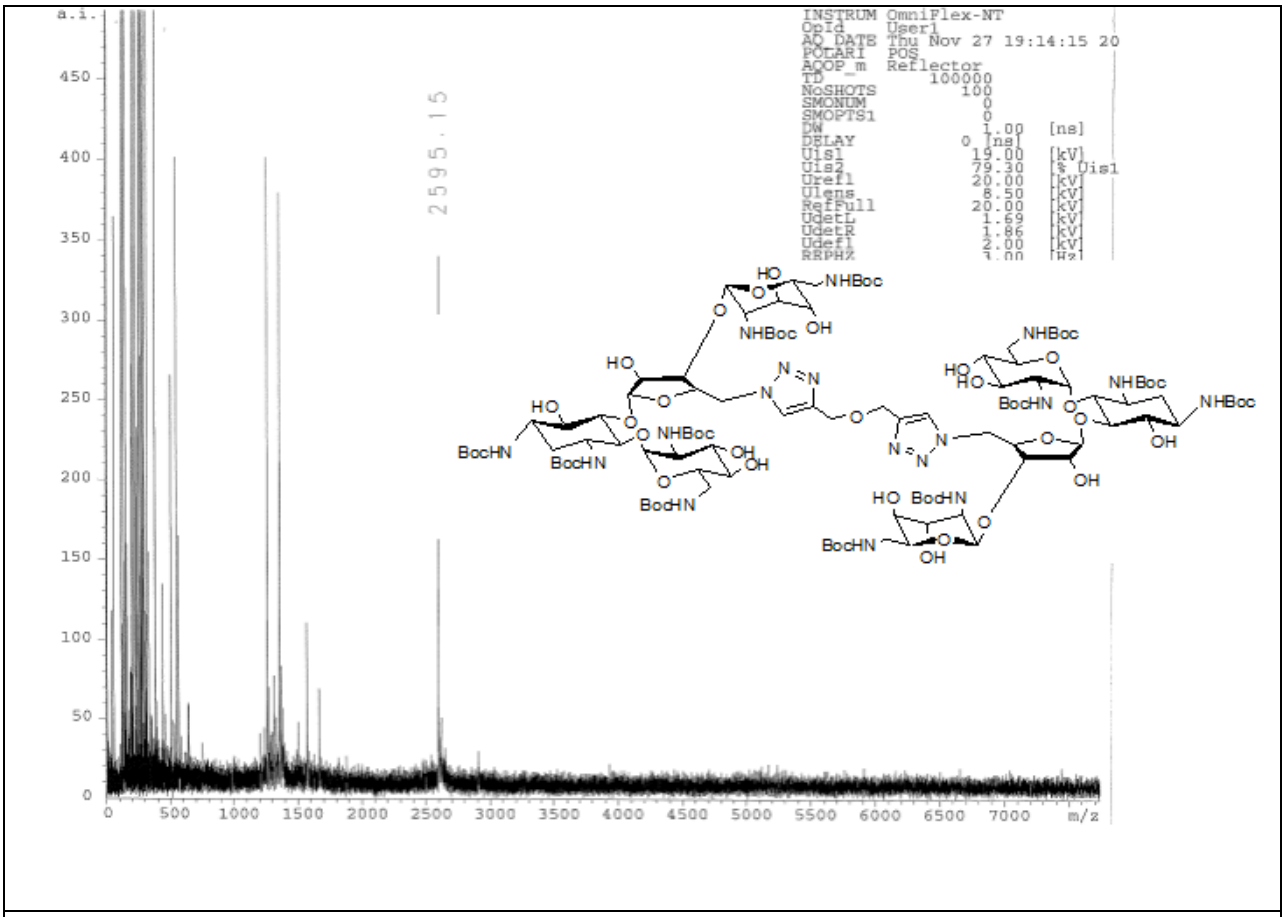

Figure S2.3. MALDI-TOF of N-Boc DPA51.

DPA51.

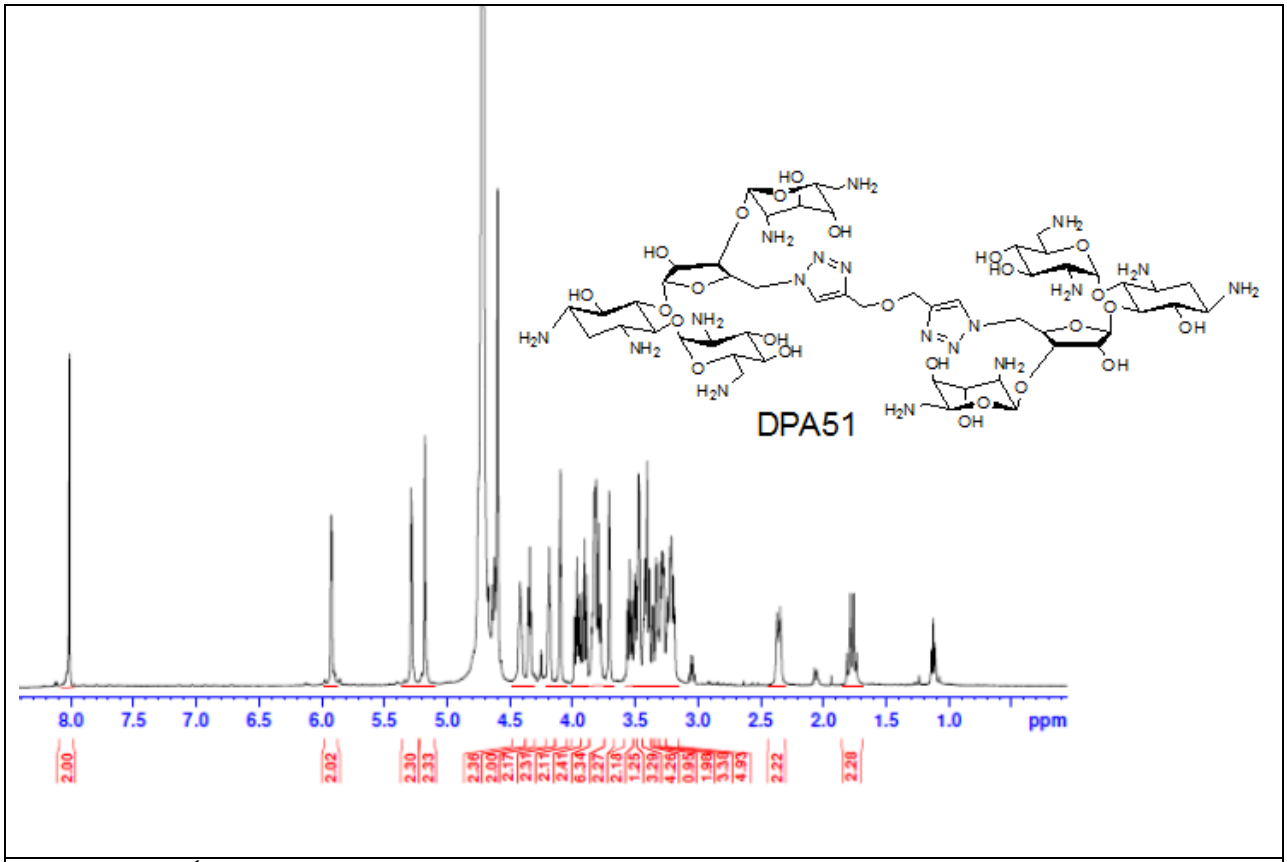

Figure S2.1. ^{1}H-NMR of DPA51.

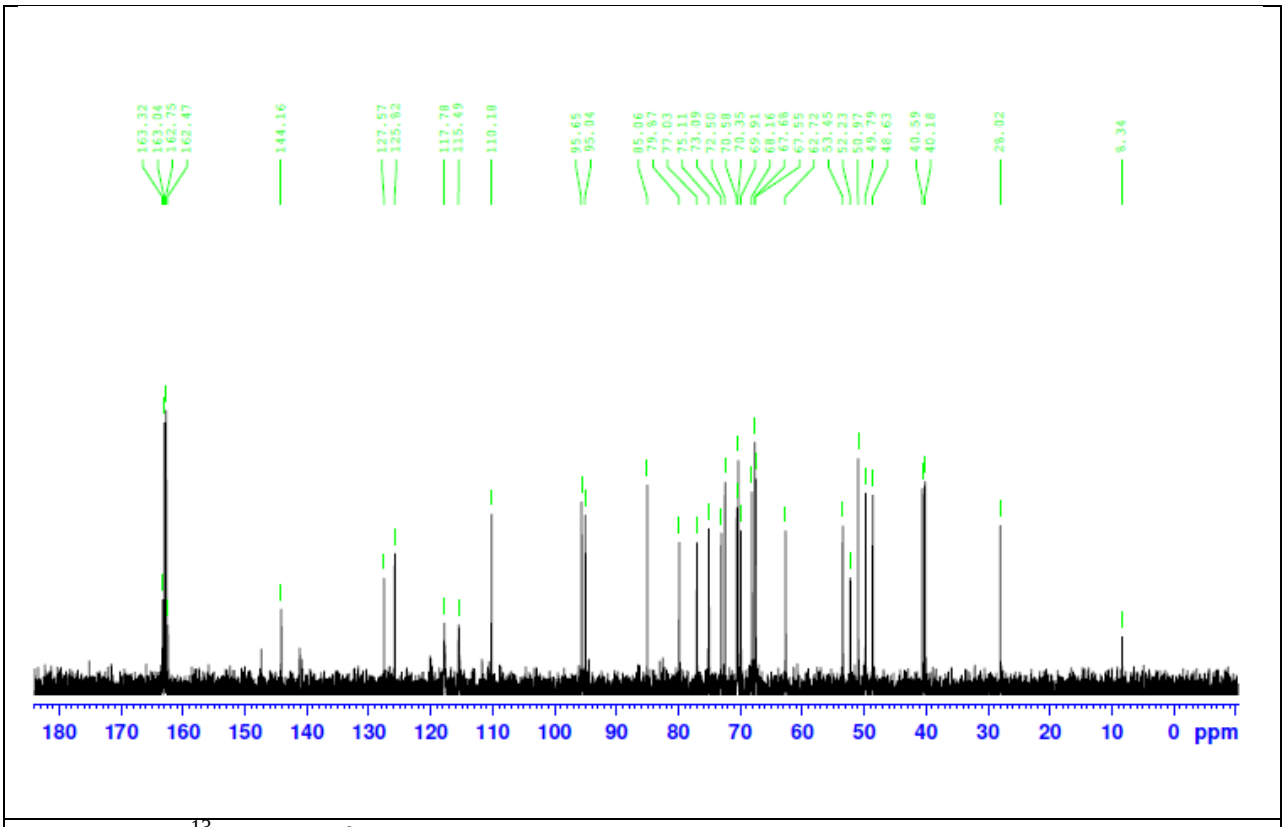

Figure S2.2. ^{13}C-NMR of DPA51.

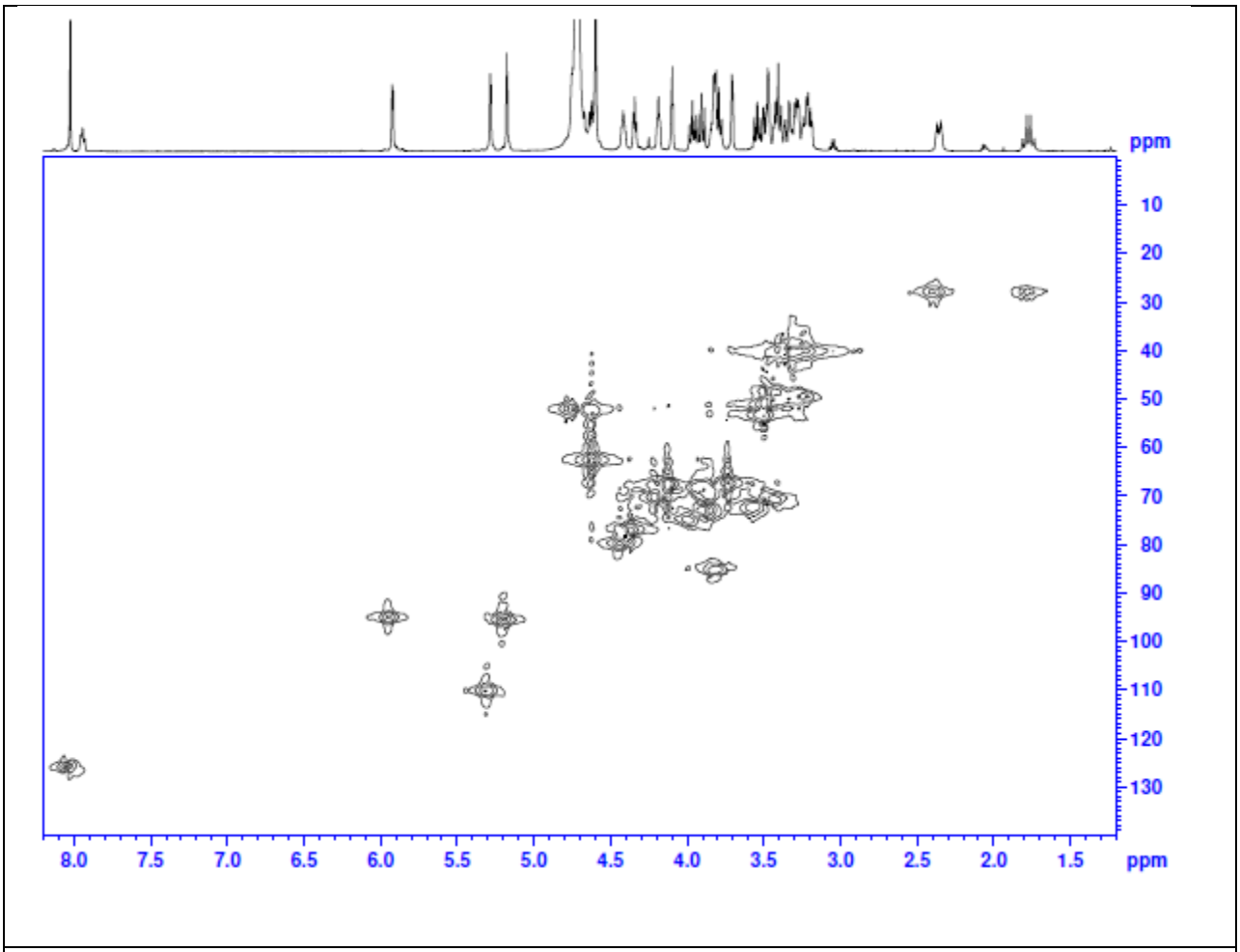

Figure S2.3. HMBC-NMR of DPA51.

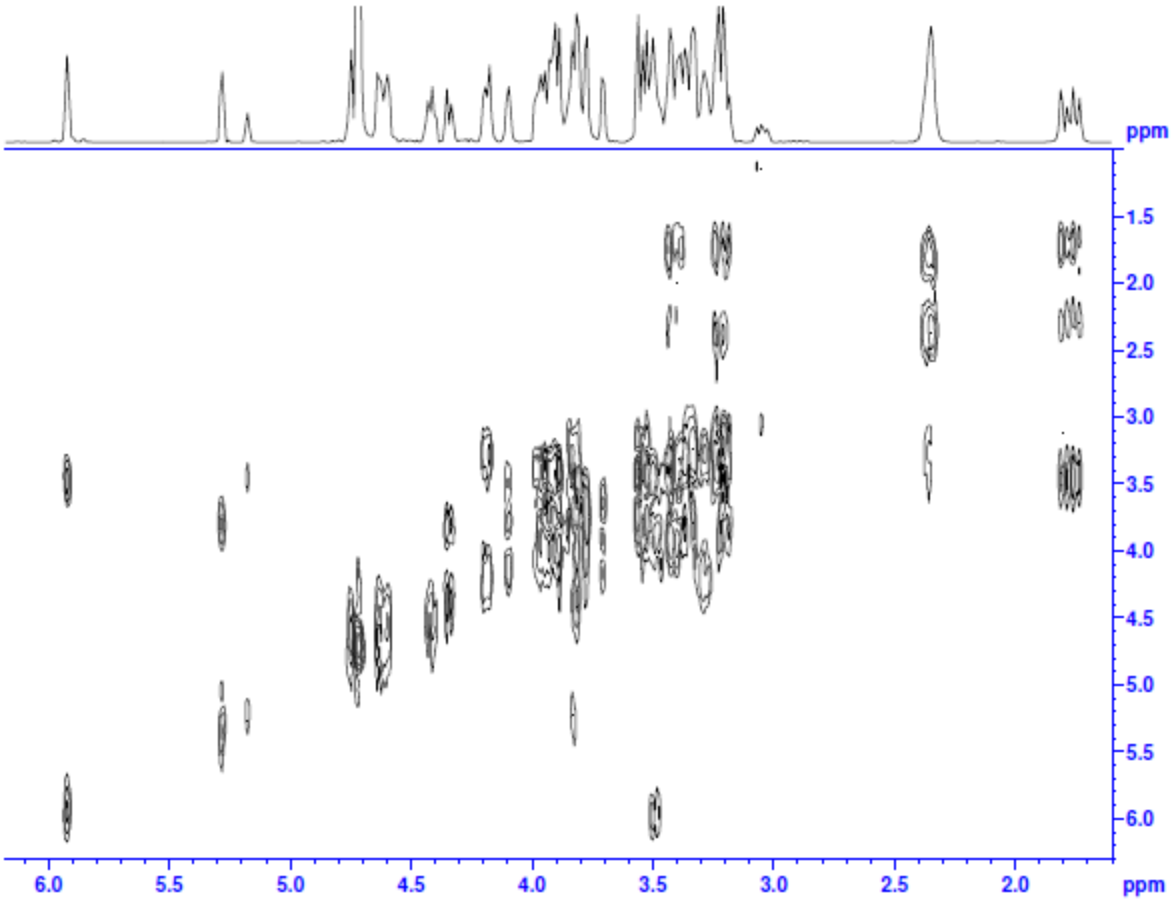

Figure S2.4. COSY-NMR of DPA51.

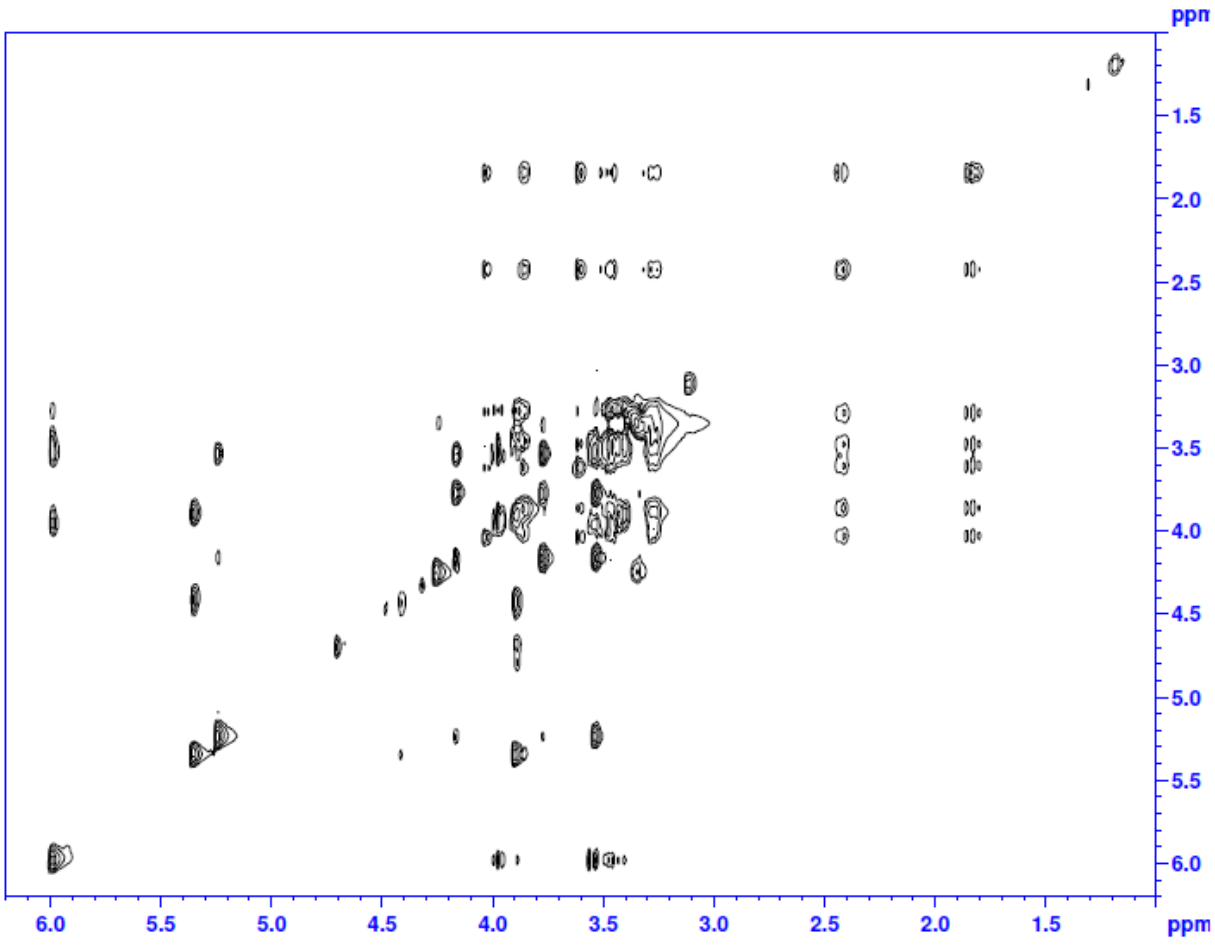

Figure S2.5. TOCSY-NMR of DPA51.

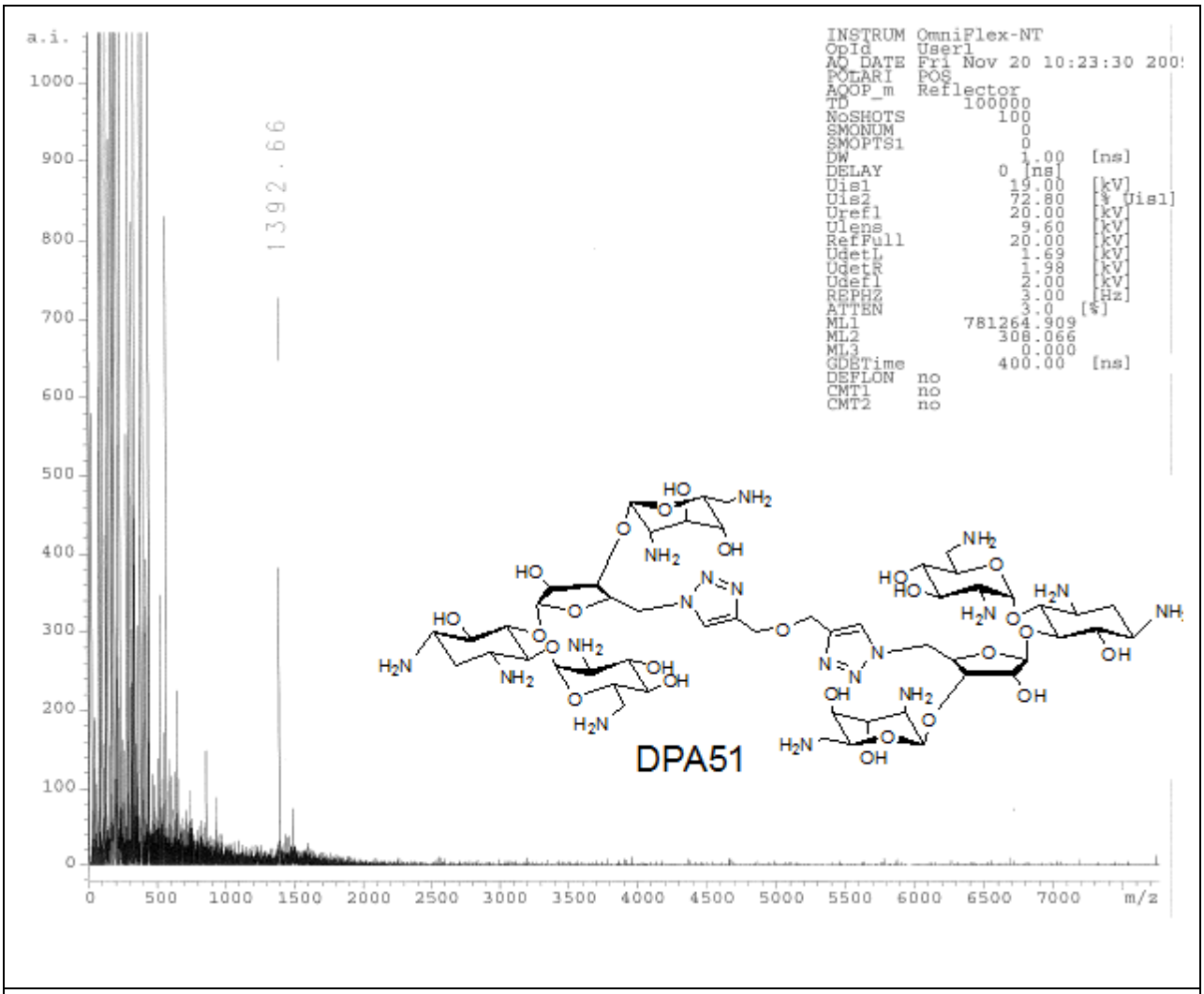

Figure S2.6. MALDI-TOF of DPA51.

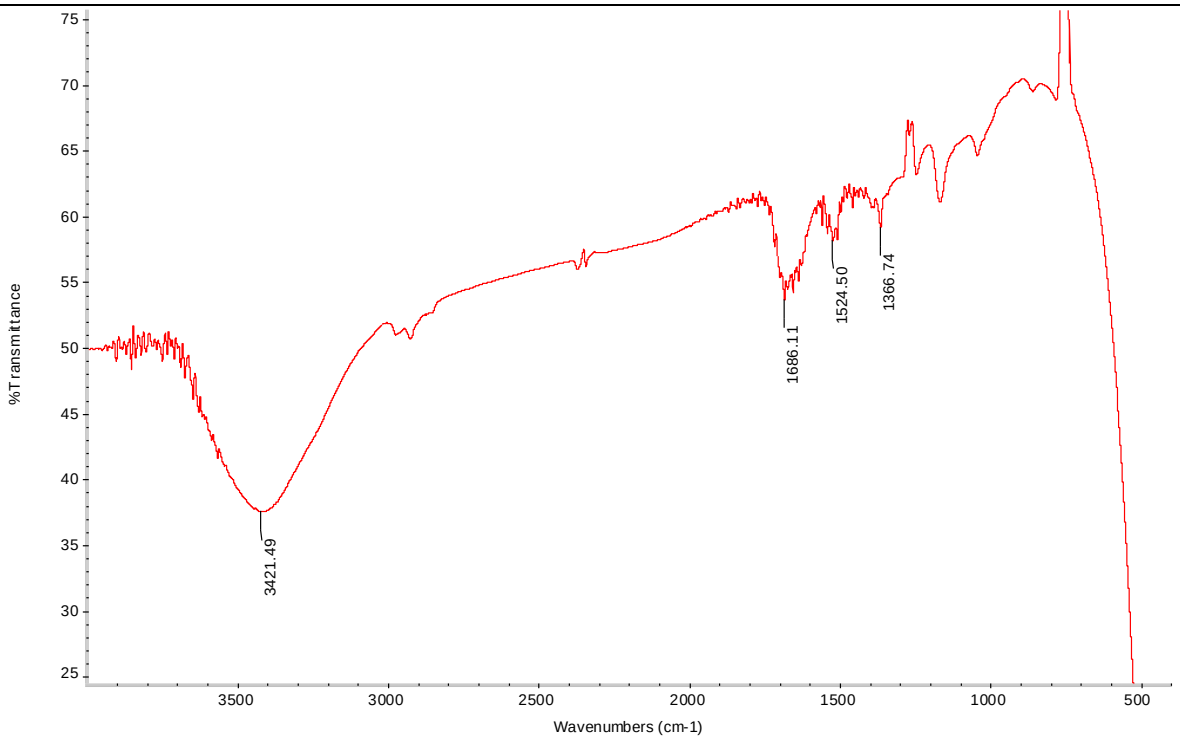

Figure S2.7. IR of DPA51.

N-Boc DPA52.

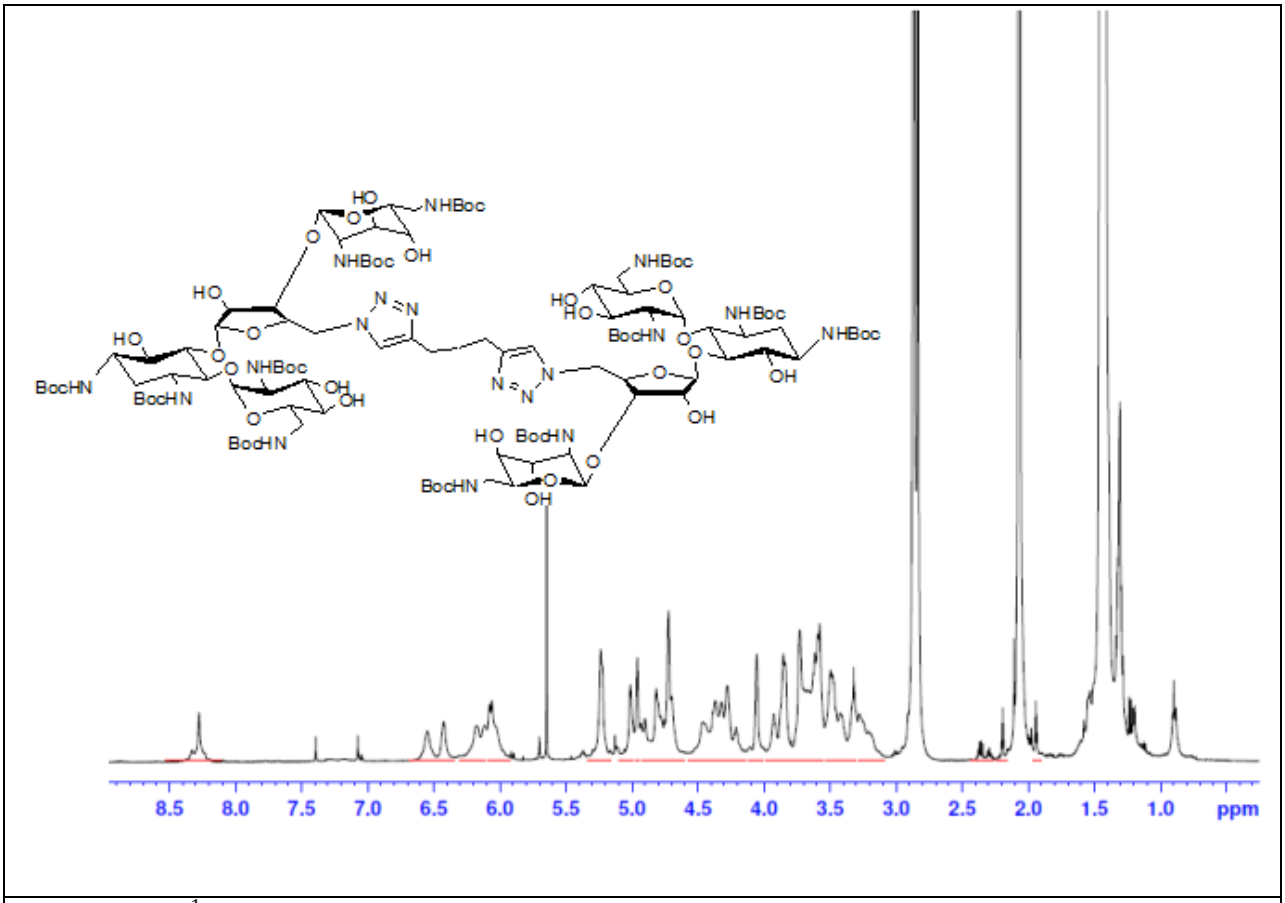

Figure S2.8. ^{1}H-NMR of N-Boc DPA52.

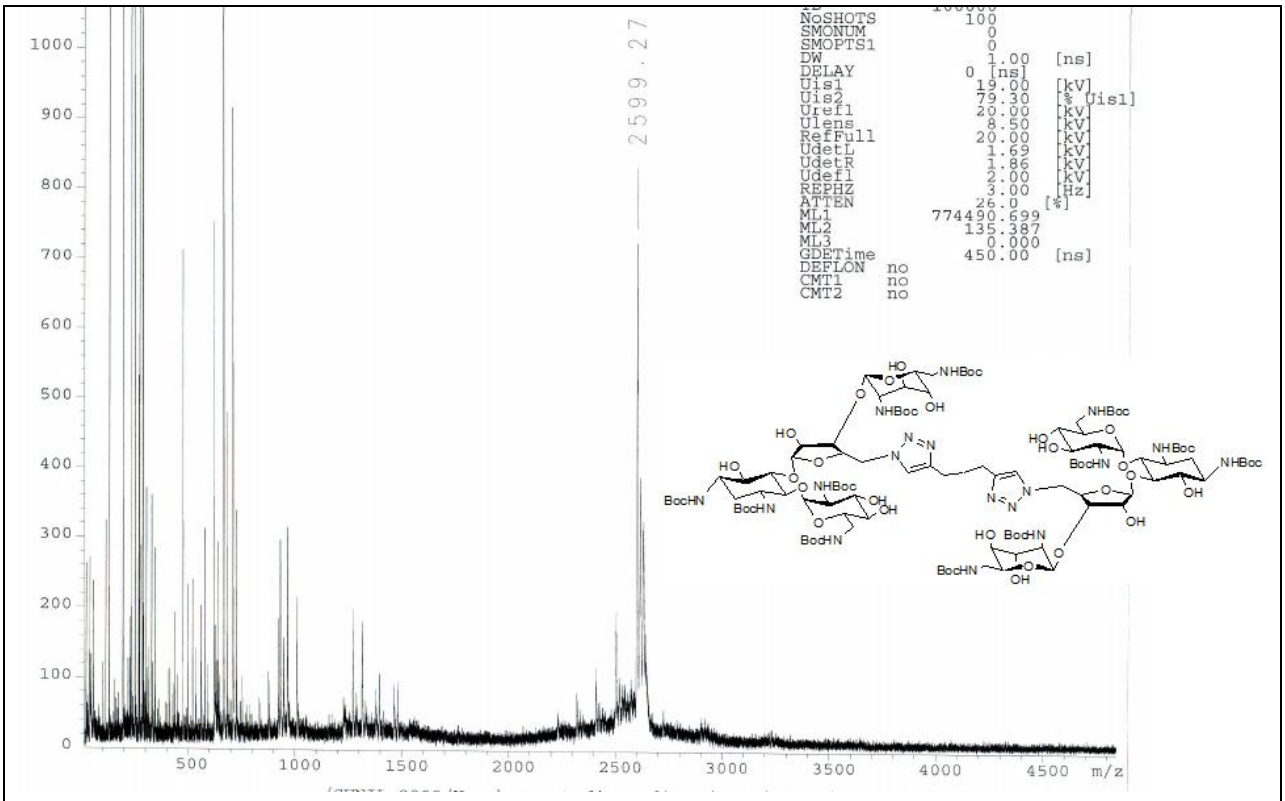

Figure S2.9. MALDI-TOF of N-Boc DPA52.

DPA52.

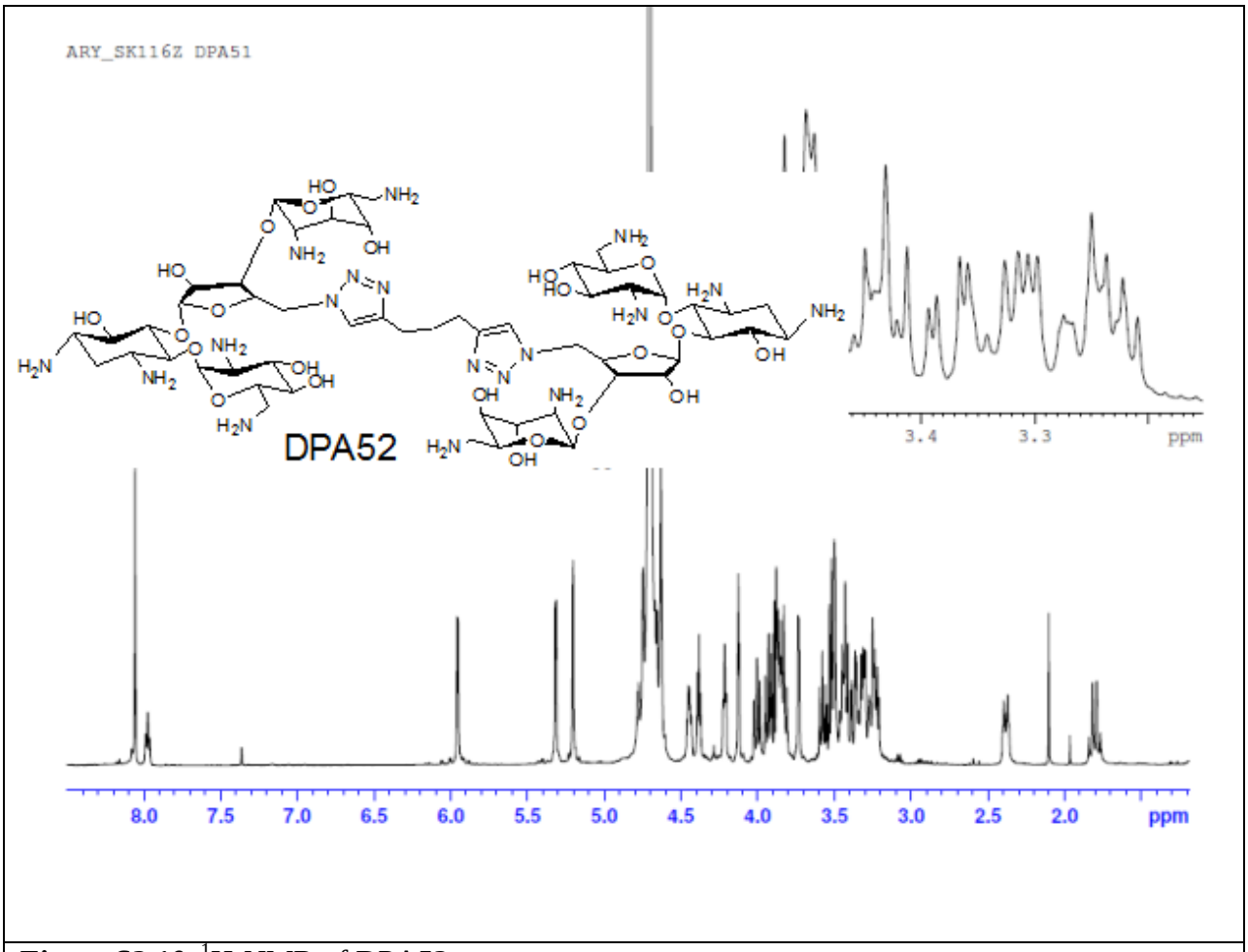

Figure S2.10. ^{1}H-NMR of DPA52.

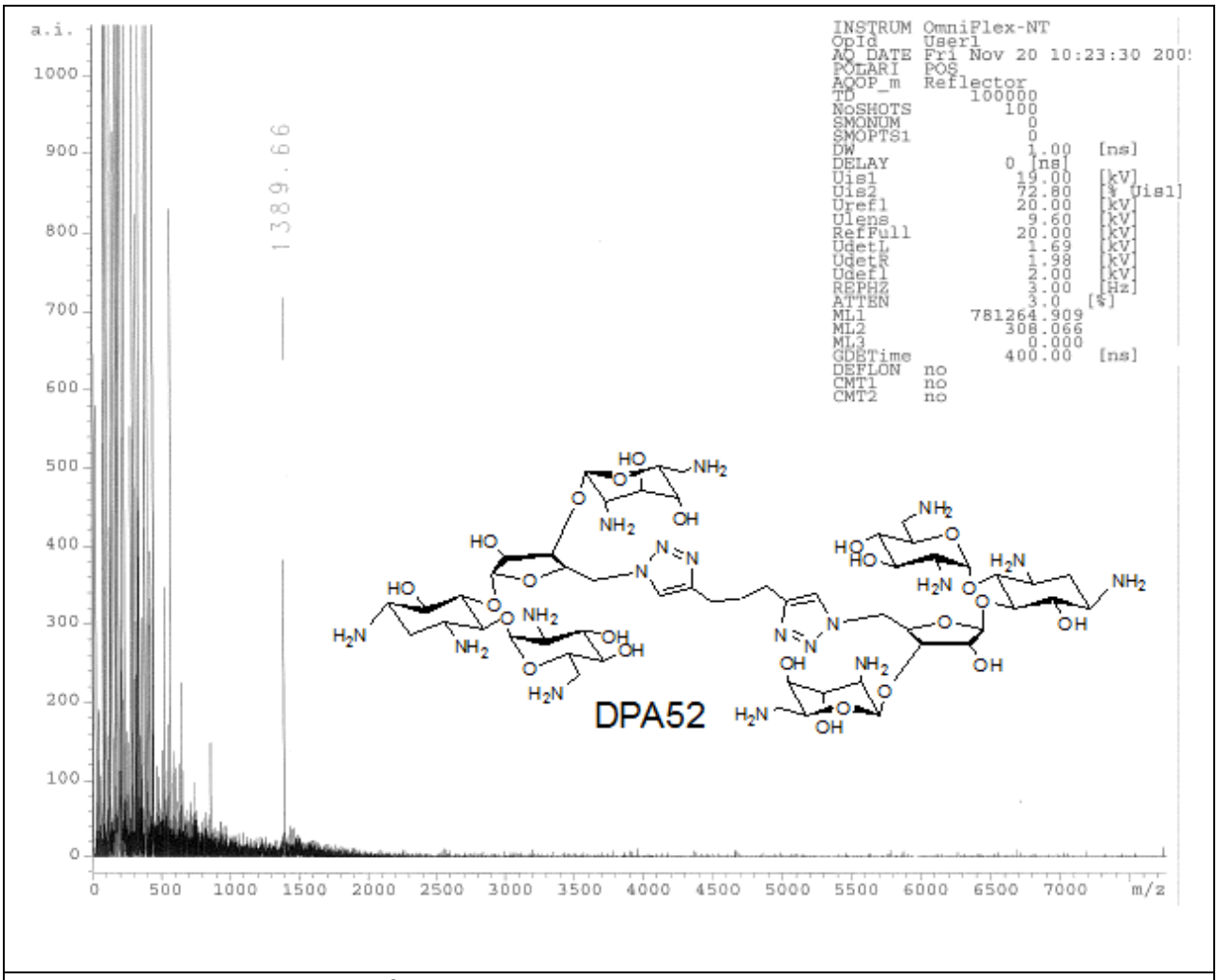

Figure S2.11. MALDI-TOF of DPA52.

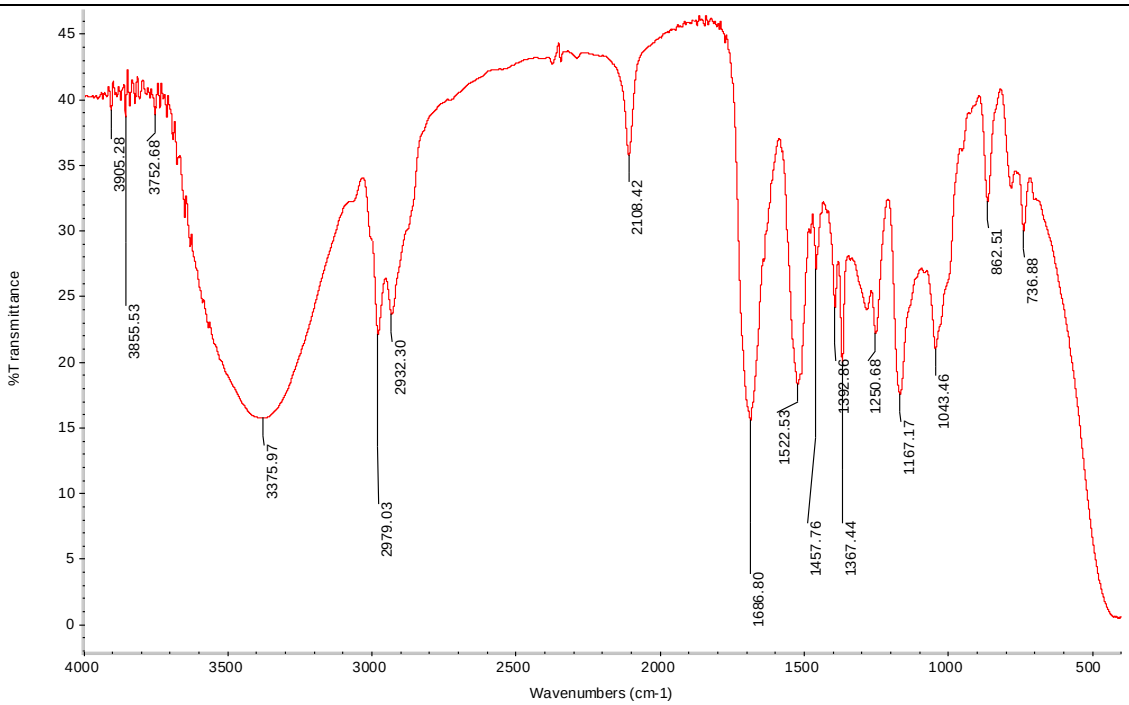

Figure S2.12. IR of DPA52.

N-Boc DPA53.

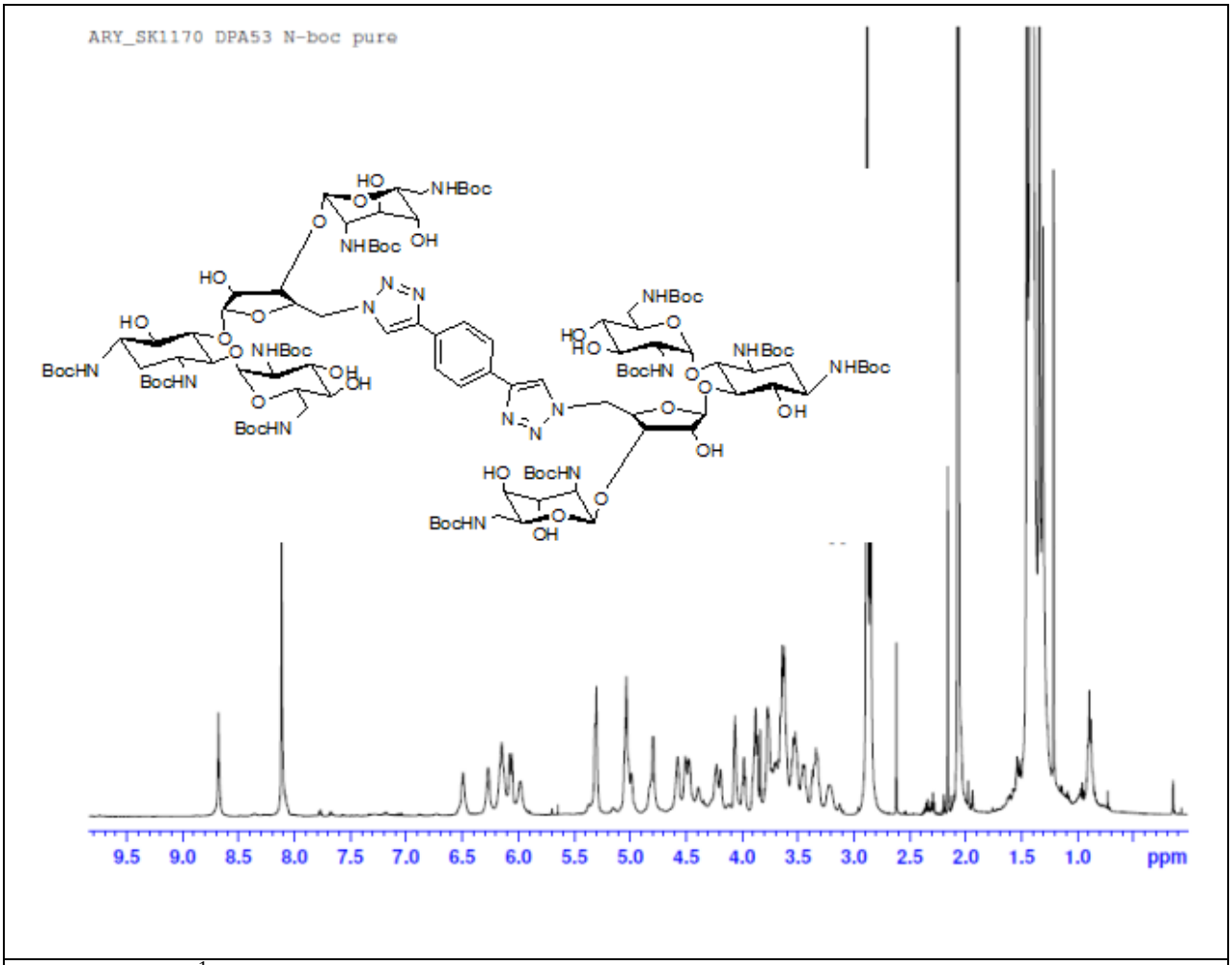

Figure S2.13. ^{1}H-NMR of N-Boc DPA53.

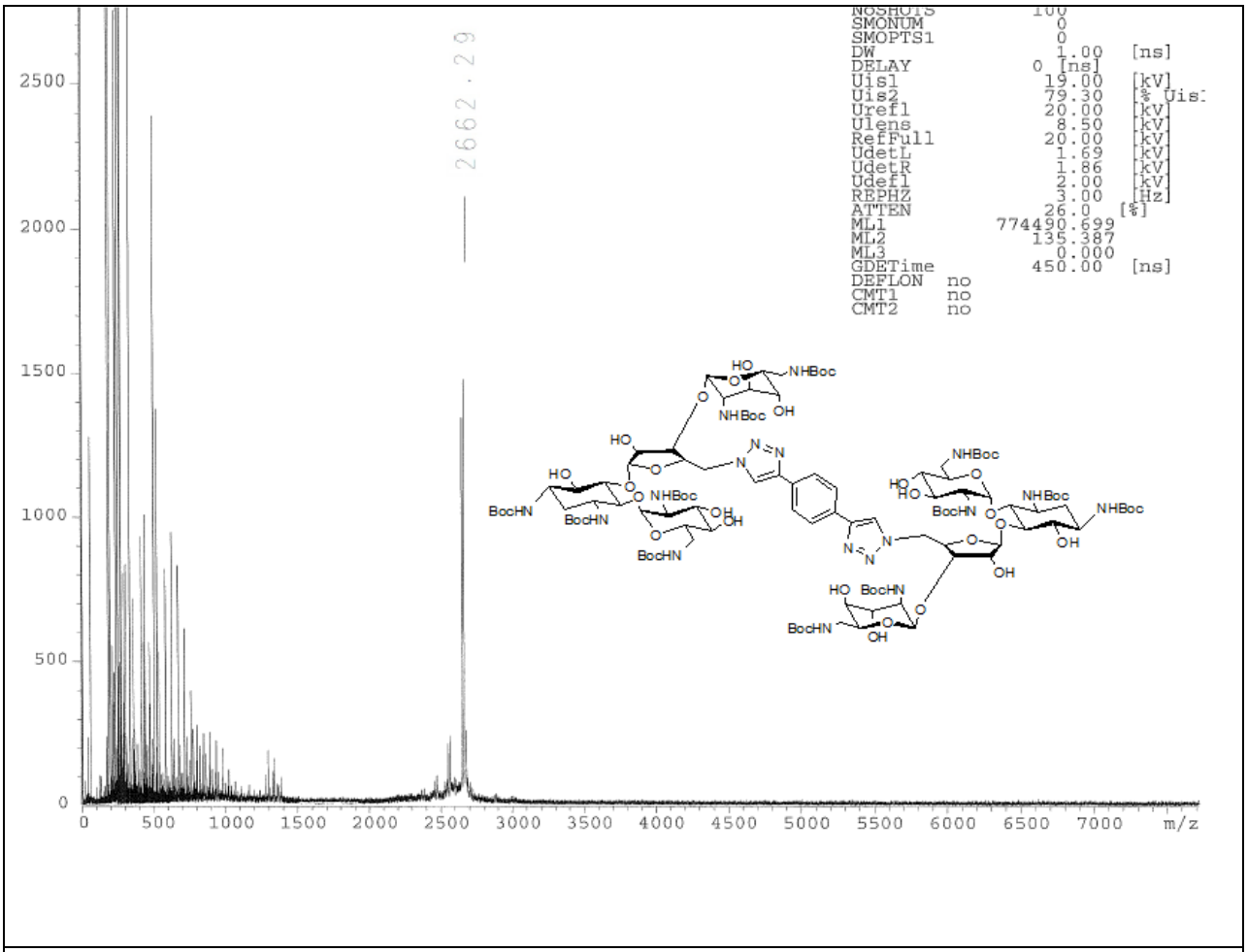

Figure S2.14. MALDI-TOF of N-Boc DPA53.

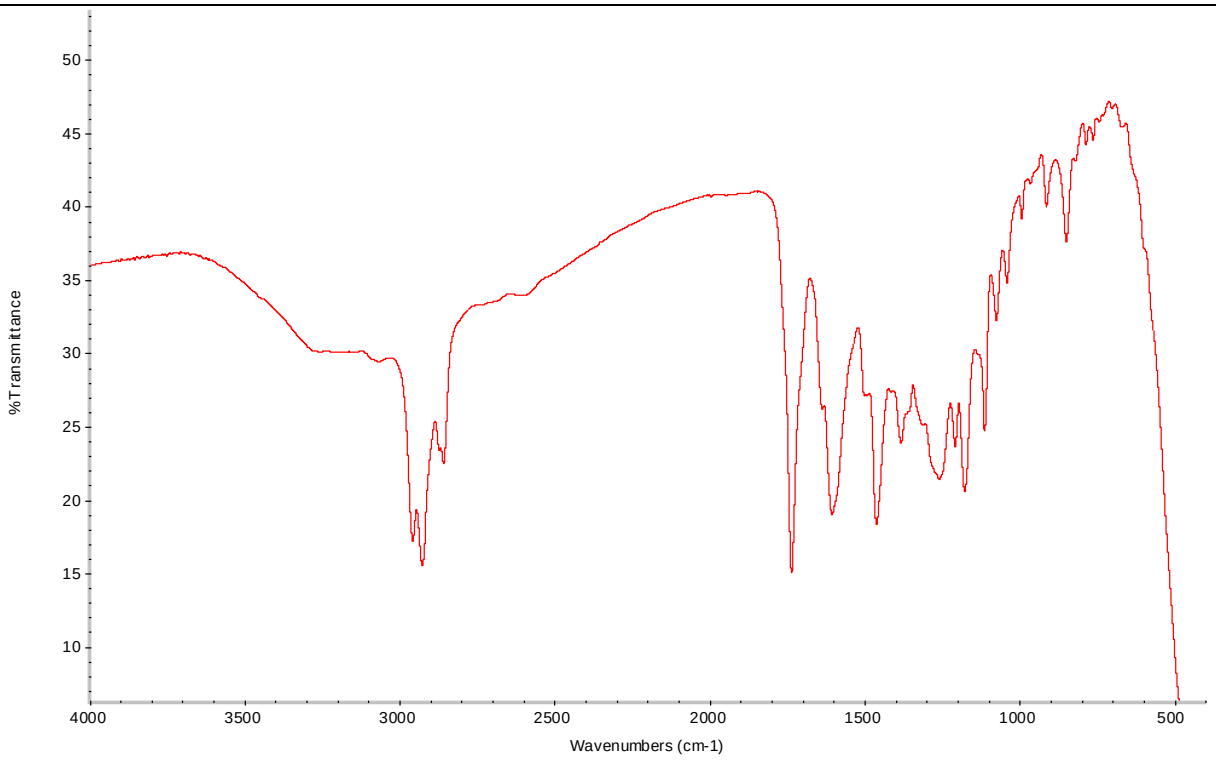

Figure S2.15. IR of of N-Boc DPA53.

DPA53.

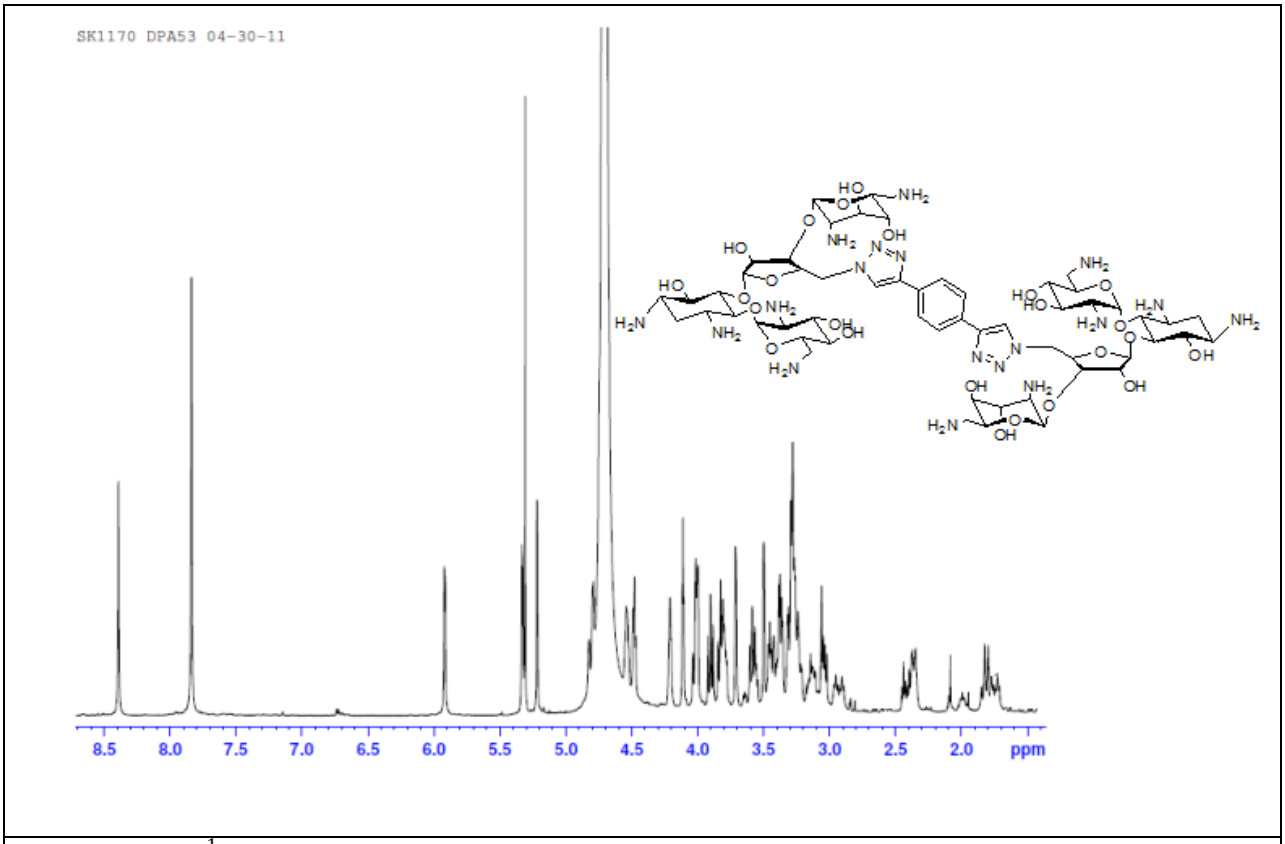

Figure S2.16. ^{1}H-NMR of DPA53.

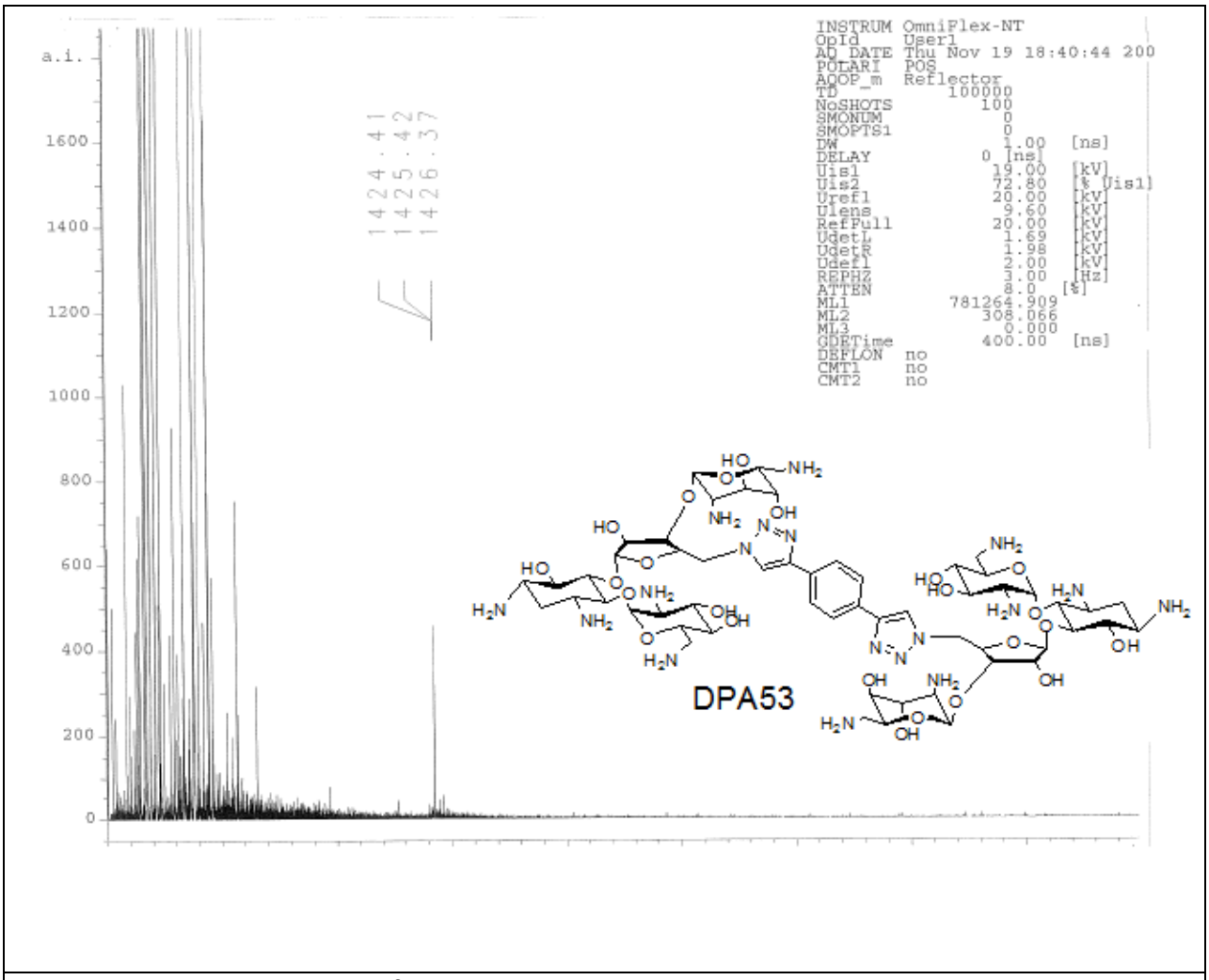

Figure S2.17. MALDI-TOF of DPA53.

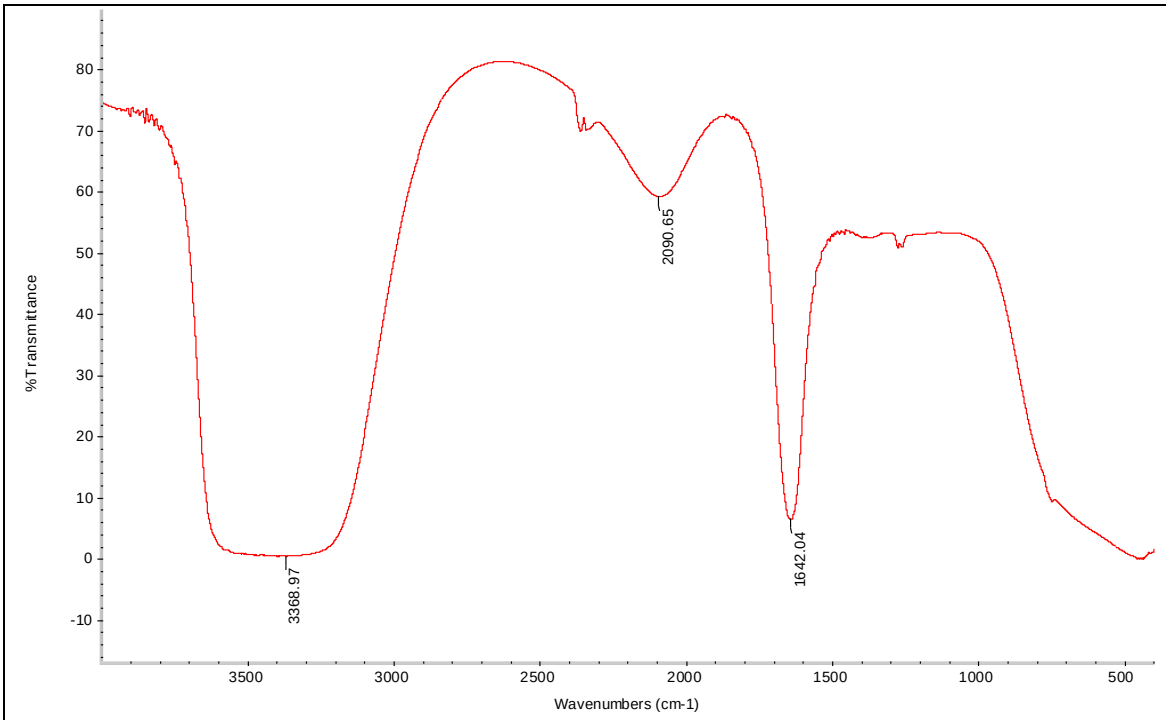

Figure S2.18. IR of DPA53.

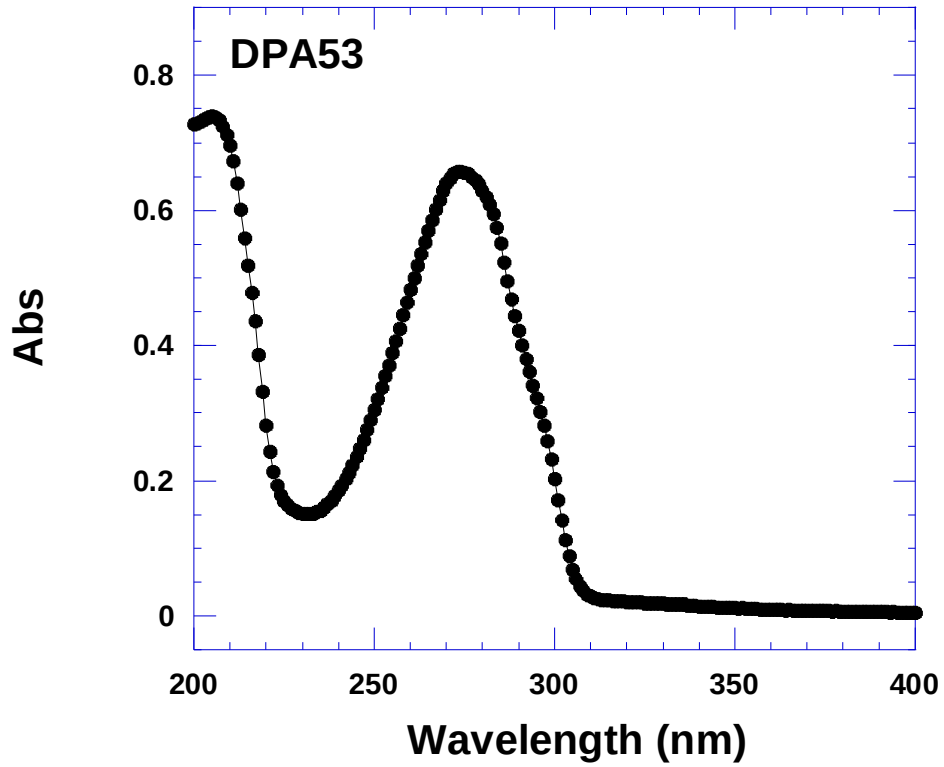

Figure S2.18. UV absorbance scan of DPA 53. Scan was taken in water and the concentration of DPA 54 was 25 µM. T = 25 °C.

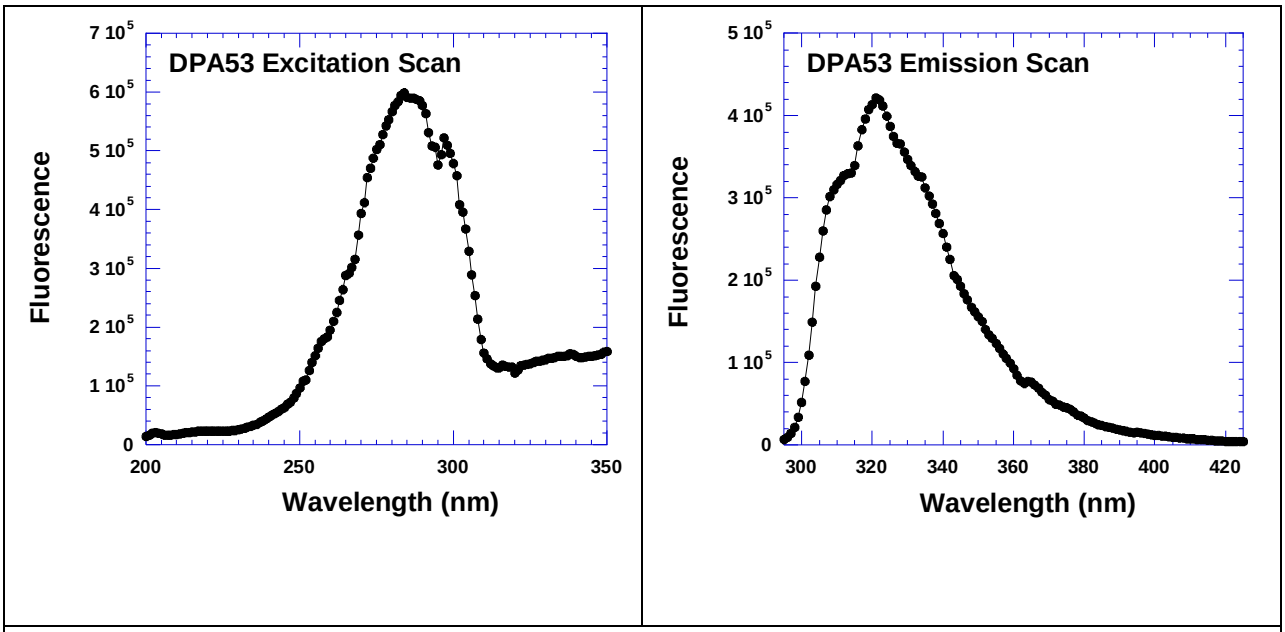

Figure S2.19. Fluorescence excitation scan of DPA 53 (left) and fluorescence emission scan of DPA 53 excited at 284nm (right). All scans were taken in water and the concentration of DPA 53 was 25 µM in all the scans. Excitation scan was performed first and wavelength with the highest fluorescence (284nm) was then used for the emission scan. DPA 53 excitation wavelength is now defined at 284nm, the emission maximum wavelength is defined at 321nm.

N-Boc DPA54.

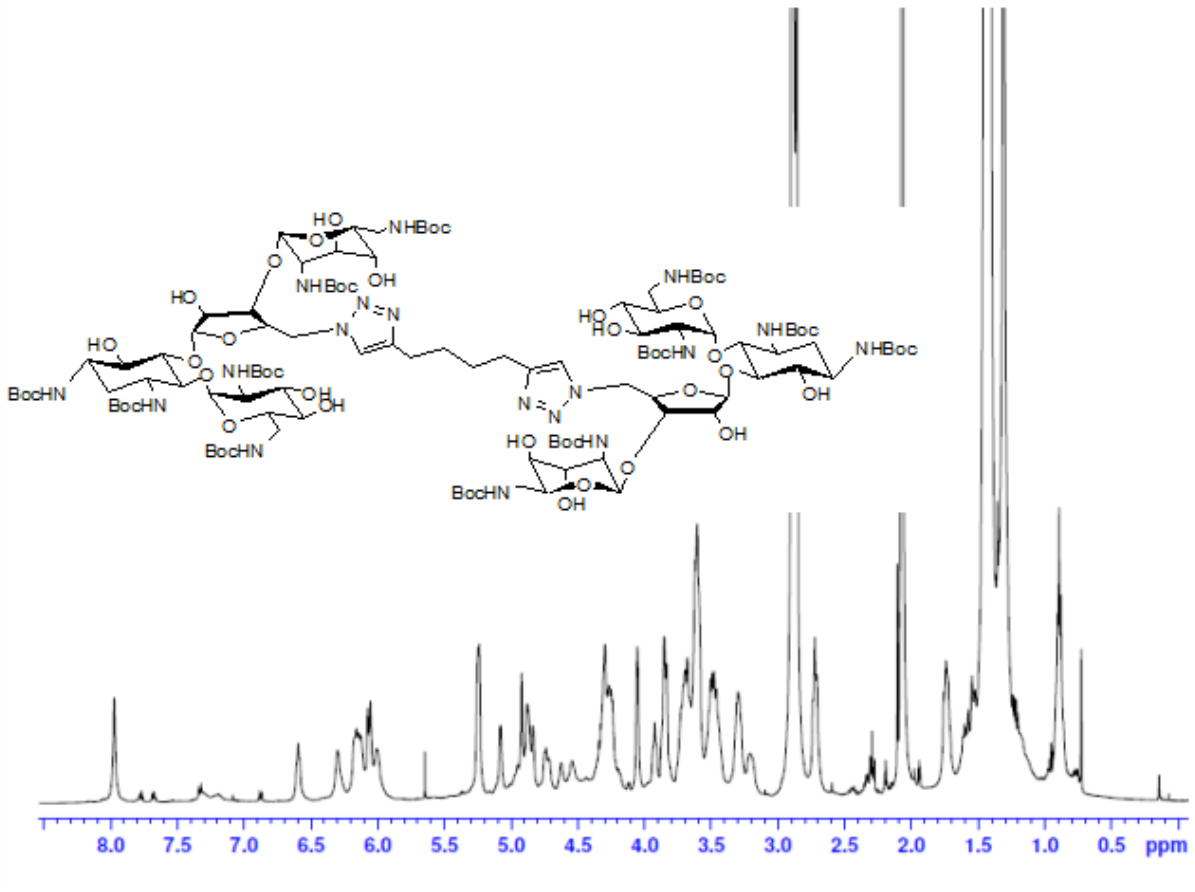

Figure S2.20. ^{1}H-NMR of N-Boc DPA54.

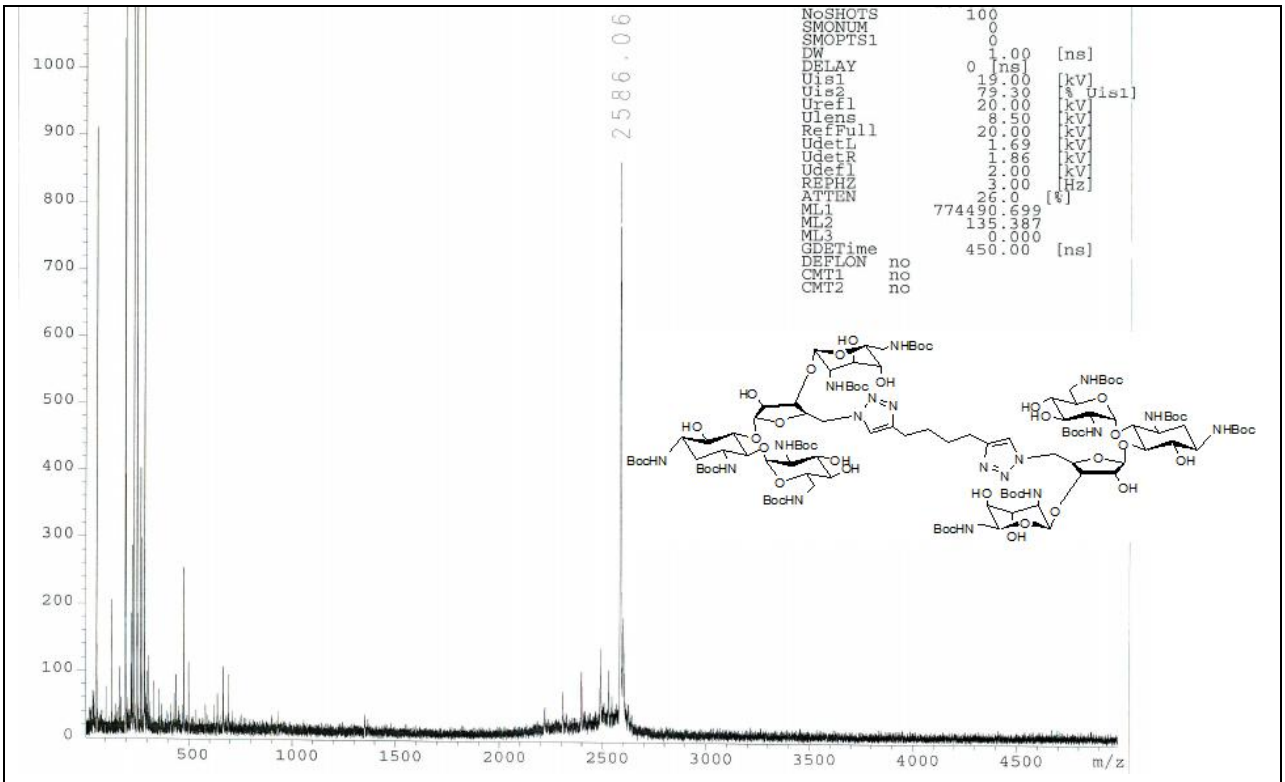

Figure S2.21. MALDI-TOF of N-Boc DPA54.

DPA54.

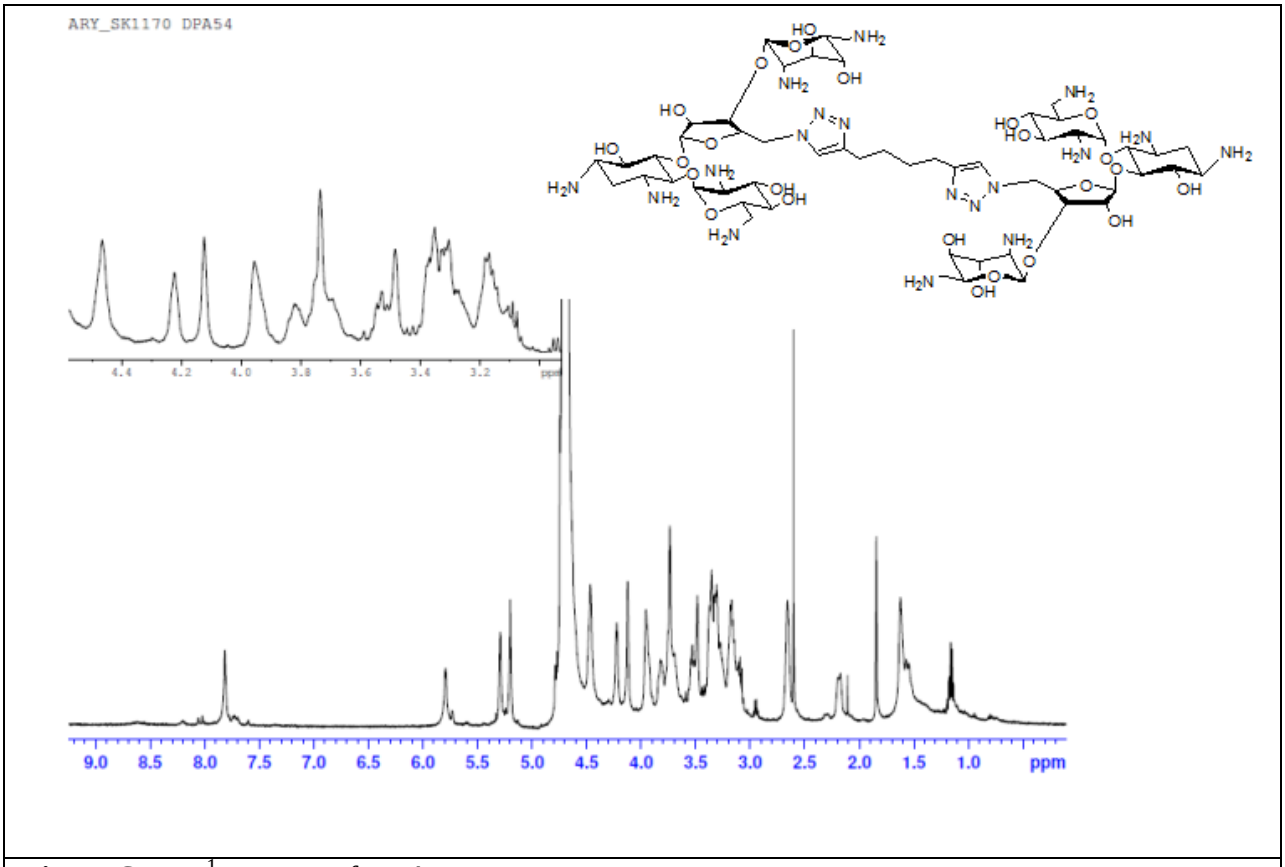

Figure S2.22. ^{1}H-NMR of DPA54.

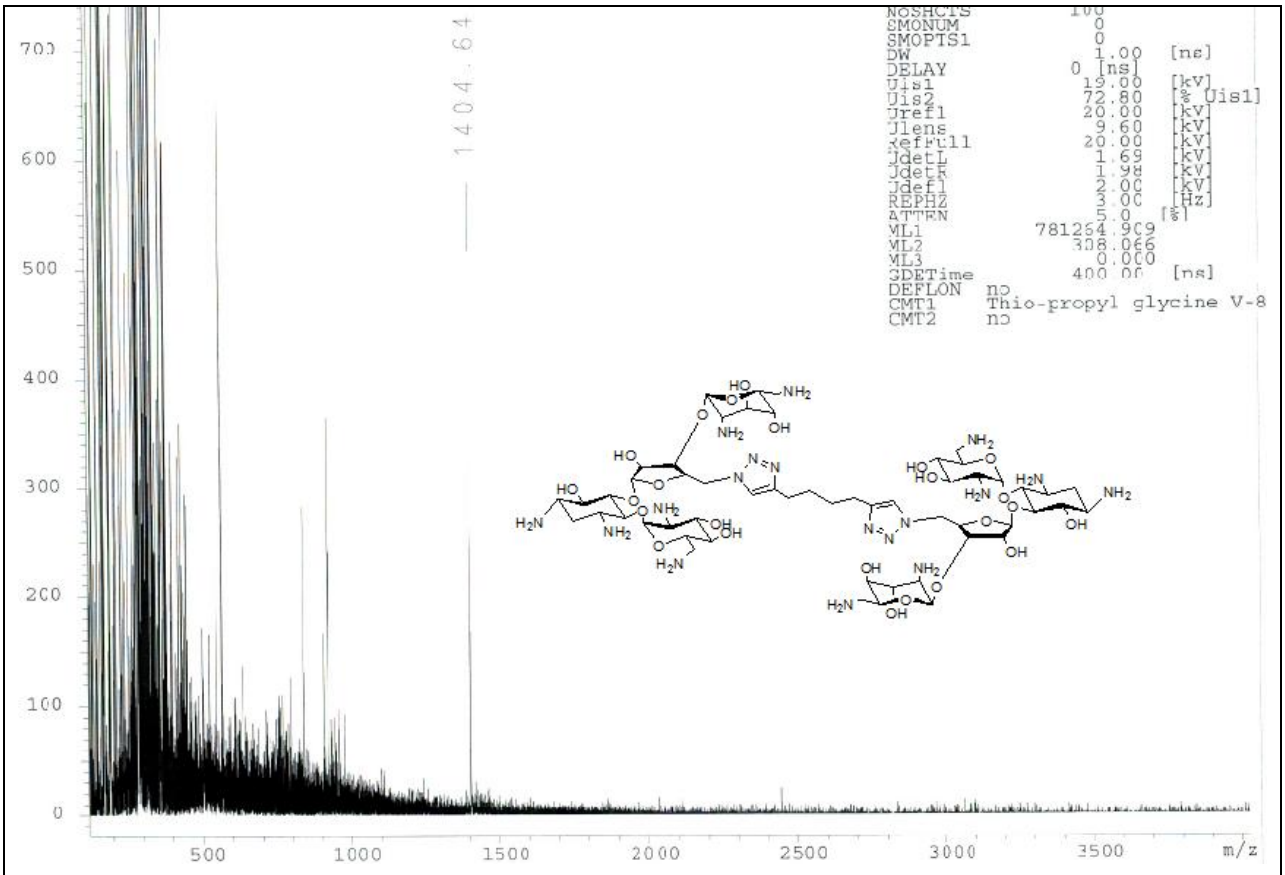

Figure S2.23. MALDI-TOF of DPA54.

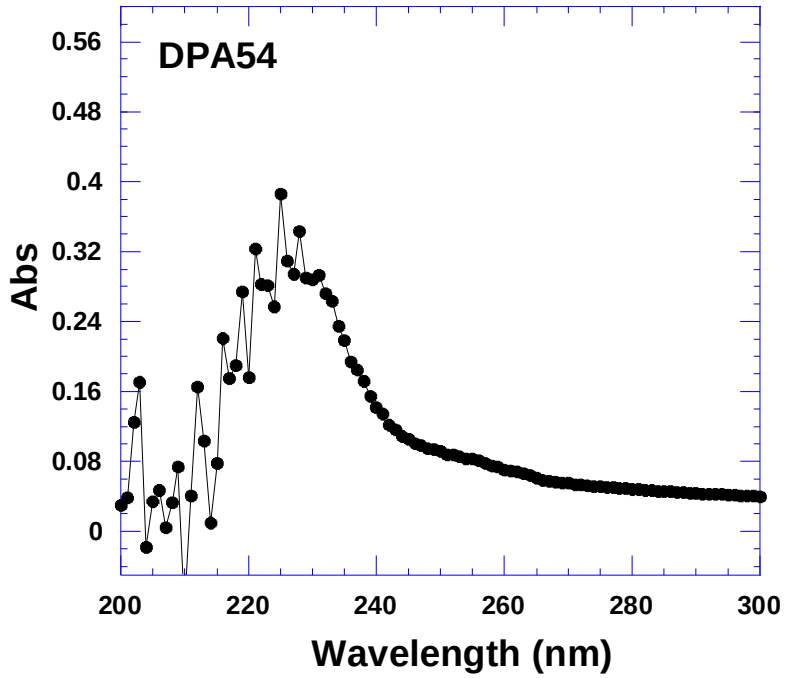

Figure S2.24. UV absorbance scan of DPA 54. Scan was taken in water and the concentration of DPA 54 was 25 µM. T = 25 °C.

N-Boc DPA55.

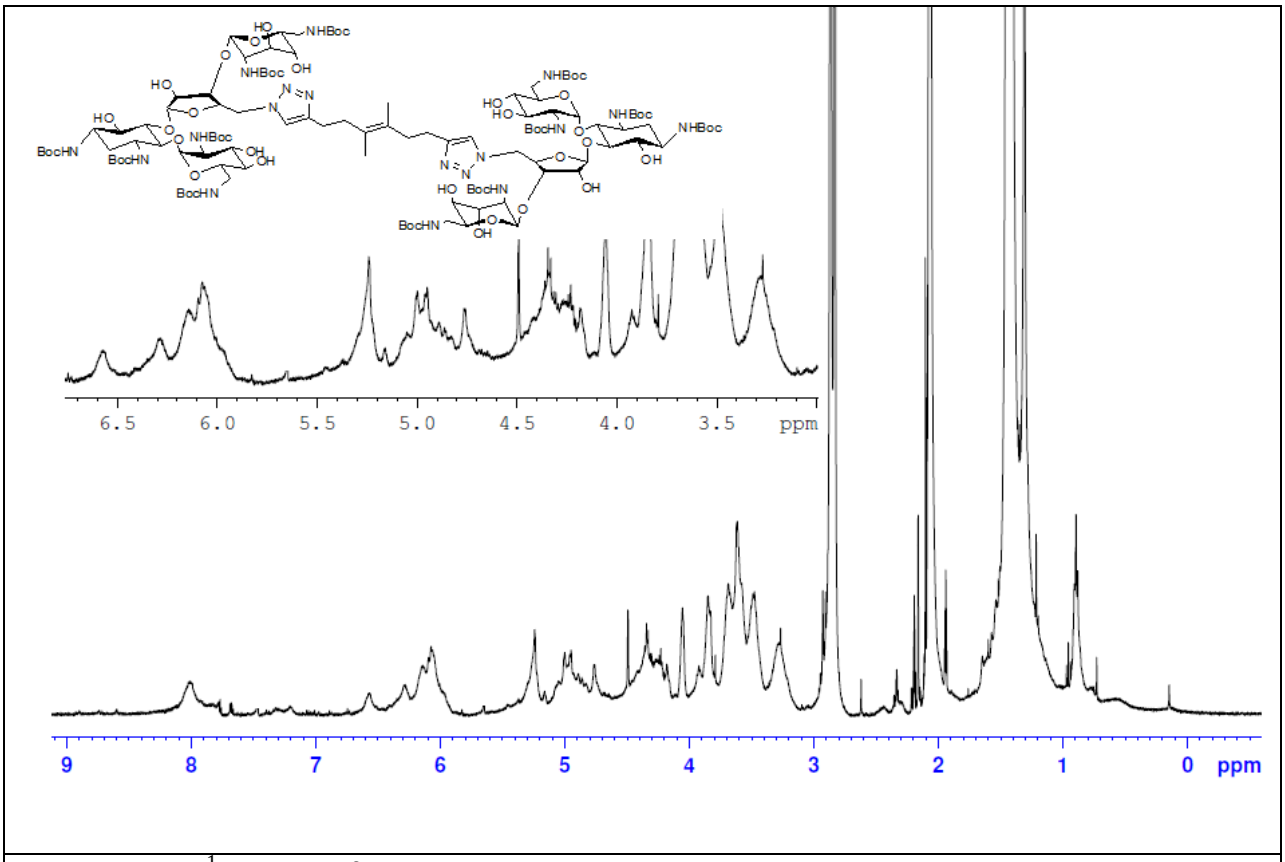

Figure S2.25. ^{1}H-NMR of N-Boc DPA55.

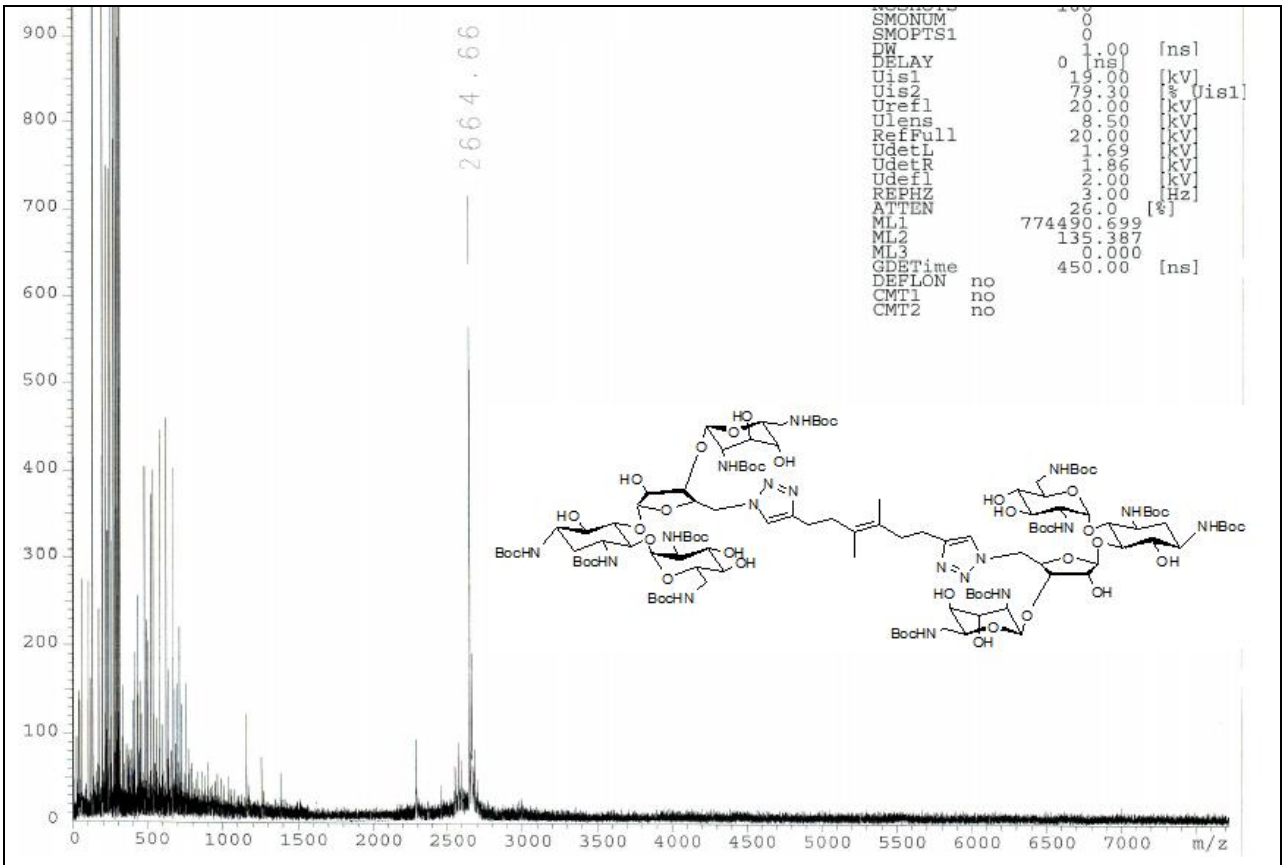

Figure S2.26. MALDI-TOF of N-Boc DPA55.

DPA55.

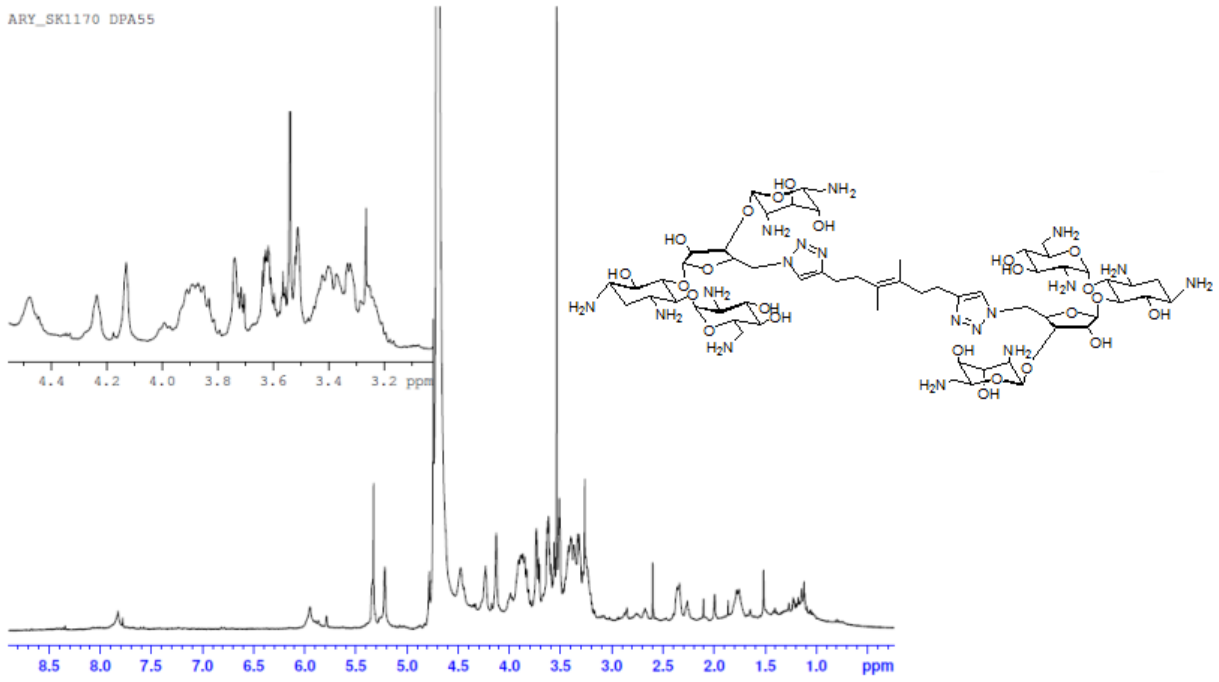

Figure S2.27. ^{1}H-NMR of DPA55.

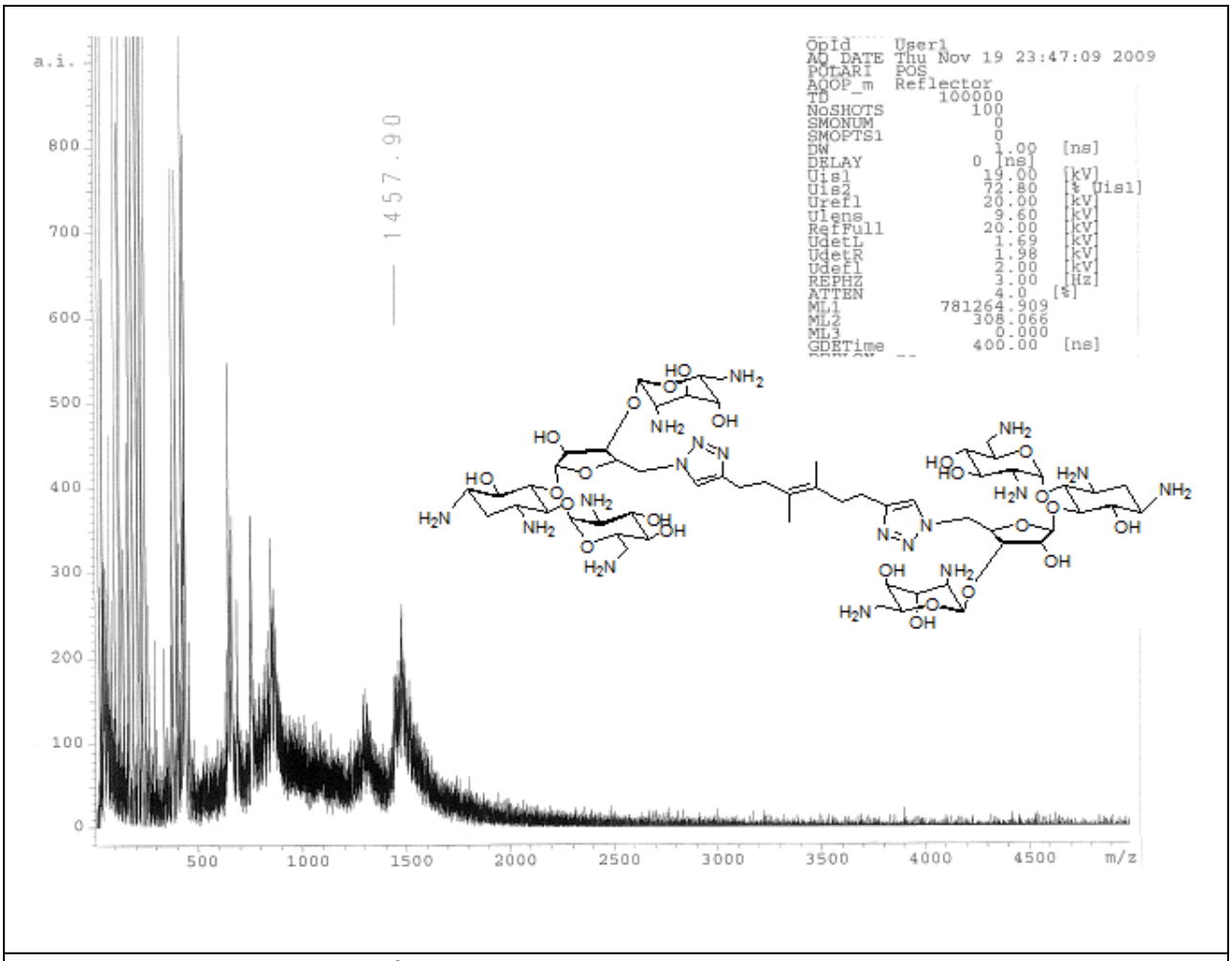

Figure S2.28. MALDI-TOF of DPA55.

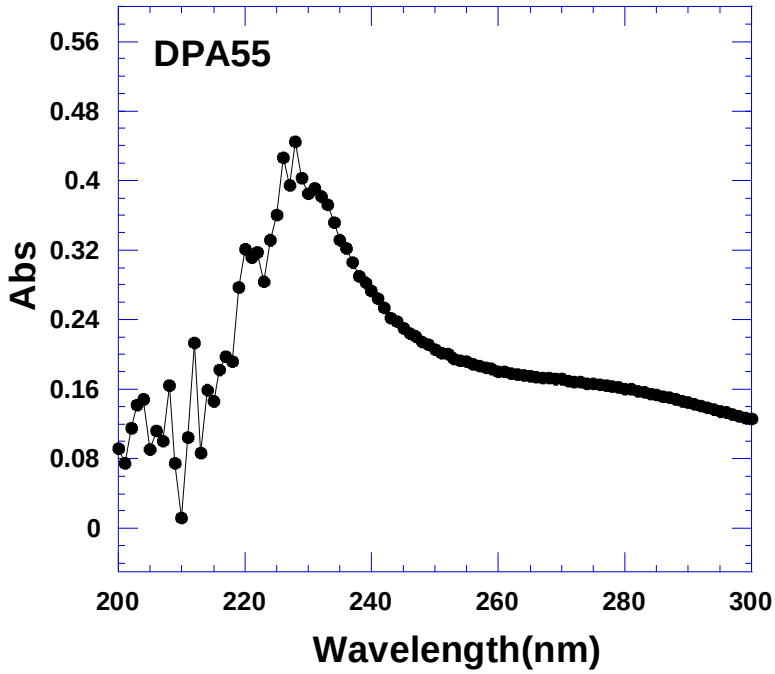

Figure S2.29. UV absorbance scan of DPA 55. Scan was taken in water and the concentration of DPA 55 was 25 µM. T = 25 °C.

N-Boc DPA56.

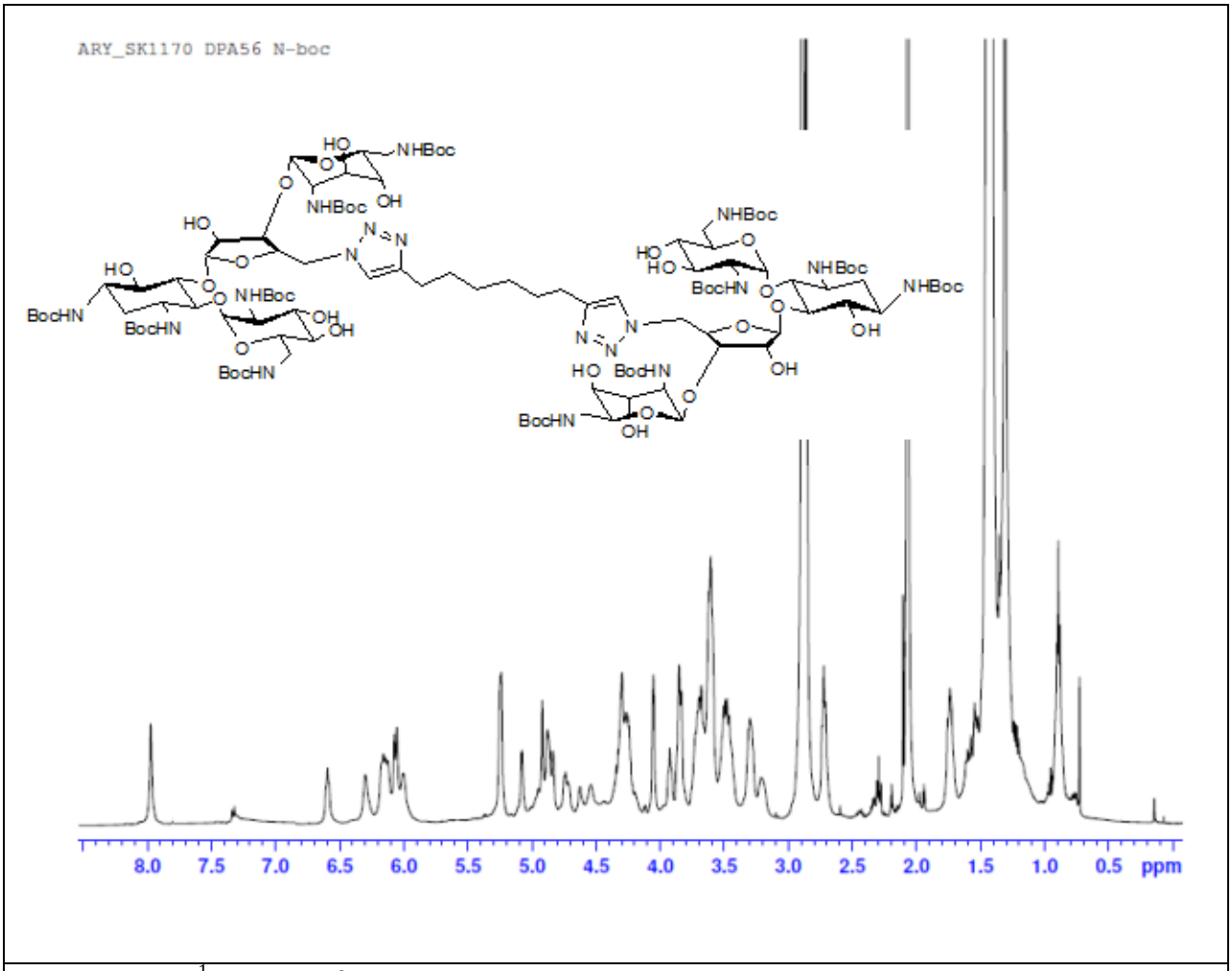

Figure S2.30. ^{1}H-NMR of N-Boc DPA56.

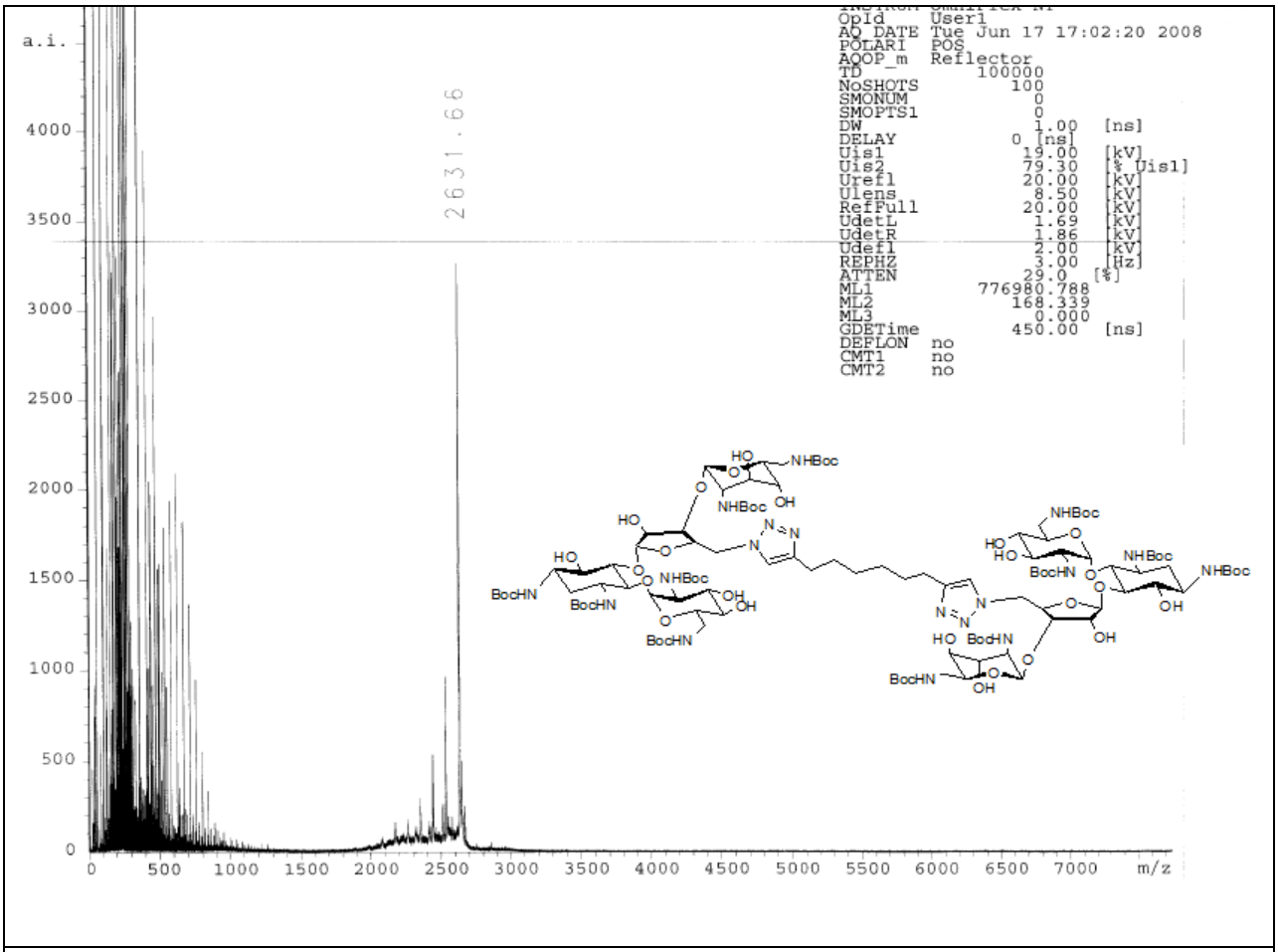

Figure S2.31. MALDI-TOF of N-Boc DPA56.

DPA56.

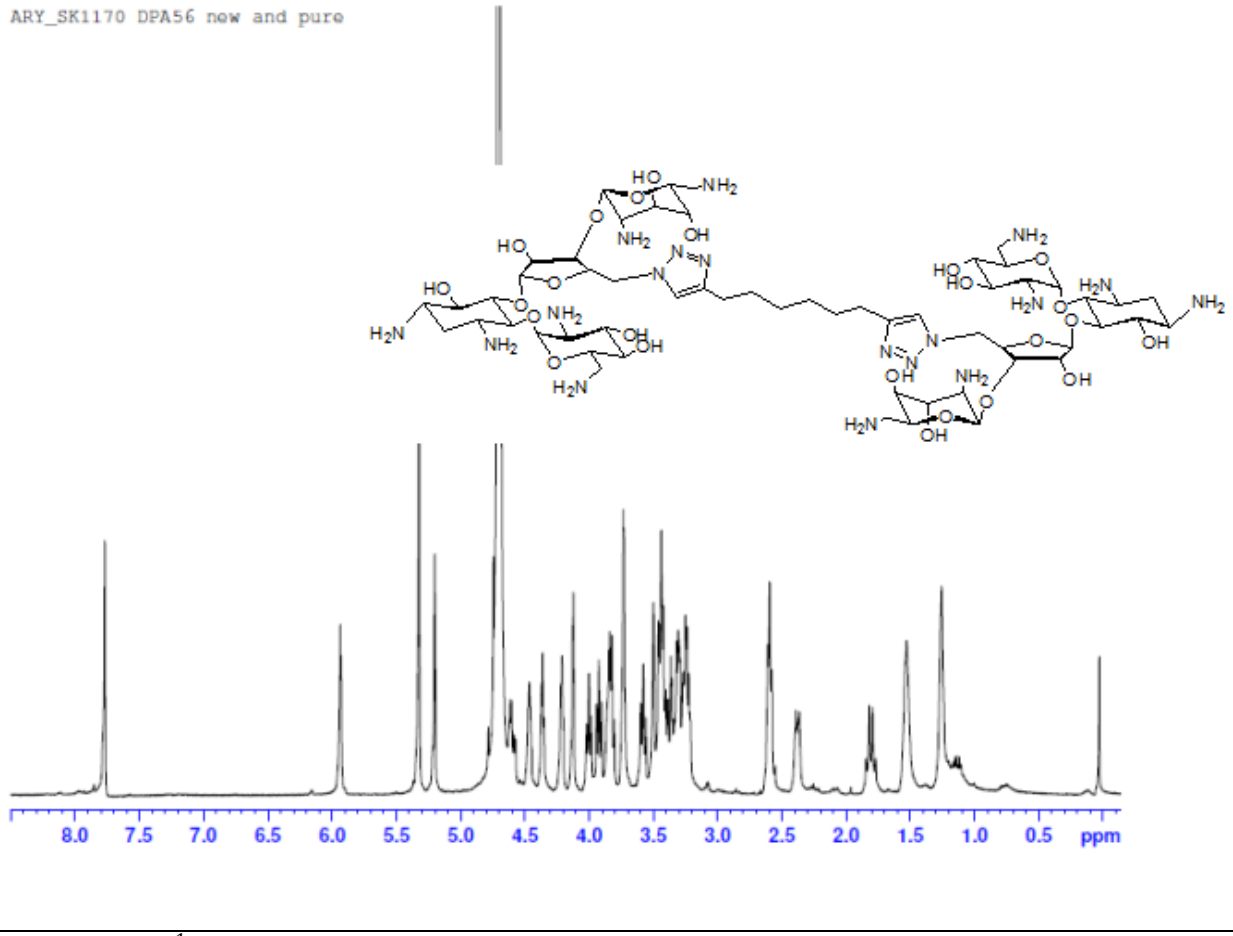

Figure S2.32. ^{1}H-NMR of DPA56.

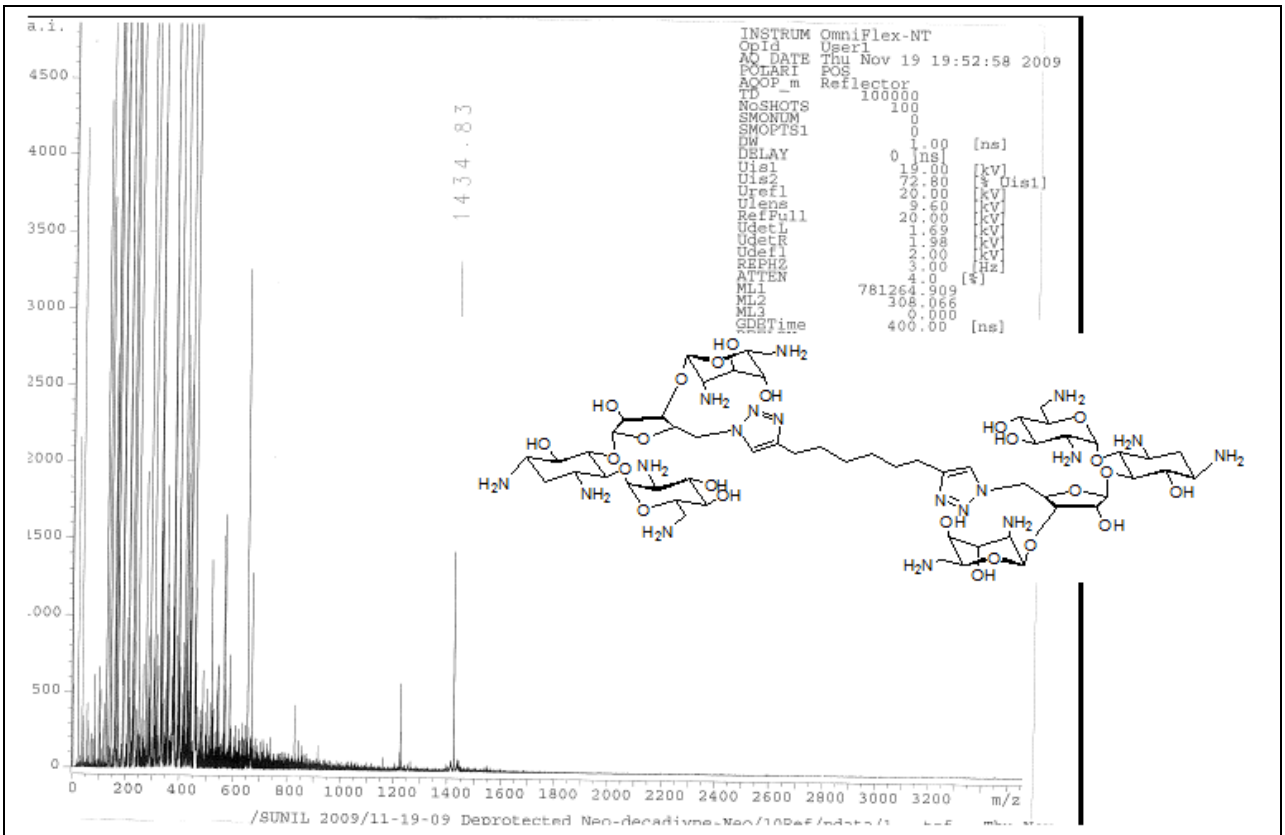

Figure S2.33. MALDI-TOF of DPA56.

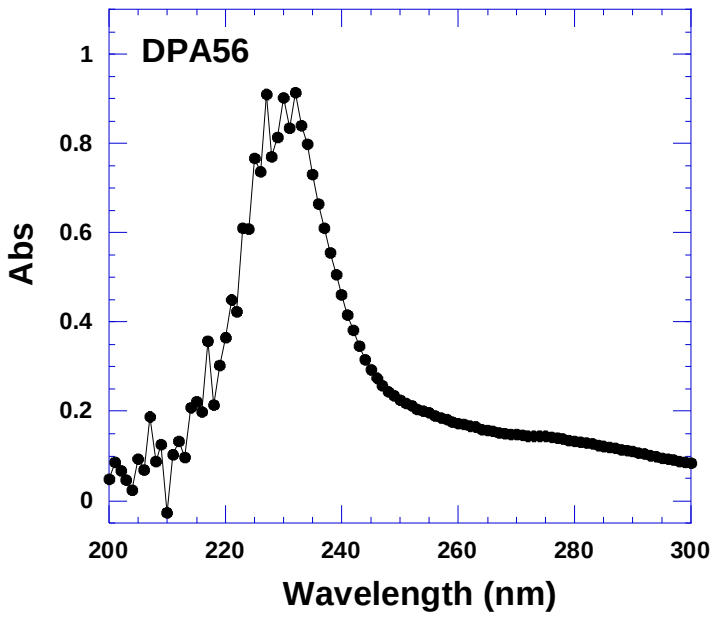

Figure S2.34. UV absorbance scan of DPA56. Scan was taken in water and the concentration of DPA56 was 25 μM. T = 25 °C.

N-Boc DPA58.

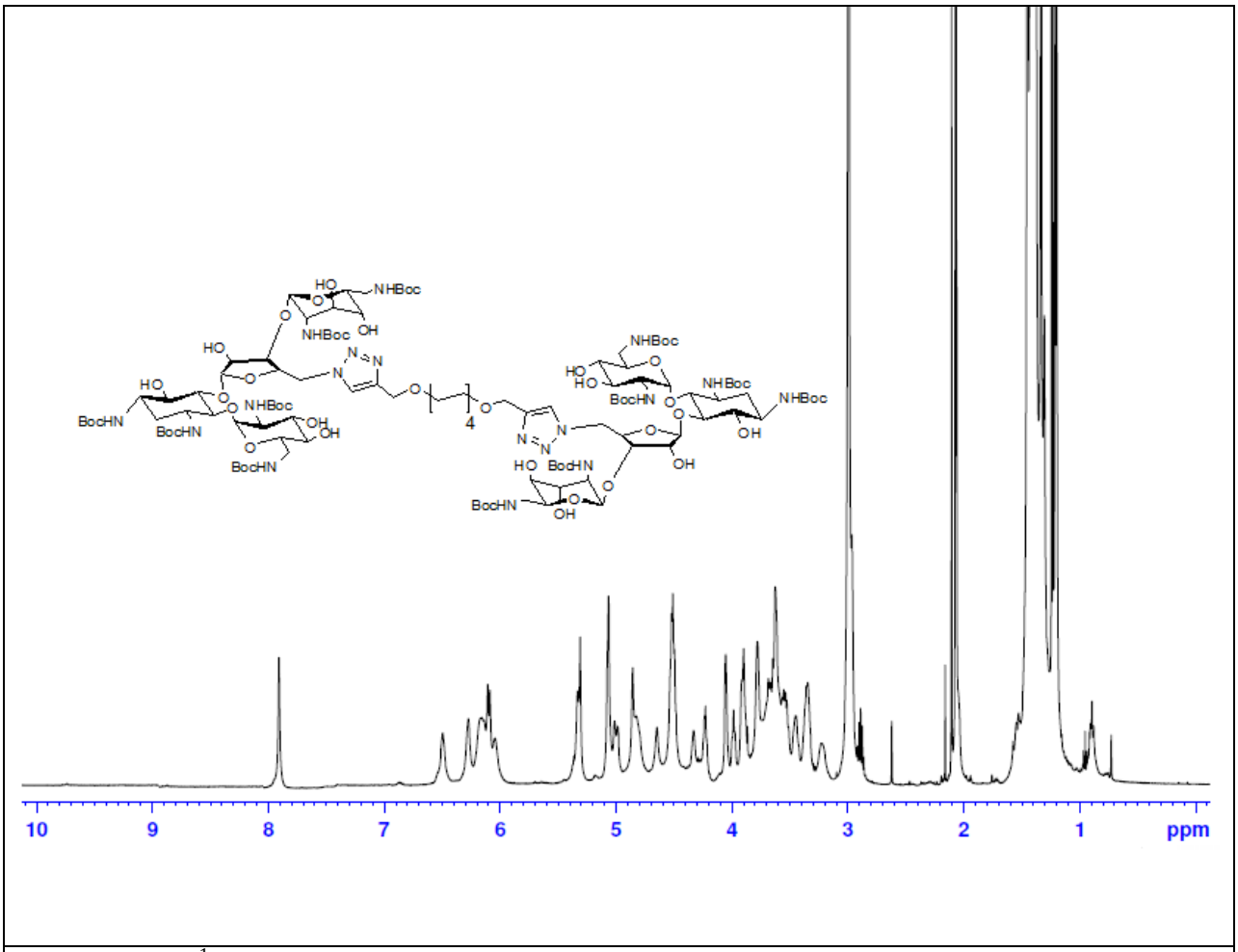

Figure S2.35. ^{1}H-NMR of N-Boc DPA58.

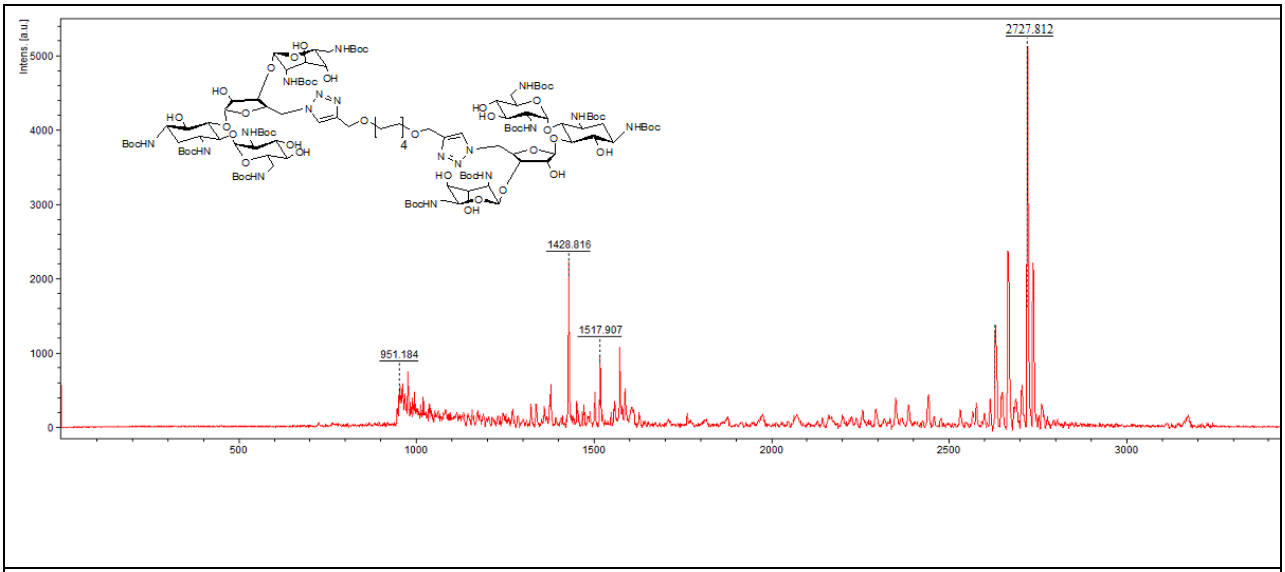

Figure S2.36. MALDI-TOF of N-Boc DPA58.

DPA58.

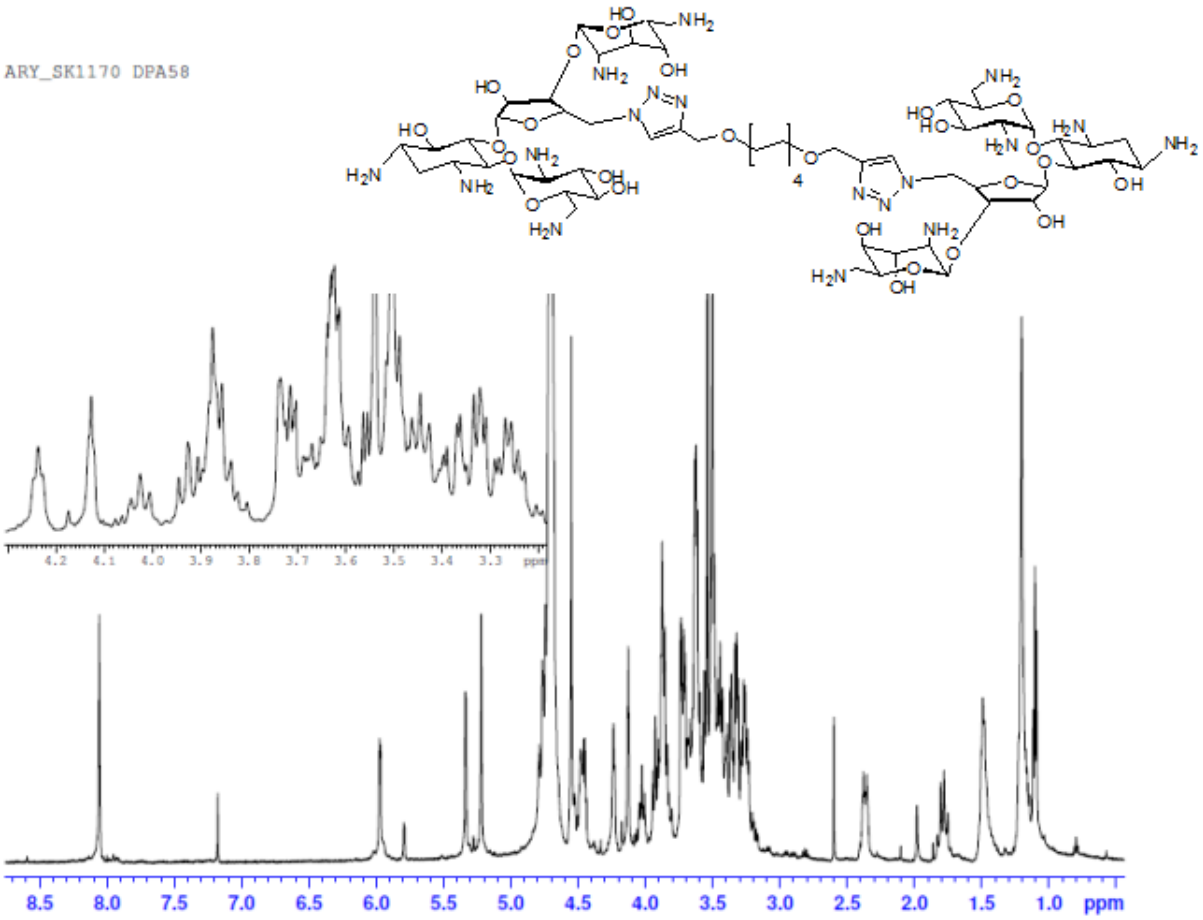

Figure S2.37. ^{1}H NMR of DPA58.

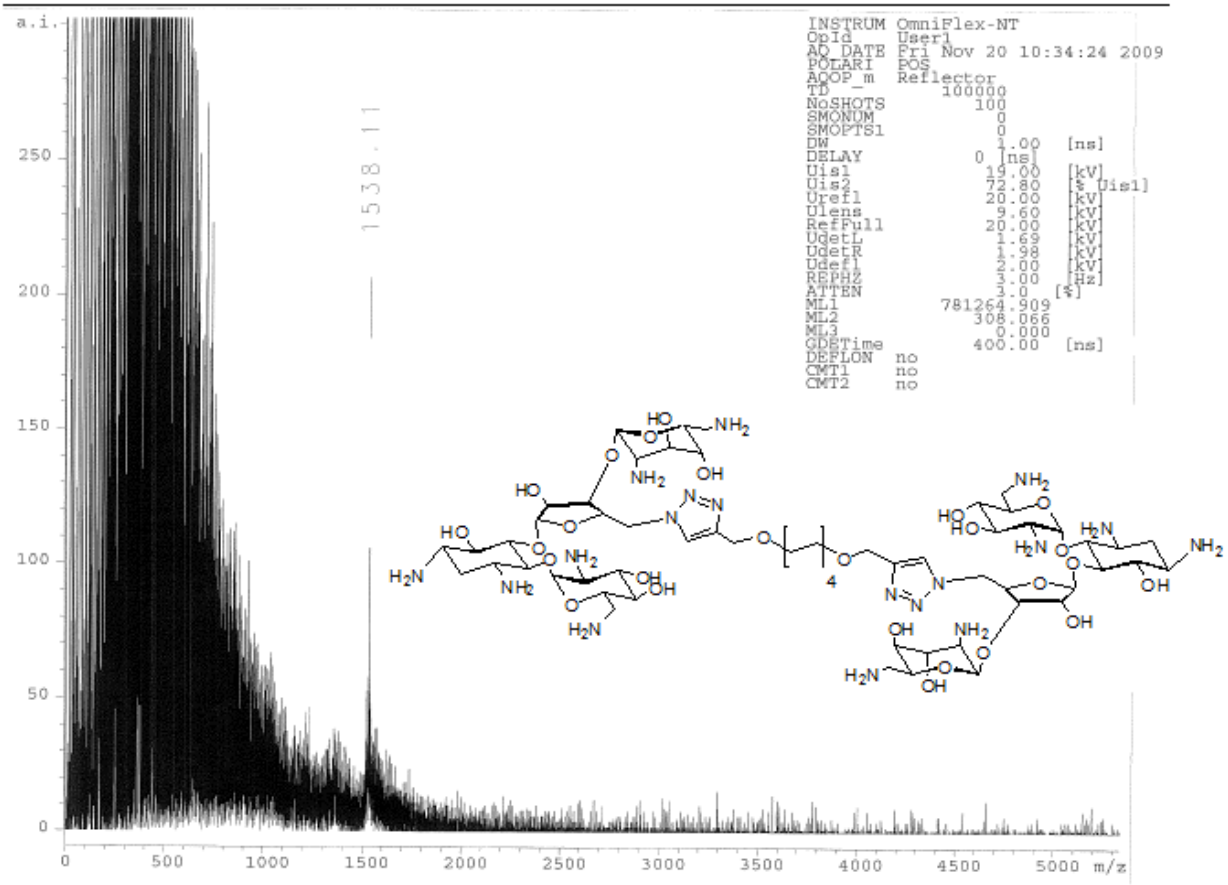

Figure S2.38. MALDI-TOF of DPA58.

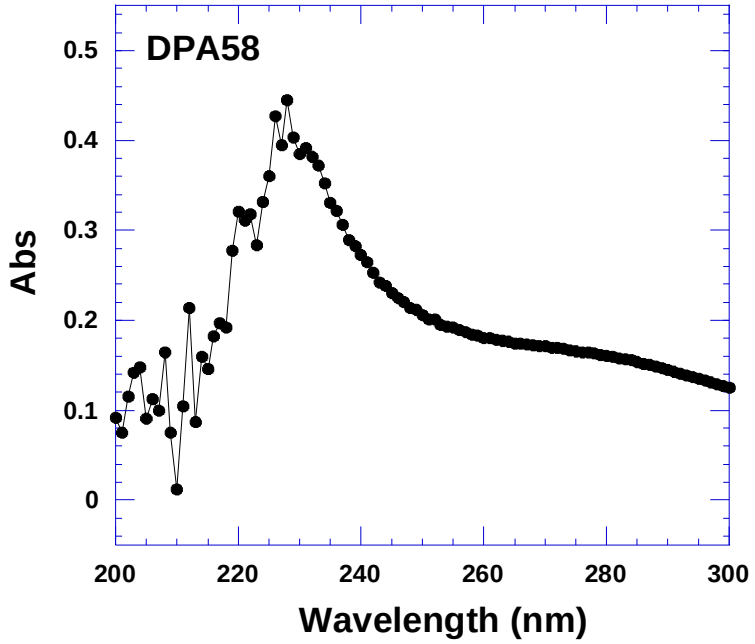

Figure S2.39. UV absorbance scan of DPA58. Scan was taken in water and the concentration of DPA58 was 25 μM. T = 25 °C.

N-Boc DPA60.

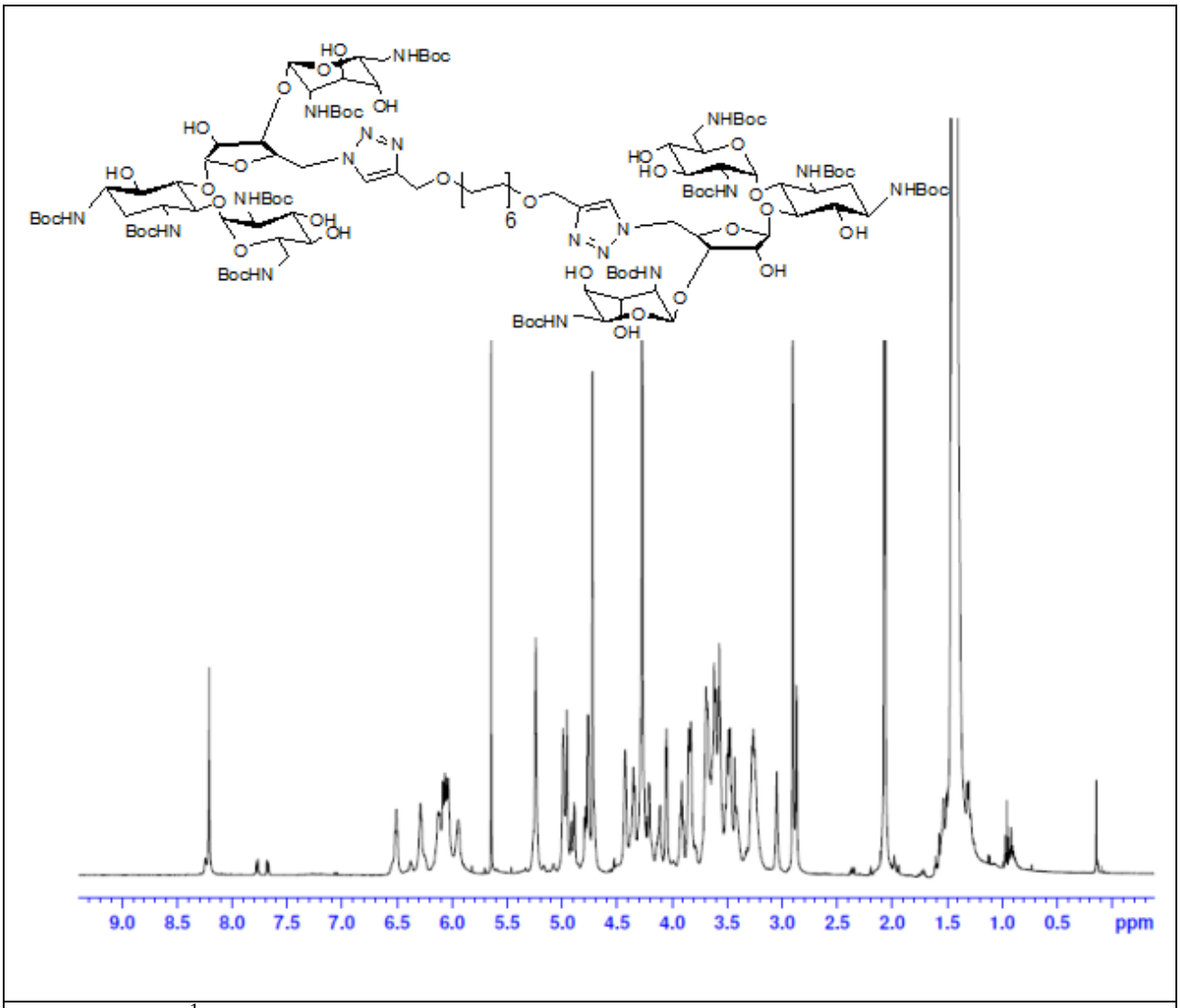

Figure S2.40. ^{1}H-NMR of N-Boc DPA60.

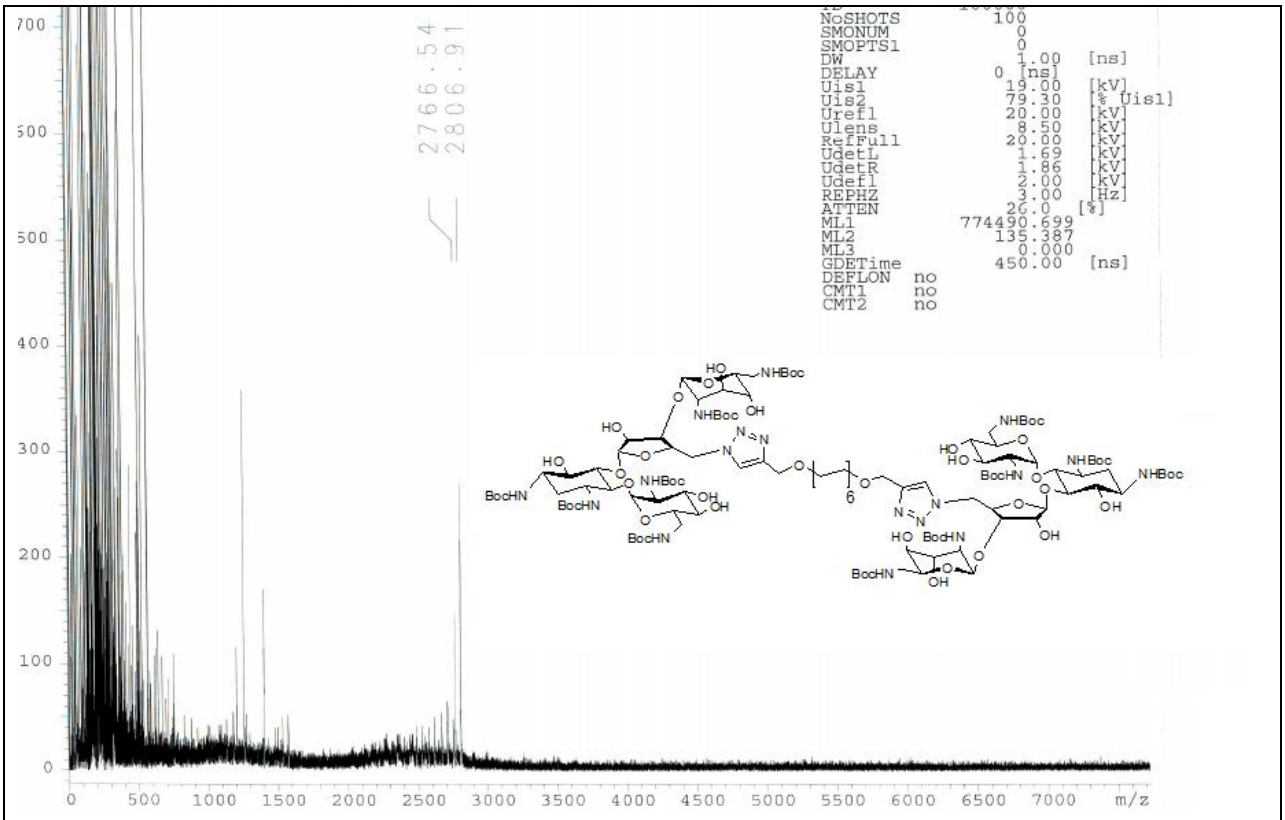

Figure S2.41. MALDI-TOF of N-Boc DPA60.

DPA60.

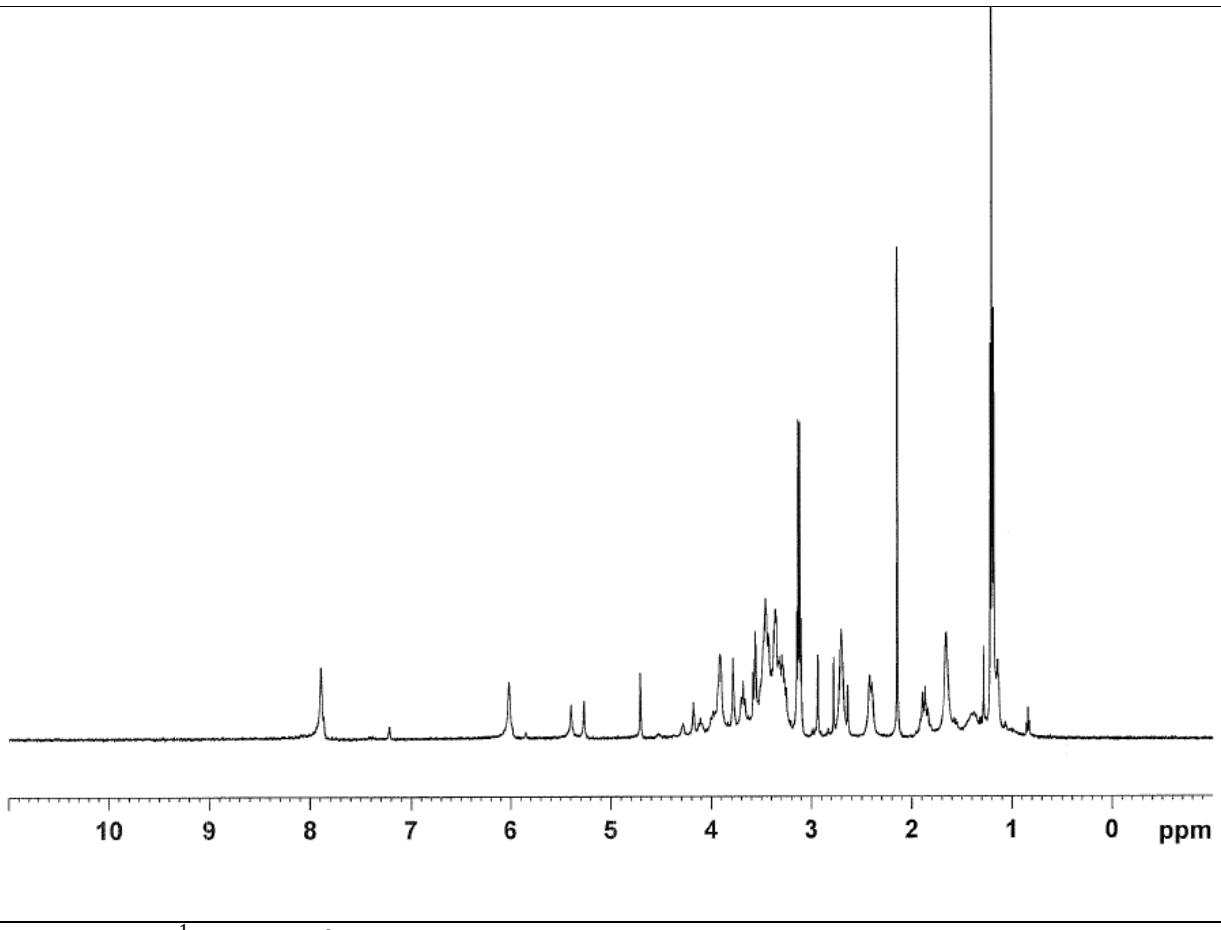

Figure S2.42. ^{1}H-NMR of DPA60.

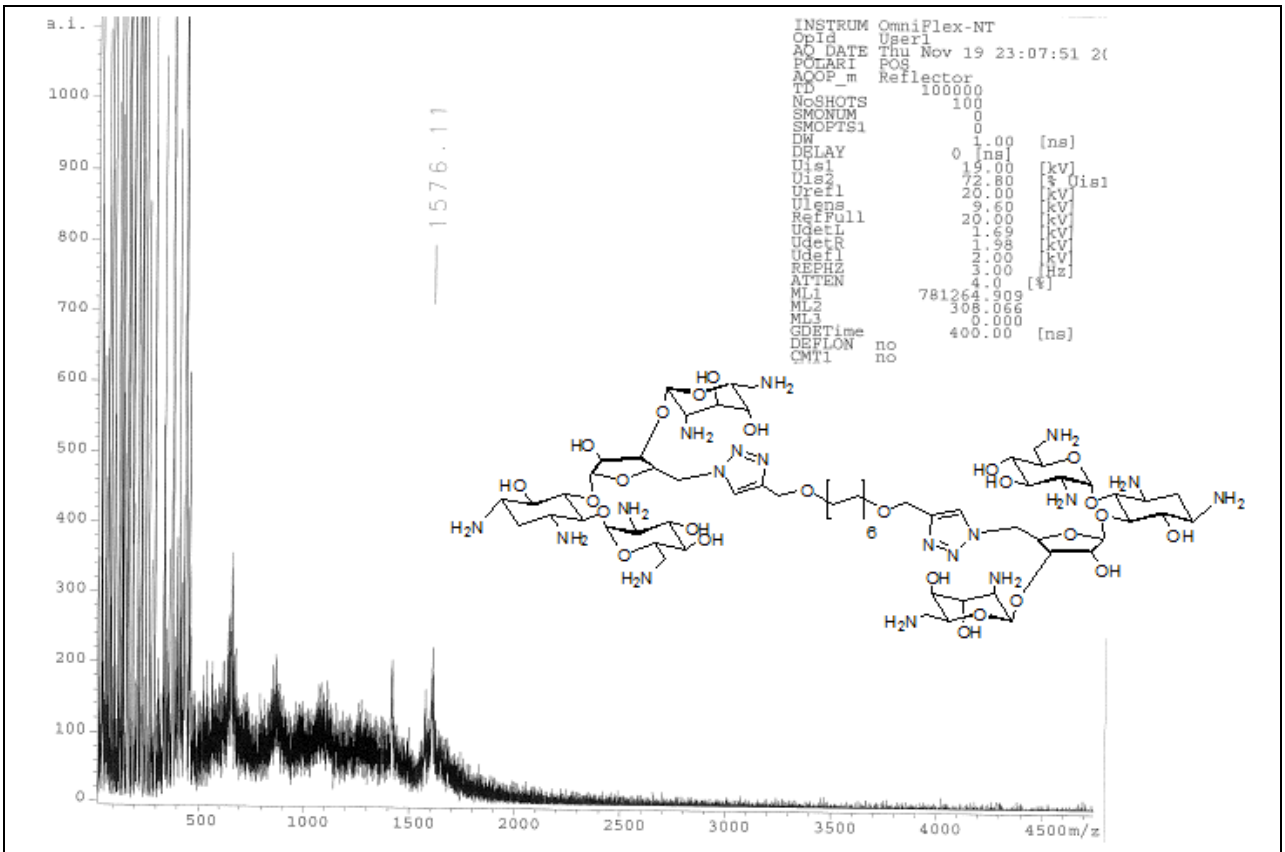

Figure S2.43. MALDI-TOF of DPA60.

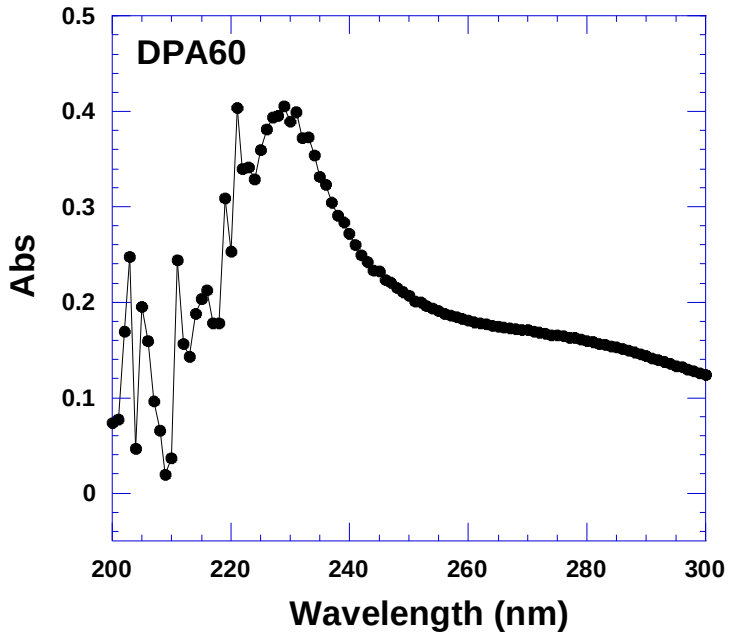

Figure S2.44. UV absorbance scan of DPA60. Scan was taken in water and the concentration of DPA60 was 25 μM. T = 25 °C.

N-Boc DPA65.

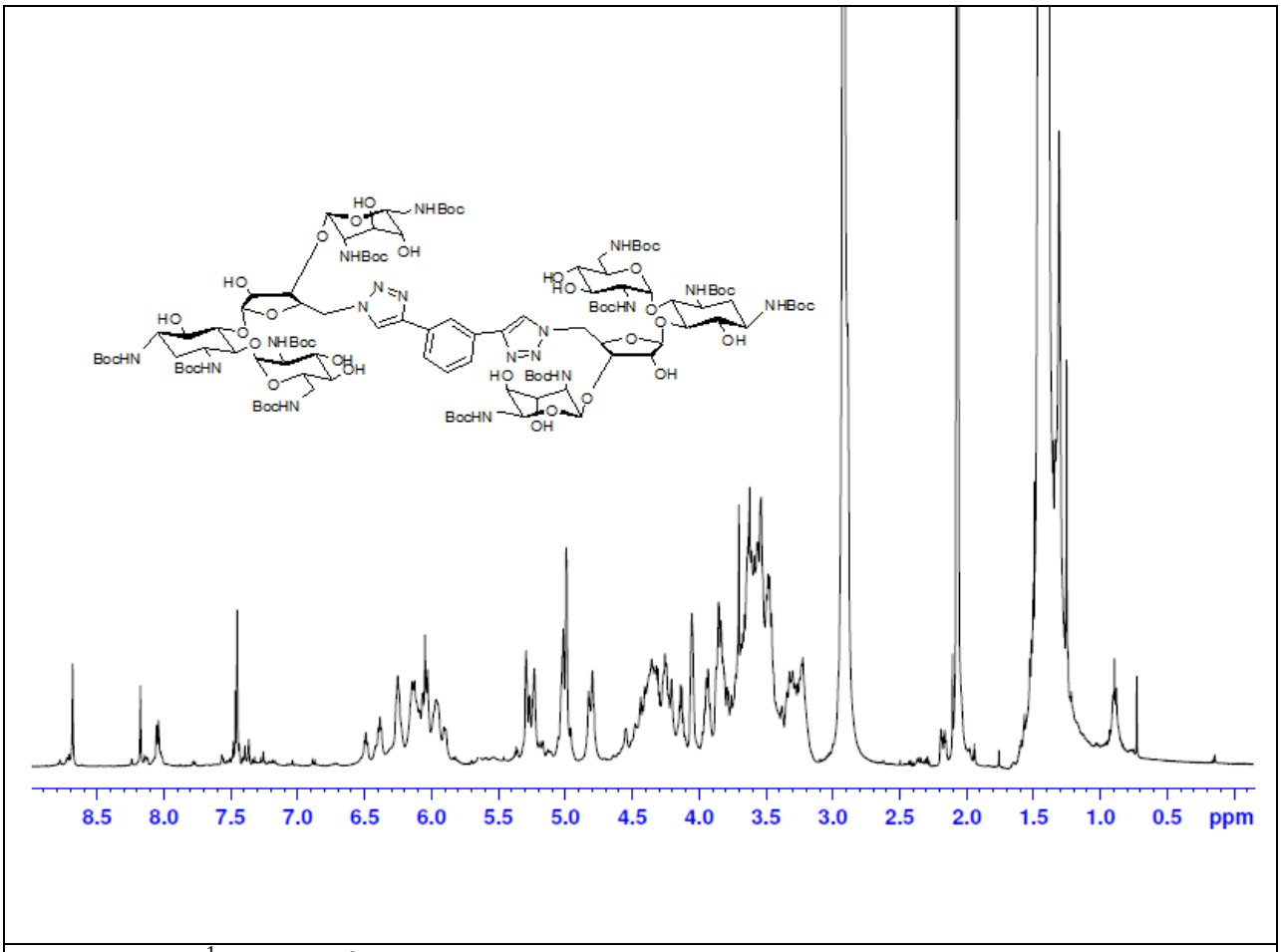

Figure S2.45. ^{1}H NMR of N-Boc DPA65.

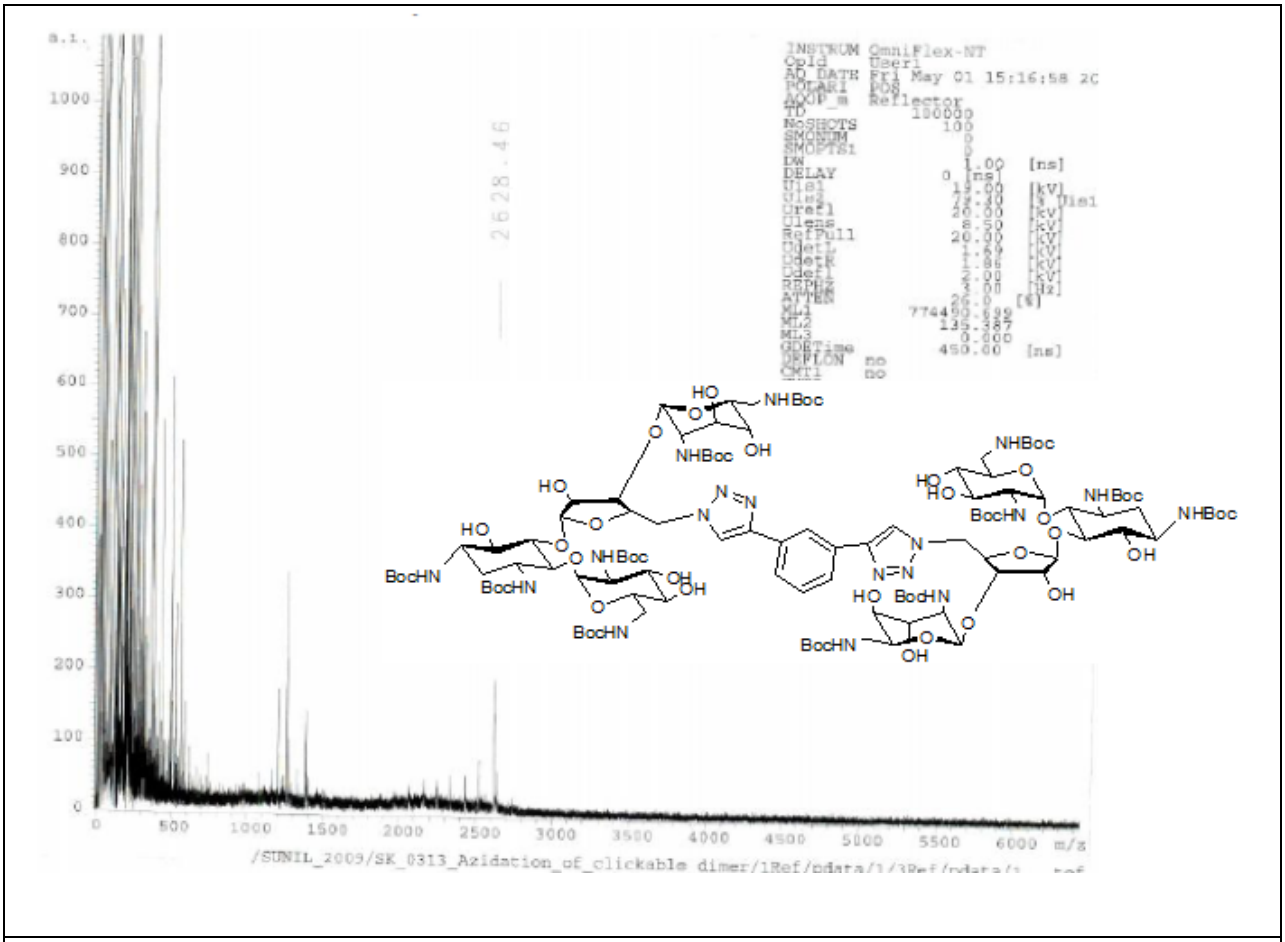

Figure S2.46. MALDI-TOF of N-Boc DPA65.

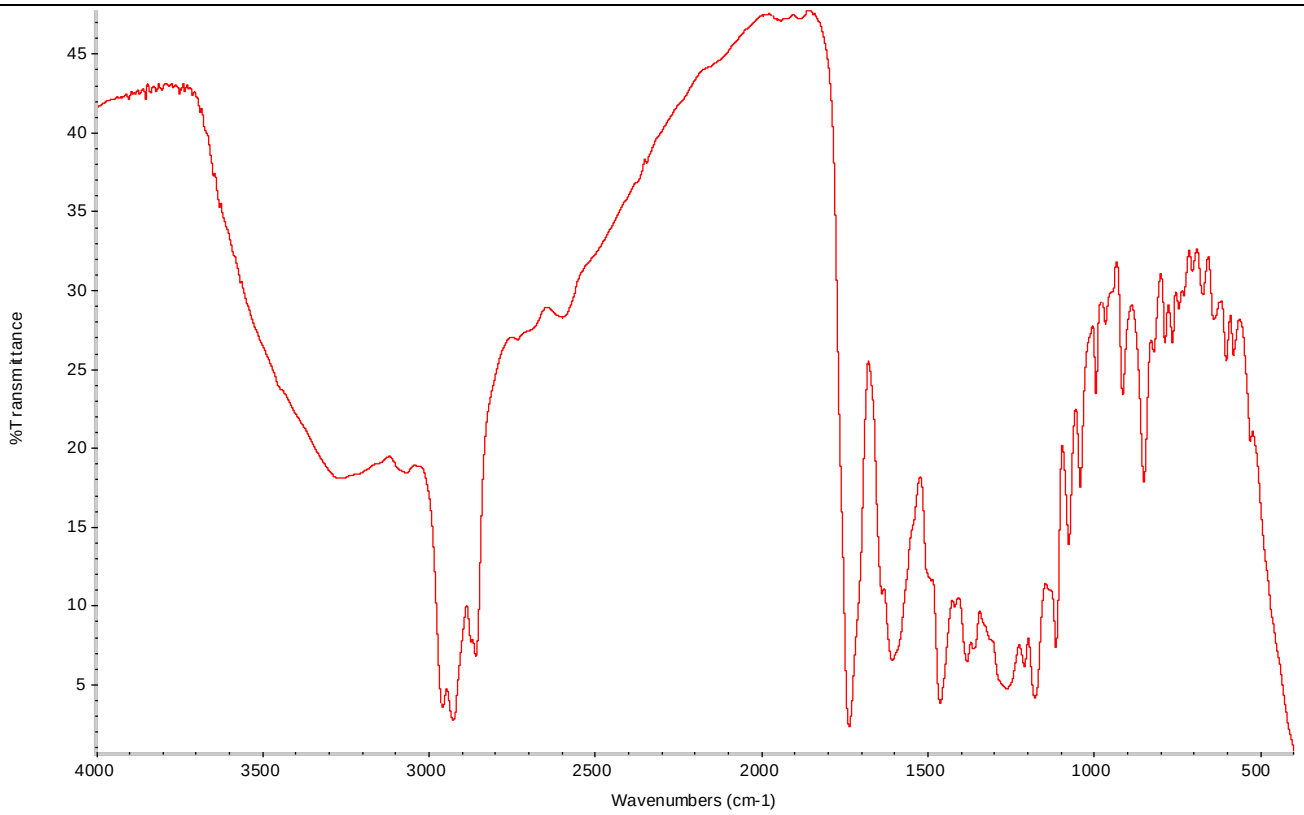

Figure S2.47. IR of N-Boc DPA65.

DPA65.

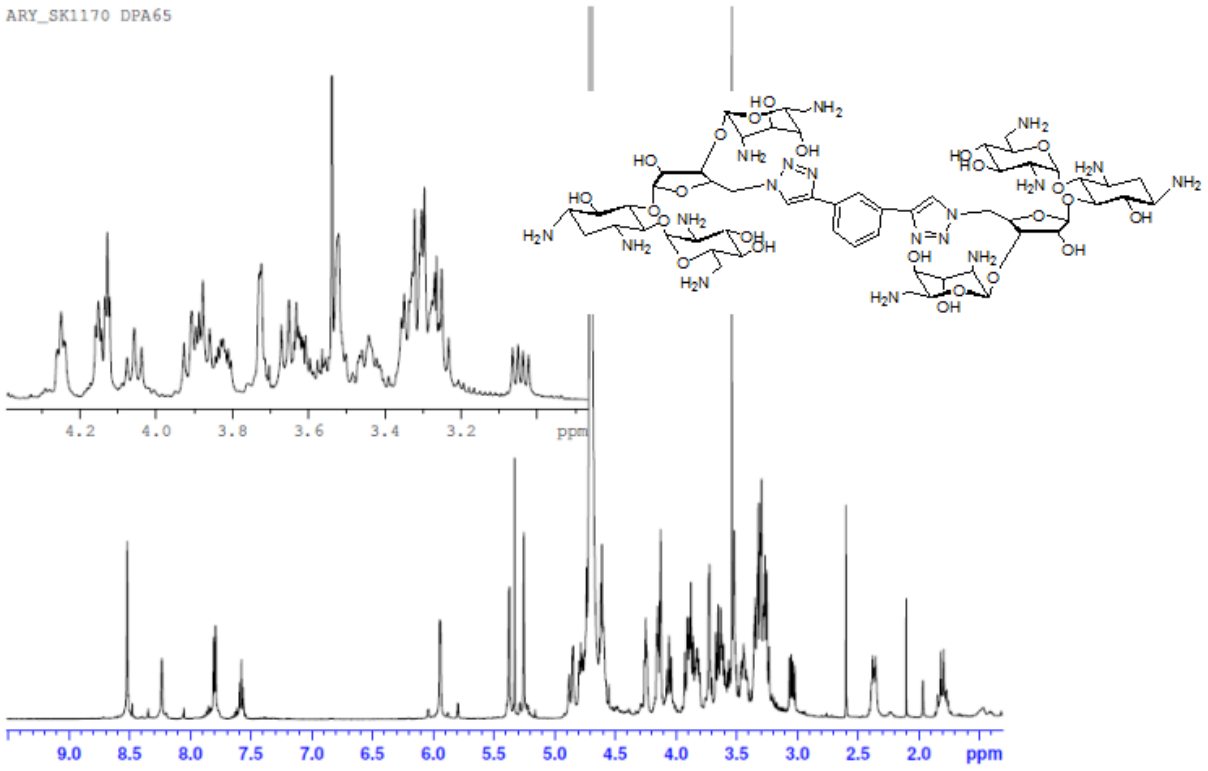

Figure S2.48. ^{1}H-NMR of DPA65.

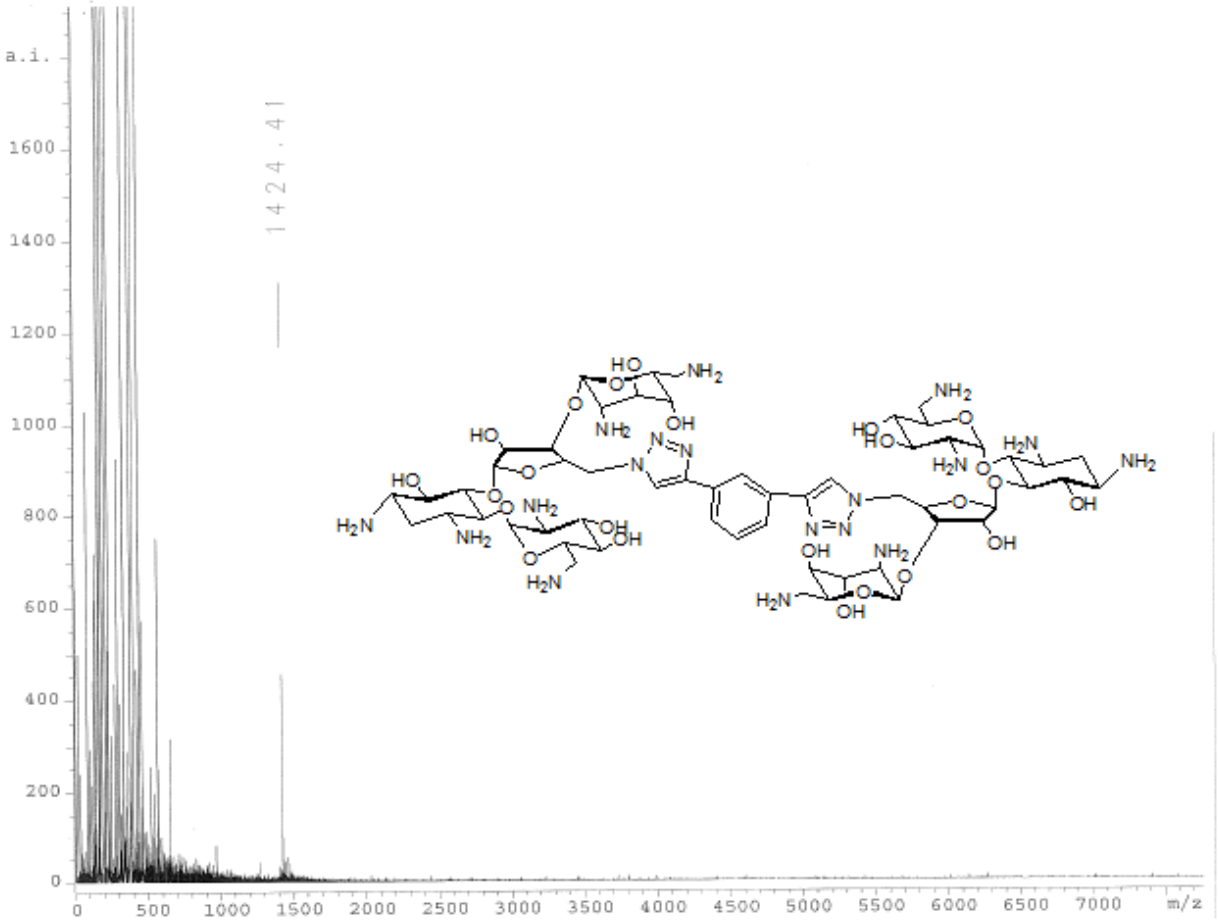

Figure S2.49. MALDI-TOF of DPA65.

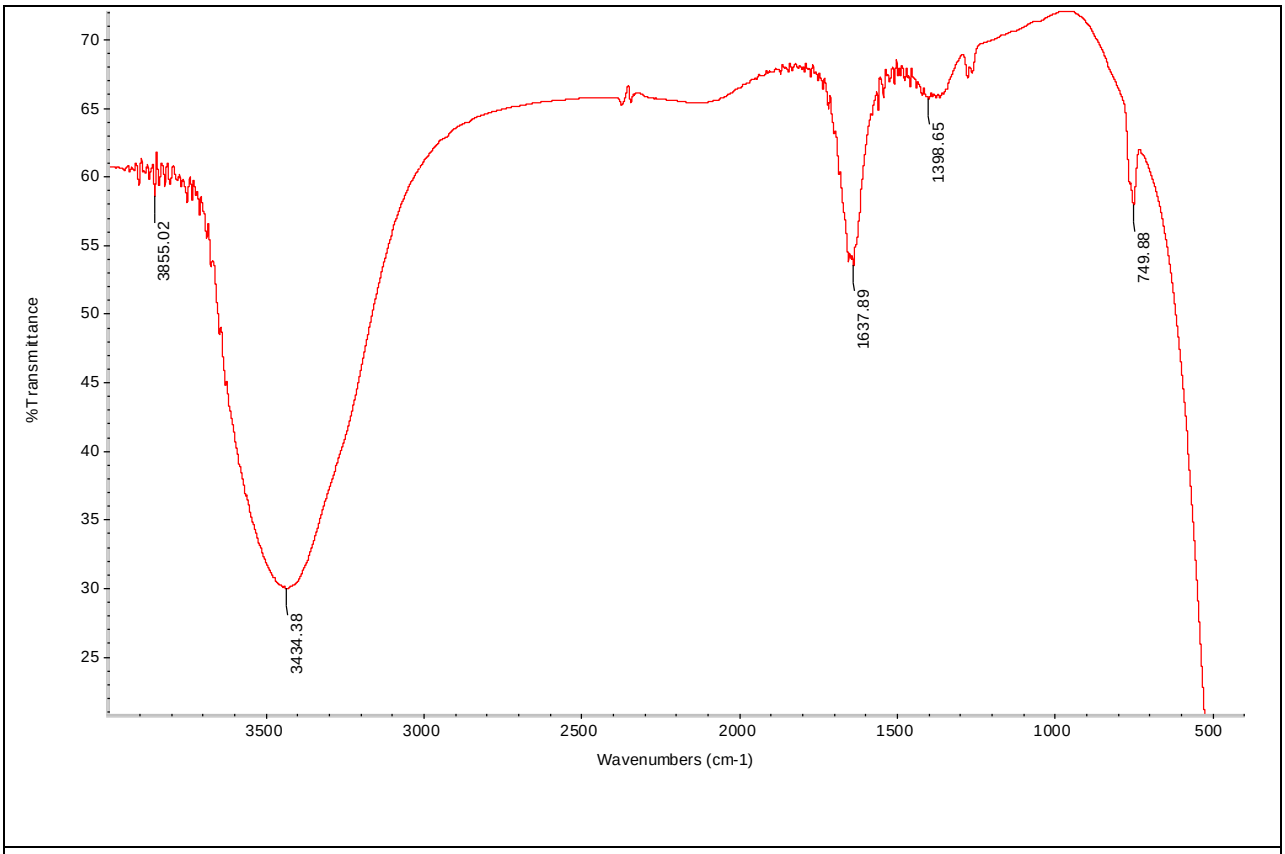

Figure S2.50. IR of DPA65.

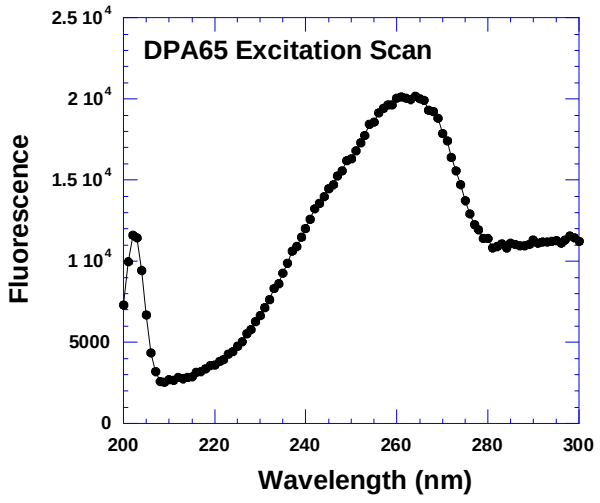

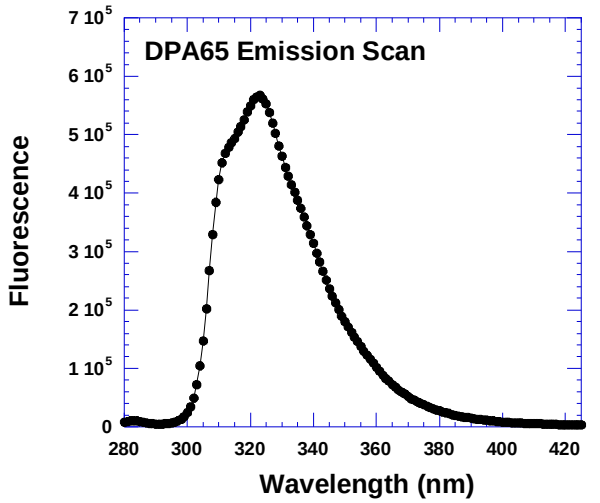

Figure S2.51. Fluorescence excitation scan of DPA 65 (left) and fluorescence emission scan of DPA 65 excited at 284nm (right). All scans were taken in water and the concentration of DPA 65 was 25 µM in all the scans. Excitation scan was performed first and wavelength with the highest fluorescence (260nm) was then used for the emission scan. DPA 65 excitation wavelength is now defined at 260nm, the emission maximum wavelength is defined at 235nm.

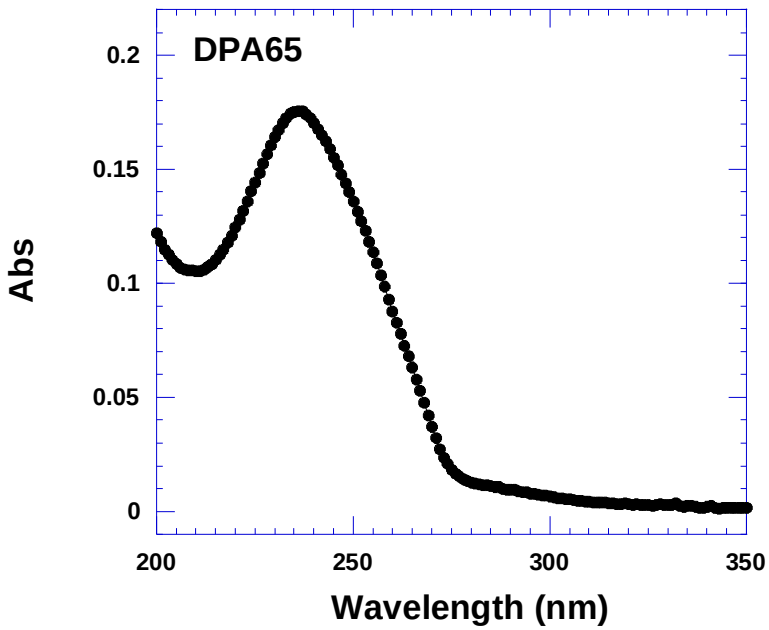

Figure S2.52. UV absorbance scan of DPA 65. Scan was taken in water and the concentration of DPA 65 was 25 µM. T = 25 °C.

N-Boc DPA51.

[R_f 0.38 in 10% EtOH in DCM (v/v)]; ^{1}H NMR (500 MHz, CD_3COCD_3) δ 8.28 (s, 2 H, triazole), 6.55 (s, 2 H), 6.43 (s, 2 H, NH_{6IV}), 5.95-6.25 (m, 12 H, $NH_{6II,}$ NH_{1I}, NH_{3I}, NH_{2IV}, and NH_{2II}), 5.20-5.18 (d, *J* = 8.36 Hz, 4 H), 5.03 (s, 2H), 5.00-.80 (m, 10 H), 4.75-4.65 (m, 8 H), 4.43-4.55 (br, 4 H), 4.40-4.30 (m, 4 H), 4.27 (br, 6 H), 4.06 (s, 4 H), 3.93 (m, 2 H), 3.90-3.82 (m, 6 H), 3.80-3.55 (m, 20 H), 3.53-3.37 (m, 8 H), 3.35-3.15 (m, 8 H), 1.85-1.35 (m, 110 H, 6 × boc, H_{2Ieq}); MS (MALDI-TOF) calcd. for $C_{112}H_{192}N_{18}O_{49}$,2595.80, found 2595.15 [$(M+Na^+)$].

N-Boc DPA52.

[R_f 0.42 in 10% EtOH in DCM (v/v)] ^{1}H NMR (500 MHz, CD_3COCD_3) δ 8.26 (s, 2 H, triazole), 6.56 (s, 2 H), 6.42 (s, 2 H, NH_{6IV}),6.28- 5.97 (m, 12 H, $NH_{6II,}$ NH_{1I}, NH_{3I}, NH_{2IV}, and NH_{2II}), 5.30-5.18 (d, *J* = 7.41 Hz, 4 H), 5.07-4.99 (m, 4H), 4.98-4.94 (s, 2 H), 4.90-4.77 (m, 8 H), 4.77-4.65 (m, 8 H), 4.57-4.44 (m, 4 H), 4.42-4.32 (m, 8 H), 4.31-4.16 (m, 16 H), 4.06 (s, 4 H), 3.96-3.90 (t, *J* = 6.30 Hz, 2H), 3.90-3.80 (m, 6 H),3.78- 3.64-3 (m, 18 H),3.53- 3.37 (m, 8 H), 3.37-3.15 (m, 10 H), 2.37-2.27 (m, 2 H, H_{2Ieq}), 1.52-1.23 (m, 110 H, H_{2Iax}, 12 × Boc); MS (MALDI-TOF) *m/z* calcd. for $C_{113}H_{194}N_{18}O_{48}$ 2598.80, found: 2599.27$(M+2H+Na^+)$.

N-Boc DPA53.

[R_f 0.40 in 10% EtOH in DCM (v/v)]; IR (neat, cm^{-1}) 2980, 2930, 2880, 2910, 1720, 1608, 1480; ^{1}H NMR (500 MHz, CD_3COCD_3) δ 8.69 (s, 2 H, triazole), 8.14-8.04 (s, 4 H, Aromatic ring protons), 6.50 (s, 2 H), 6.28 (s, 2 H, NH_{6IV}), 6.23-5.97- (m, 12 H, $NH_{6II,}$ NH_{1I}, NH_{3I}, NH_{2IV}, and NH_{2II}), 5.26-5.41 (m, 4 H), 5.11-5.03 (m, 4H), 5.03-4.95 (d, *J* = 12.45 Hz, 2 H), 4.93-4.74 (m, 6 H), 4.65 (s, 2 H),4.59- 4.44 (m, 8 H),4.27- 4.19 (m, 2 H), 4.05 (s, 2 H),4.04- 3.95 (t, *J* = 6.31 Hz,

2 H), 3.95-3.85 (m, 4H),3.83- 3.75 (m, 4 H),3.72- 3.58 (m, 10 H), 3.58-3.49 (m, 4 H), 3.49-3.41 (m, 2 H), 3.41-3.29 (m, 4 H), 3.27-3.15 (br, 2 H),2.88 (t, J = 6.94 Hz, 2 H), 1.50-1.25-1.50 (m, 110 H, H_{2Iax}, 12 × Boc); MS(MALDI-TOF), *m/z* calcd. for $C_{116}H_{192}N_{18}O_{48}$ 2629.86, found 2662.29 ($M+Na^+$),.

N-Boc DPA54.

[R_f 0.42 in 10% EtOH in DCM (v/v)], ^{1}H NMR (500 MHz, CD_3COCD_3) δ 8.26 (s, 2 H, triazole), 6.53 (s, 2 H), 6.41 (s, 2 H, NH_{6IV}), 6.27-5.92 (m, 12 H, $NH_{6II,}$ NH_{1I}, NH_{3I}, NH_{2IV}, and NH_{2II}), 5.30-5.16 (m, 4 H), 5.05-4.87 (m, 8 H), 4.87-4.62 (m, 10 H), 4.57-4.41 (br, 4 H), 4.41-4.24 (m, 8 H), 4.24-4.15 (m, 2 H), 4.09-4.00 (s, 4 H), 3.97-3.90 (m, 2 H), 3.90-3.79 (m, 6 H), 3.79-3.54 (m, 16 H), 3.54-3.36 (m, 8 H), 3.37-3.10 (m, 8 H), 1.52-1.35 (m, 110 H, H_{2Iax}, 6 × Boc); MS (MALDI-TOF) *m/z* calcd. for $C_{114}H_{196}N_{18}O_{48}$ (M^+), 2586.87 found 2586.06.

N-Boc DPA55.

[R_f 0.44 in 10% EtOH in DCM (v/v)]; ^{1}H NMR (500 MHz, CD_3COCD_3) δ 8.02 (s, 2 H, triazole), 6.50-6.64 (br, s, 2 H), 6.39-6.23 (br, s, 2 H, NH_{6IV}), 6.23-5.90 (m, 10 H, NH_{1I}, NH_{6II}, NH_{3I}, NH_{2IV}, and NH_{2II}), 5.35-5.20 (m, 4 H), 5.12-5.03 (m, 2 H), 5.03-4.80 (m, 8 H), 4.79-4.70 (m, 2 H), 4.49 (s, 2 H), 4.40-4.21 (m, 8 H), 4.20-4.14 (m, 2 H), 4.06 (s, 2 H), 3.93 (t, J = 7.10 Hz, 2 H), 3.90-3.80 (m, 6 H), 3.77-3.54 (m, 16 H), 3.55-3.39 (m, 8 H), 3.38-3.13 (m, 6 H), 2.93 (m, 2 H), 2.38-2.26 (m, 2 H, H_{2Ieq}), 2.23-2.14 (m, 2 H), 1.96-1.93 (m, 2 H, linker protons), 1.68-1.20 (m, 110 H, 6 × Boc and linker protons, H_{2Iax}); MS MALDI-TOF m/z for $C_{118}H_{202}N_{18}O_{48}$ $[M+H_2O]^+$, calcd 2663.94, found 2664.66.

N-Boc DPA56.

[R_f 0.44 in 10% EtOH in DCM (v/v)], ^{1}H NMR (500 MHz, CD_3COCD_3): δ 7.97 (s, 2 H, triazole), 6.60 (t, *J* = 2.0 Hz, 2 H), 6.30 (s, 2 H, NH_{6IV}), 6.23-6.10 (m, 4 H, NH_{1I} and NH_{6II}), 6.10-5.90 (m, 6 H, NH_{3I}, NH_{2IV}, and NH_{2II}), 5.29-5.19 (m, 4 H), 5.07 (d, *J* = 2.68 Hz, 2 H), 4.92 (s, 2 H), 4.90-4.80 (m, 4 H), 4.78-4.67 (m, 2 H), 4.58-4.50 (br, s, 2 H), 4.40-4.15 (m, 8 H), 4.05 (s, 2 H), 3.92 (t, *J* = 5.99 Hz, 2 H), 3.89-3.78 (m, 4 H), 3.76-3.65 (m, 8H), 3.65-3.55 (m, 8 H), 3.55-3.38 (m, 6 H), 3.37-3.25 (m, 4 H), 3.24-3.15 (m, 2 H), 2.78-2.66 (m, 4 H), 2.37-2.27 (m, 2 H, H_{2Ieq}), 1.80-1.67 (m, 4 H, H_{2Iax} and linker protons), 1.50-1.30 (m, 112 H, 6 × Boc and linker protons); MS (MALDI-TOF) *m/z* calcd. for $C_{116}H_{200}N_{18}O_{48}$ $[M+H_2O]^+$ 2632.94, found 2631.66.

N-Boc DPA58.

[R_f 0.42 in 10% EtOH in DCM (v/v)], ^{1}H NMR (500 MHz, CD_3COCD_3) δ 7.93 (s, 2 H, triazole), 6.50 (m, 2 H), 6.28 (s, 2 H, NH_{6IV}), 6.23-5.95 (m, 10 H, NH_{1I}, NH_{6II}, NH_{3I}, NH_{2IV}, and NH_{2II}), 5.42-5.27 (m, 4 H), 5.13-5.03 (s, 4 H), 4.98 (d, *J* = 12.45 Hz, 2 H), 4.92-4.73 (m, 6 H), 4.78-4.67 (m, 2 H), 4.65 (br, s, 2 H), 4.59-4.42 (m, 8 H), 4.33 (s, 2 H), 4.27-4.19 (m, 2 H), 4.05 (m, 2 H), (t, *J* = 6.13 Hz, 2 H), 3.95-3.85 (m, 4 H), 3.83-3.75 (m, 4 H), 3.73-3.58 (m, 12 H), 3.57-3.49 (m, 4 H), 3.49-3.41 (m, 4 H), 3.41-3.29 (m, 4 H), 3.28-3.14 (br, s, 2 H), 2.92-2.85 (m, 2 H), 1.69-1.03 (m, 122 H, $H_{2Iax,}$ linker protons, 12 × Boc); MS (MALDI-TOF) *m/z* calcd.for $C_{120}H_{208}N_{18}O_{50}$ $[M+Na]^+$2727.03, found 2727.81.

N-Boc DPA60.

[R_f 0.44 in 10% EtOH in DCM (v/v)]; ^{1}H NMR (500 MHz, CD_3COCD_3) δ 7.91 (s, 2 H, triazole), 6.57-6.47 (t, *J* = 5.83 Hz, 2 H), 6.33-6.22 (s, 2 H, NH_{6IV}), 6.18-5.98 (m, 10 H, NH_{1I}, NH_{6II},

NH_{3I}, NH_{2IV}, and NH_{2II}), 5.30-5.19 (m, 4 H), 5.03-4.93 (m, 4 H), 4.94-4.87 (m, 2 H), 4.84-4.74 (m, 4 H), 4.74-4.66 (m, 4 H), 4.47-4.41 (br, s, 2 H), 4.38-4.32 (m, 4 H), 4.32-4.25 (m, 10 H), 4.22-4.17 (m, 2 H), 4.16-4.08 (m, 2 H), 4.08-4.02 (m, 4 H), 3.95-3.88 (t, *J* = 6.78 Hz, 2 H), 3.88-3.80 (m, 6 H), 3.74-3.53 (m, 20 H), 3.53-3.45 (m, 6 H), 3.44-3.36 (m, 2 H), 3.32-3.16 (m, 8 H), 3.05 (s, 2 H), 2.87 (s, 2 H), 1.58-1.32 (m, 126 H, H_{2Iax}, 6 × Boc, linker protons); MS (MALDI-TOF) *m/z* calcd.for $C_{124}H_{216}N_{18}O_{50}$ $[M+2Na]^+$, calcd 2805.49, found 2806.91.

N-Boc DPA65.

IR (KBr, cm^{-1}) 2910-2980 (br), 2870, 2910, 1719, 1610, 1470; [R_f 0.42 in 10% EtOH in DCM (v/v)]; ^1H NMR (500 MHz, CD_3COCD_3) δ 8.68 (s, 2 H, triazole), 8.18 (s, 1 H, Ar), 8.063 (d, *J* = 6.93 Hz, 2 H, Ar), 7.47 (s, 1 H, Ar), 6.39 (t, *J* = 5.67 Hz, 2 H, NH_{6IV}), 6.30-5.86 (m, 10 H, NH_{3I}, NH_{2IV}, NH_{2II}, NH_{1I} and NH_{6II}), 5.29 (m, 2 H), 5.27 (m, 2 H), 5.23 (m, 2 H), 5.07-4.96 (m, 6 H), 4.87-4.75 (m, 4 H), 4.51-4.29 (m, 12 H), 4.29-4.18 (m, 6 H), 4.17-4.09 (m, 2 H), 4.05 (br, 4 H), 3.99-3.90 (m, 4H), 3.89-3.77 (m, 8 H), 3.73-3.51 (m, 18 H), 3.51-3.40 (m, 10 H), 3.38-3.13 (m, 10 H), 2.23-2.13 (m, 2 H, H_{2Ieq}), 1.55-1.25 (m, 110 H, H_{2Iax}, 12 × Boc); MS (MALDI-TOF) *m/z* calcd.. for $C_{116}H_{192}N_{18}O_{48}$, 2629.86, found 2628.46 [$(M+Na^+)$].

3. UV-thermal denaturation profiles (S3).

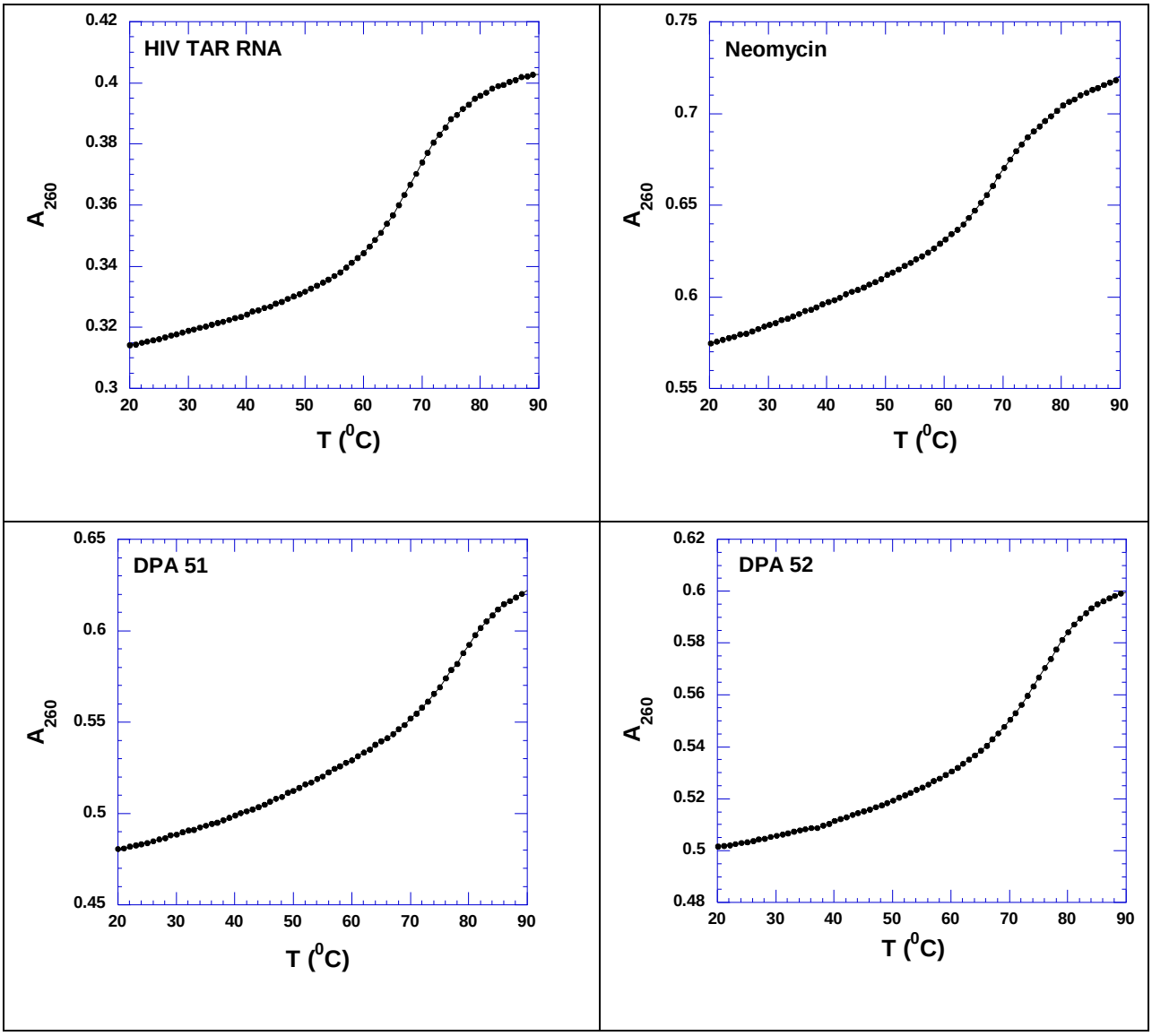

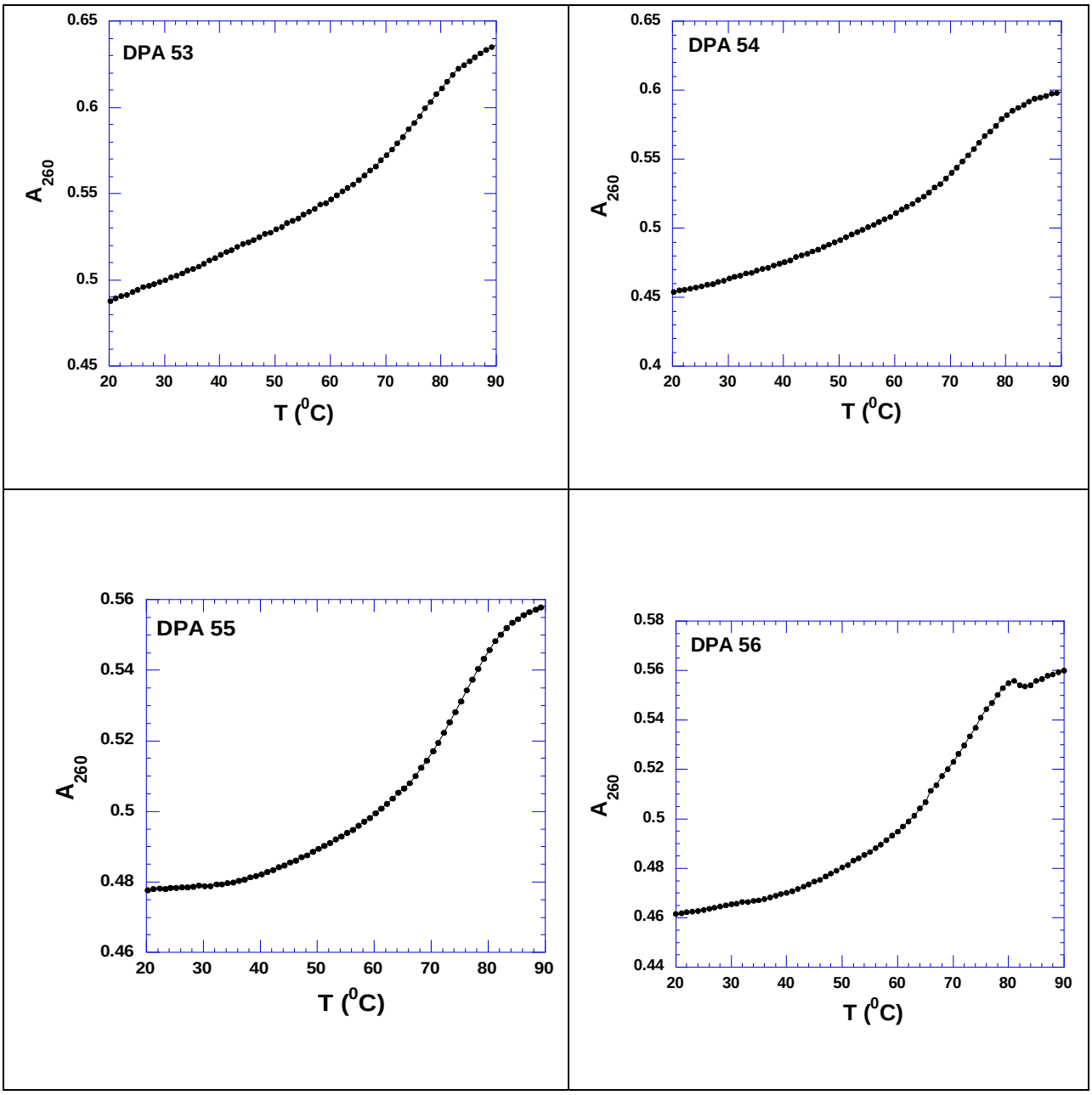
DPA 53
A260
T (0C)
DPA 54
A260
T (0C)
DPA 55
A260
T (0C)
DPA 56
A260
T (0C)

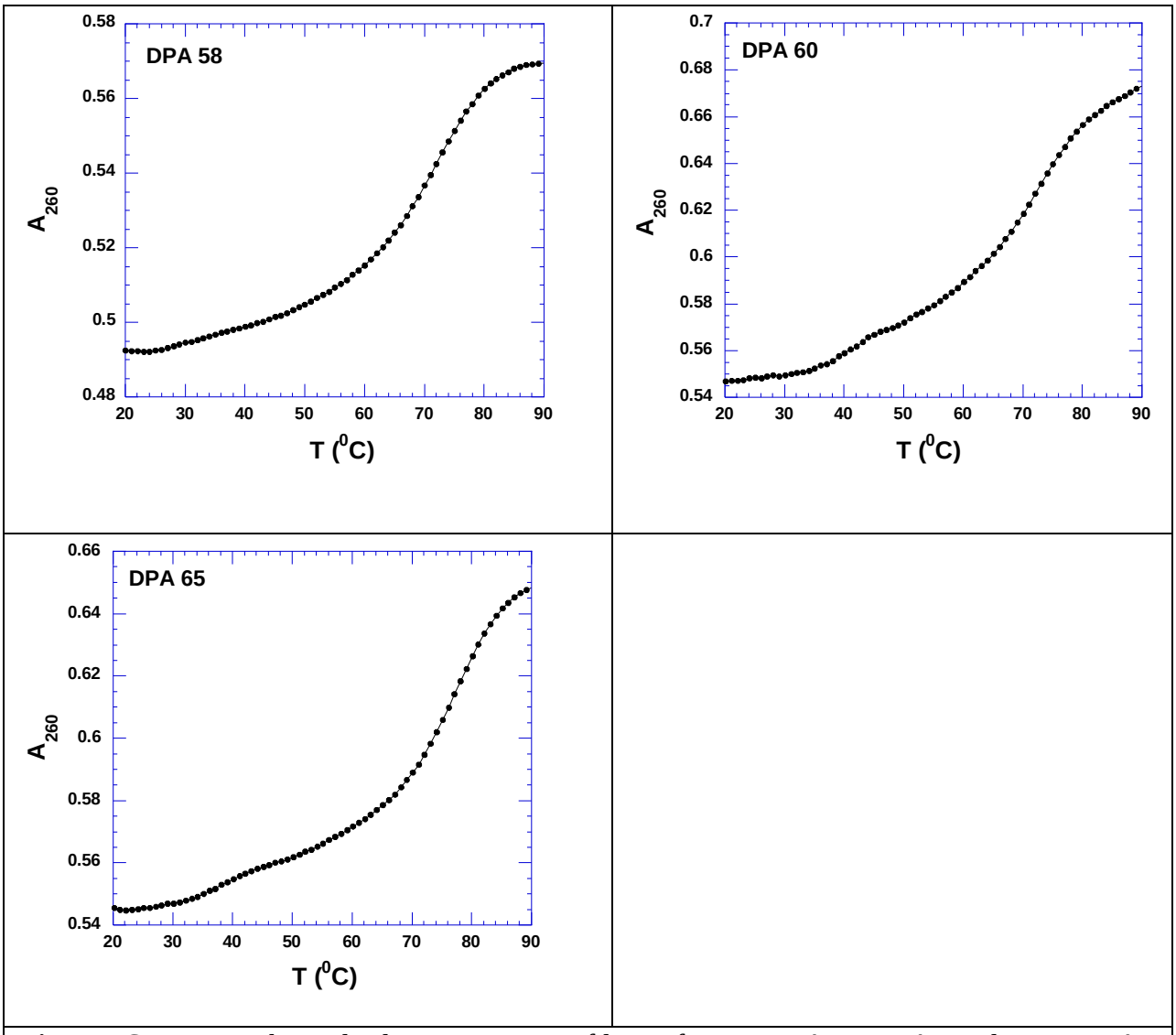

Figure S3.1. UV-thermal denaturation profiles of HIV TAR RNA and HIV TAR RNA/neomycin dimer complexes. Sample of HIV TAR RNA (1 µM/molecule) was mixed with ligand (neomycin dimer) with r_{dr} value of 1 (r_{dr} = ratio of drug to RNA concentration). Buffer conditions: 100 mM KCl, 10 mM SC, 0.5 mM EDTA, pH 6.8. Heating rate was 0.3 $^{\circ}$C/ min.

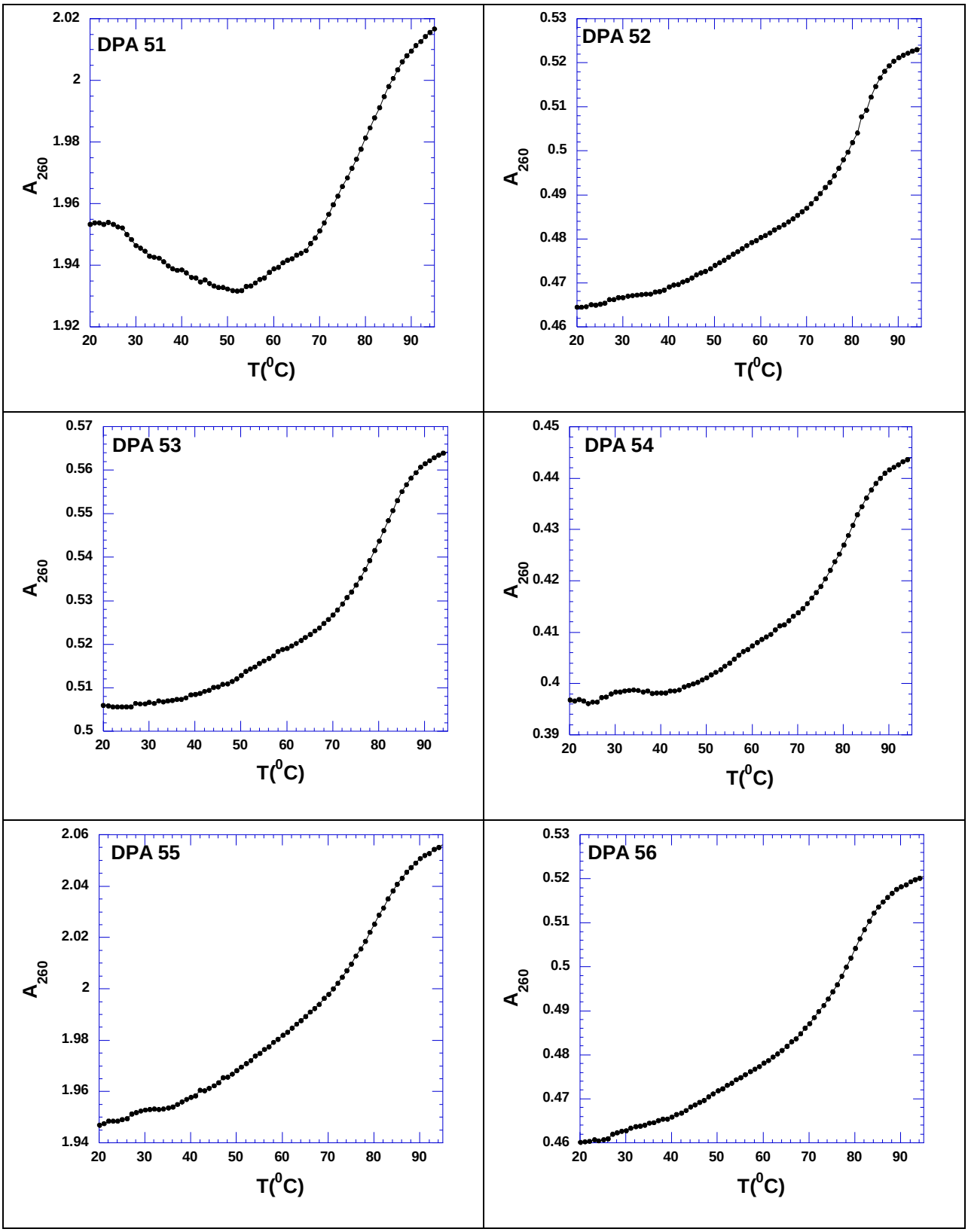
DPA 51
DPA 52
DPA 53
DPA 54
DPA 55
DPA 56
A260
T(0C)

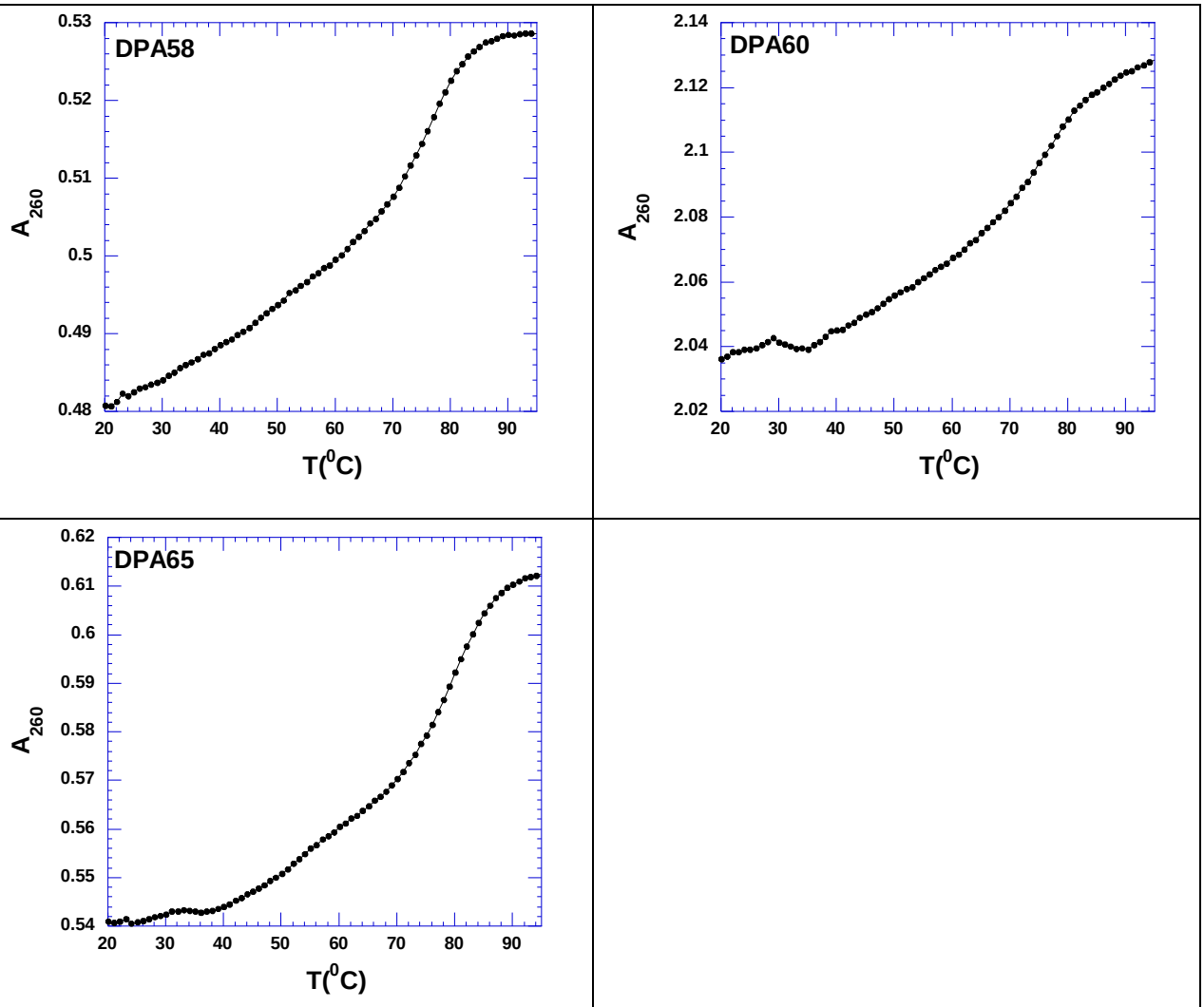

Figure S3.2. UV-thermal denaturation profiles of HIV TAR RNA and HIV TAR RNA/neomycin dimer complexes. Sample of HIV TAR RNA (1 µM/molecule) was mixed with ligand (neomycin dimer) with r_{dr} value of 2 (r_{dr} = ratio of drug to RNA concentration). Buffer conditions: 100 mM KCl, 10 mM SC, 0.5 mM EDTA, pH 6.8. Heating rate was 0.3 °C/ min.

4. Ethidium bromide displacement titrations (S4).

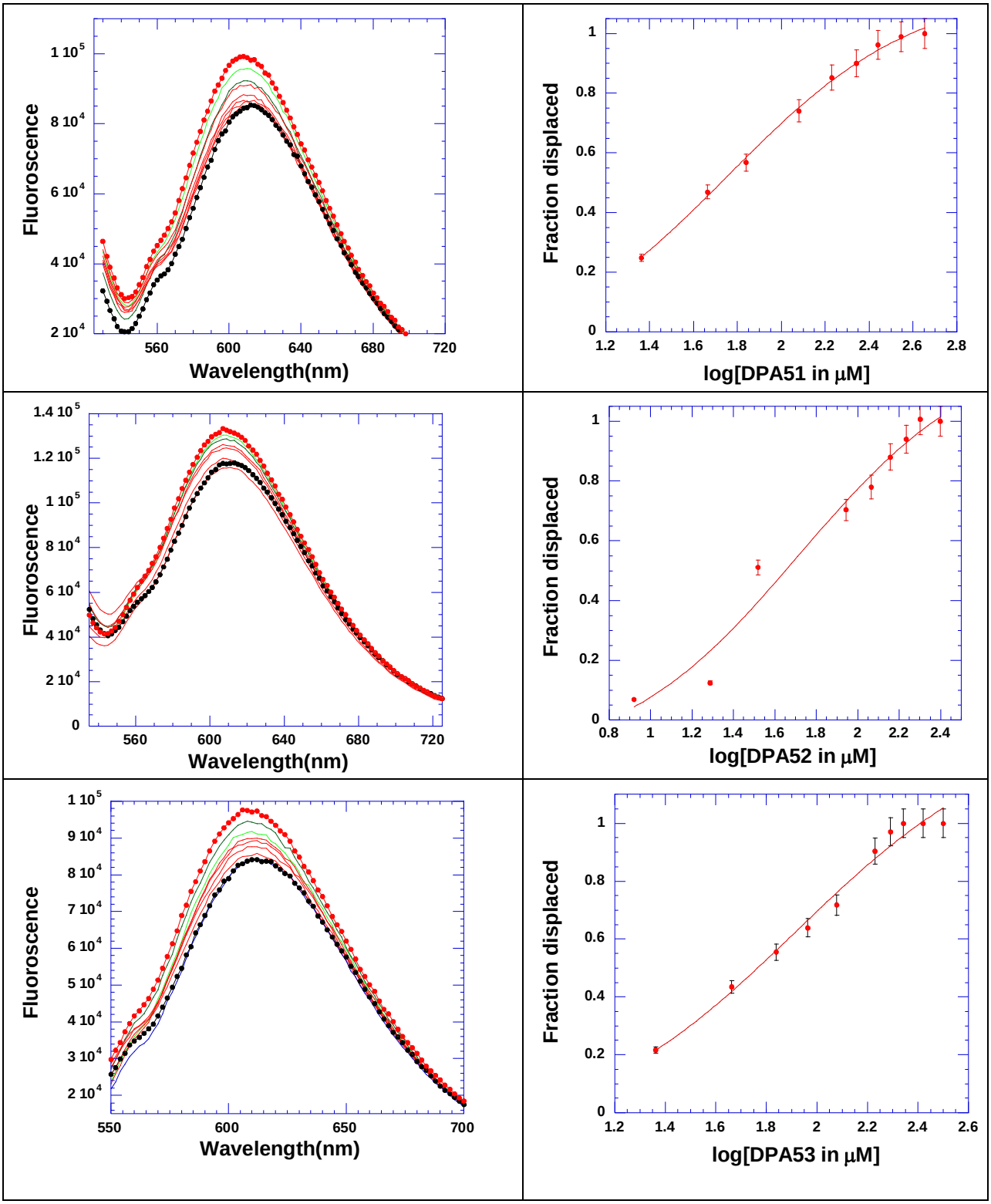

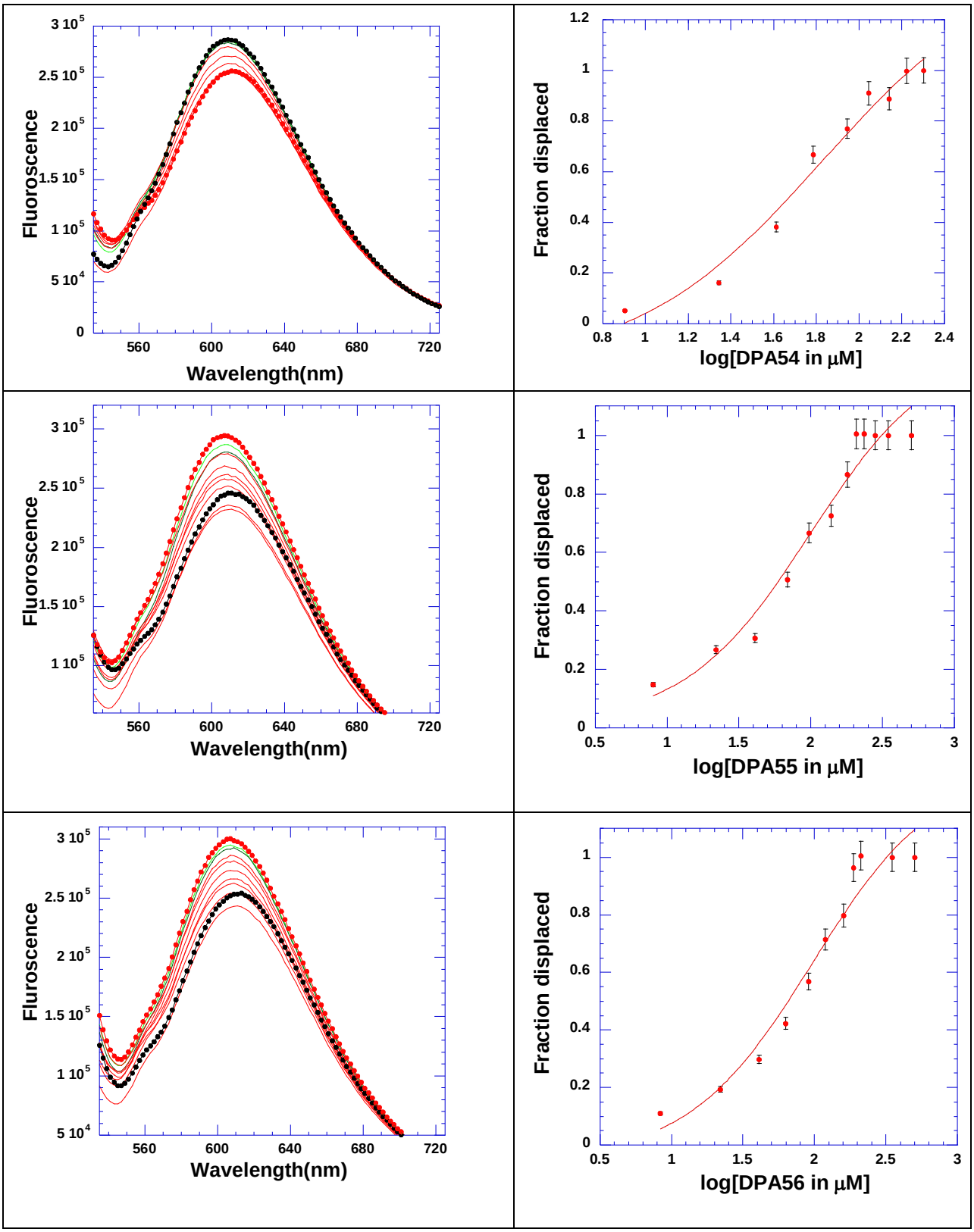
Fluoroscence
Wavelength(nm)
Fraction displaced
log[DPA54 in μM]
Fluoroscence
Wavelength(nm)
Fraction displaced
log[DPA55 in μM]
Fluroscence
Wavelength(nm)
Fraction displaced
log[DPA56 in μM]

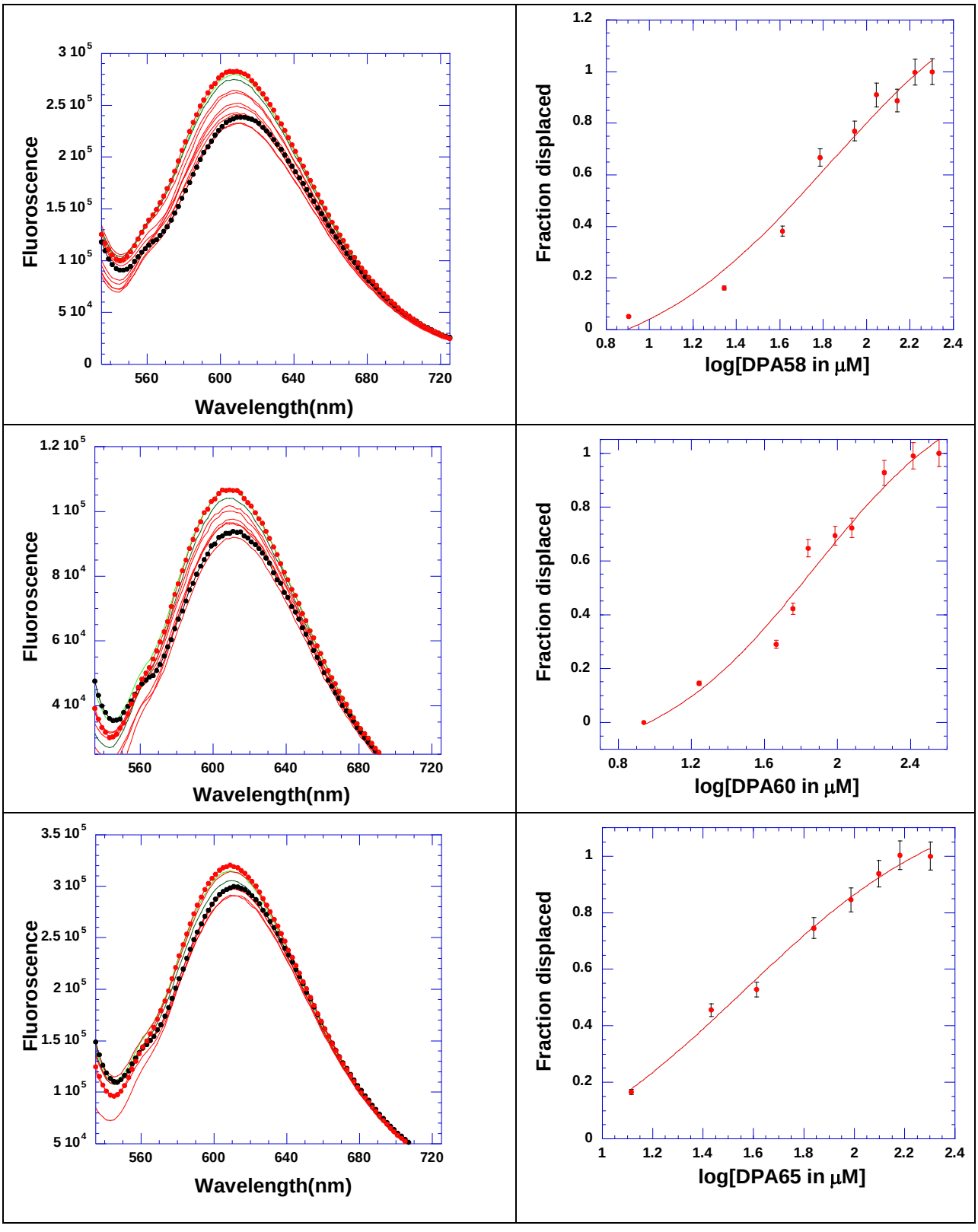
Fluoroscence
Wavelength(nm)
Fraction displaced
log[DPA58 in μM]
Fluoroscence
Wavelength(nm)
Fraction displaced
log[DPA60 in μM]
Fluoroscence
Wavelength(nm)
Fraction displaced
log[DPA65 in μM]

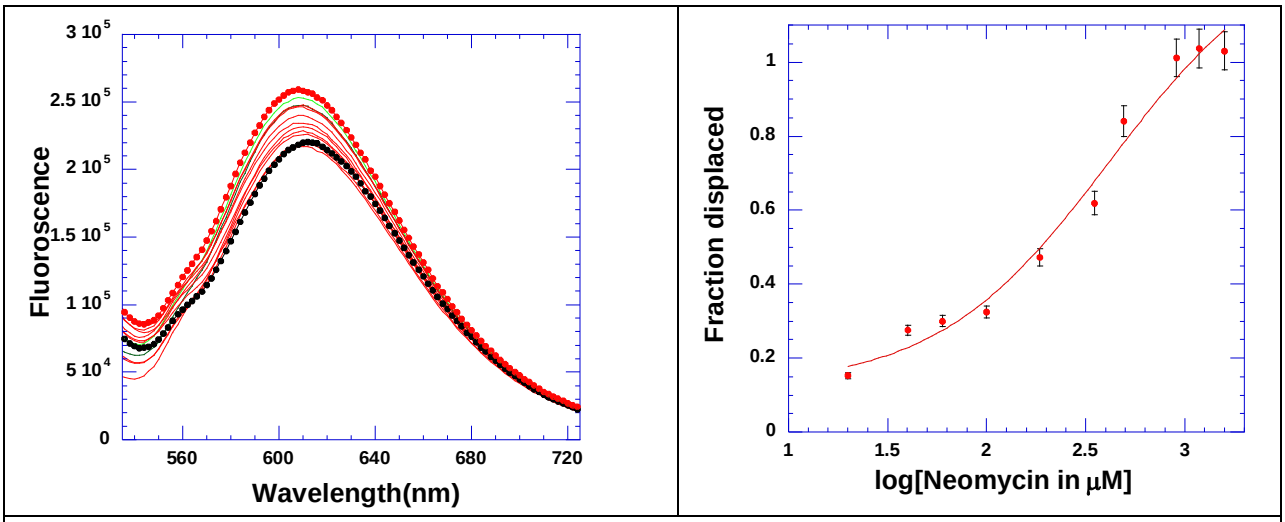

Figure S4.1. Ethidium bromide displacement titrations between HIV TAR RNA and ligands. (Left) The raw fluorescence scans of ethidium bromide displacement titrations. (Right) The plot between fractions of ethidium bromide displaced from TAR RNA as a function of conc. of ligand results in a S-shaped curve. The curve was fit by sigmoidal fit using non-linear regression which helps in determining the AC_{50} value (the concentration of ligand required to displace 50% of ethidium bromide from HIV TAR RNA). Buffer conditions: 100 mM KCl, 10 mM SC, 0.5 mM EDTA (pH 6.8).

5. FRET mediated competition binding assay (S5).

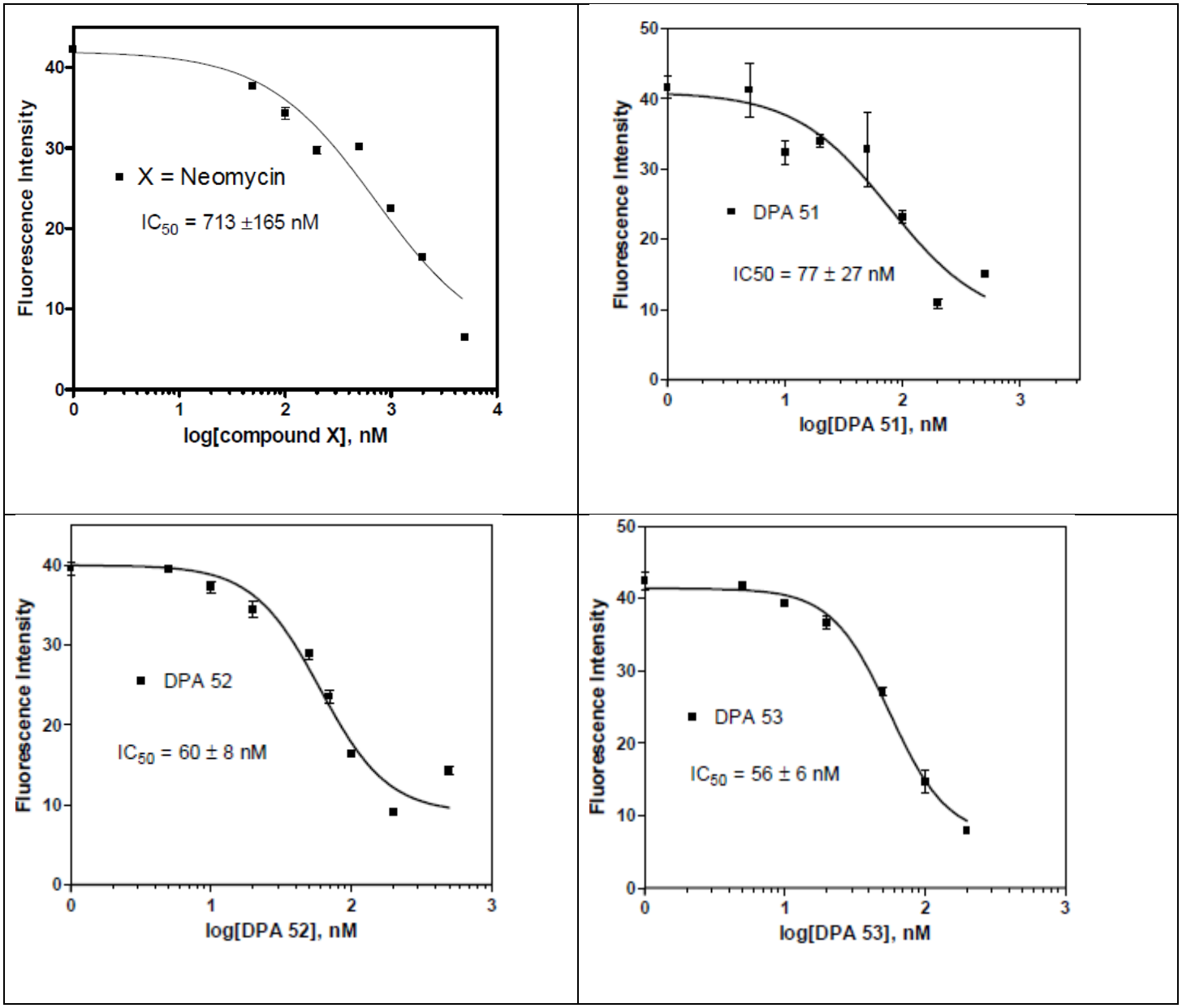

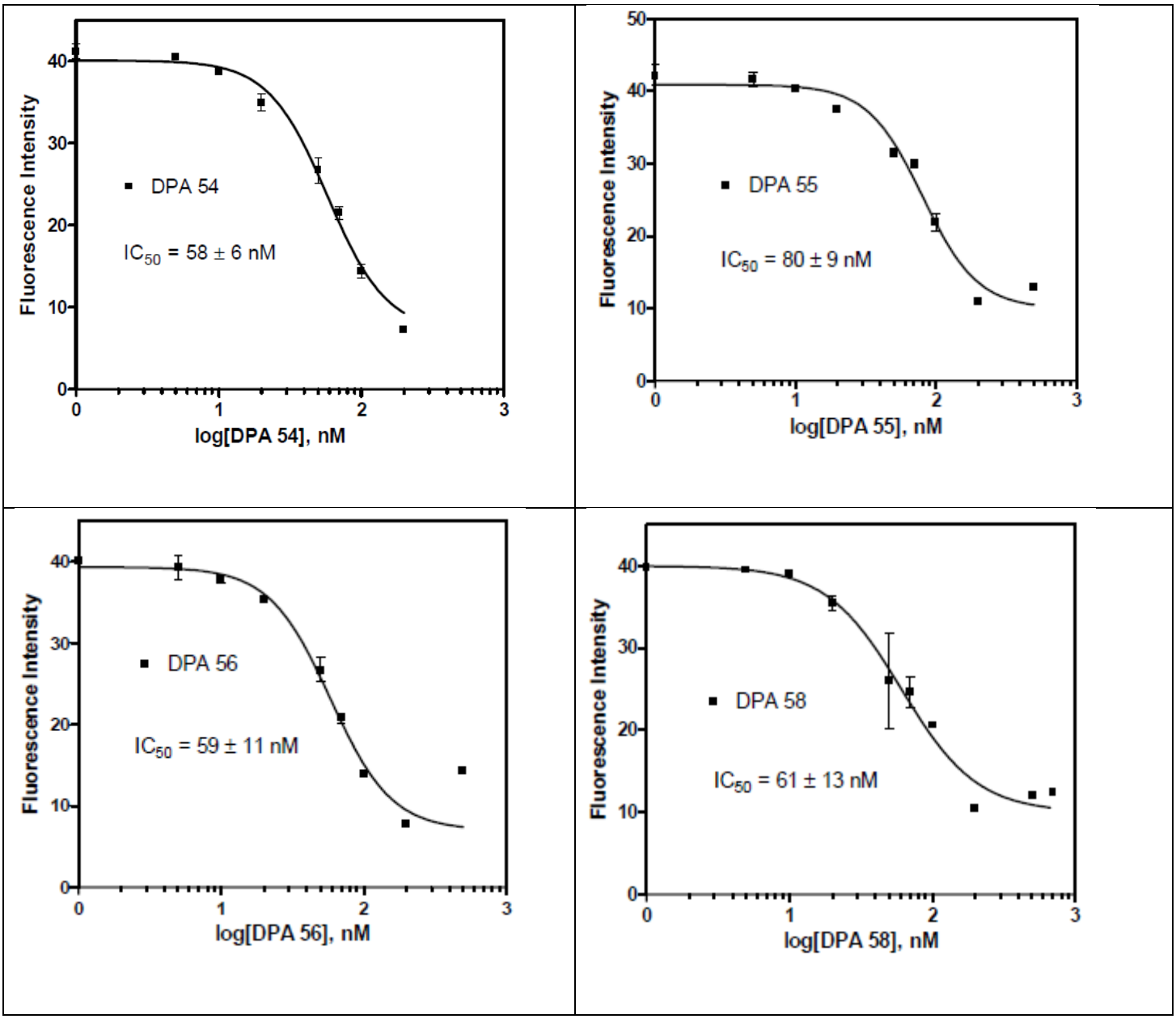
Fluorescence Intensity
DPA 54
IC50 = 58 ± 6 nM
log[DPA 54], nM
Fluorescence Intensity
DPA 55
IC50 = 80 ± 9 nM
log[DPA 55], nM
Fluorescence Intensity
DPA 56
IC50 = 59 ± 11 nM
log[DPA 56], nM
Fluorescence Intensity
DPA 58
IC50 = 61 ± 13 nM
log[DPA 58], nM

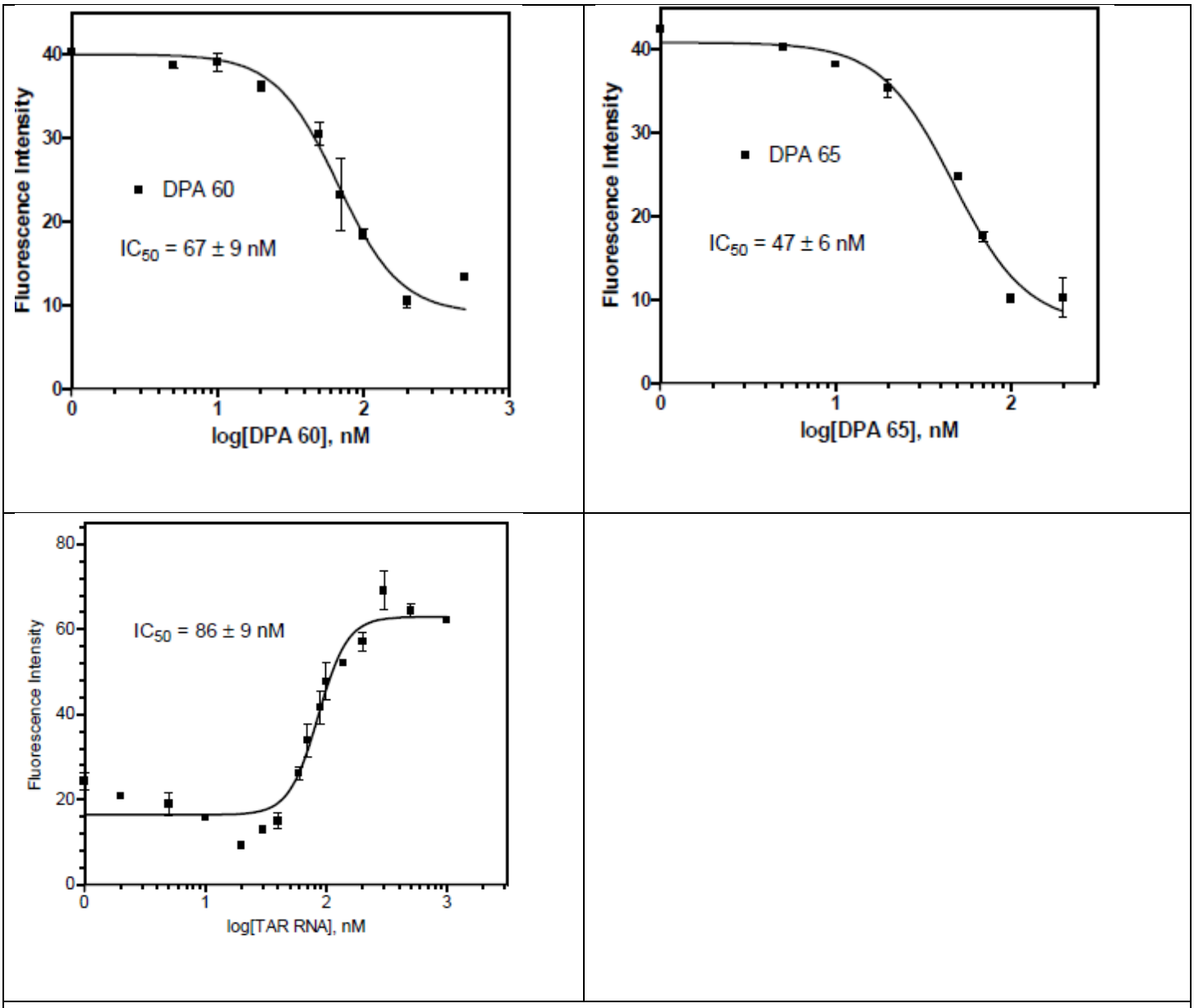

Figure S5.1. The FRET mediated competition binding assay between neomycin dimers and HIV TAR RNA. The plots showing decrease in fluorescence intensity as a function of concentration of neomycin dimers. The plots were fit using sigmoidal fit which result in a s-shaped binding isotherm and helps in determining the IC_{50} (the concentration of neomycin dimers or neomycin required to displace 50% fluorescein labeled TAT peptide). Buffer conditions: 50 mM Tris, 20 mM KCl, pH = 7.4. [HIV-1 TAR RNA] = 100 nM/strand , [fluorescein-labeled Tat peptide] = 100 nm. T = 25 °C.

6. Ethidium bromide displacement titration to determine the binding constants (S6).

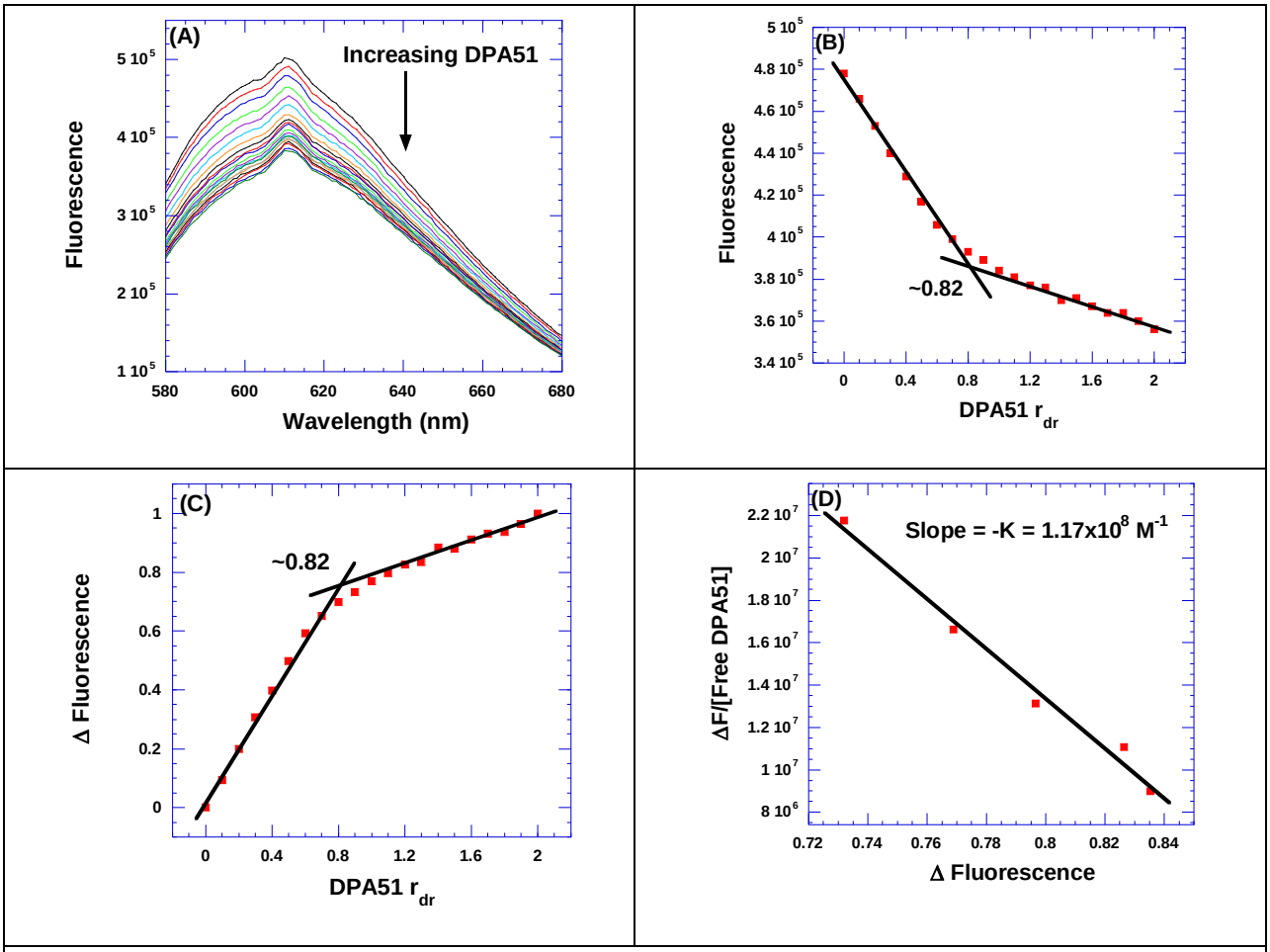

Figure S6.1. FID titration of DPA51 with HIV TAR RNA. (A) Raw fluorescence emission spectra in the presence of increasing concentration of DPA51. (B) The decrease of fluorescence intensity (at 605 nm) of HIV TAR RNA/EtBr complex with increasing concentration of DPA51 results in a saturating binding plot. (C) The plot between normalized fluorescence intensity (at 605 nm) of HIV TAR RNA-EtBr complex as a function of concentration of DPA51 results in a saturating binding plot. (D) The Scatchard plot analysis of DPA51 with HIV TAR RNA. Buffer conditions: 100 mM KCl, 10 mM SC, 0.5 mM EDTA, pH 6.8. HIV TAR RNA = 200 nM/strand. [EtBr] = 5 μM.

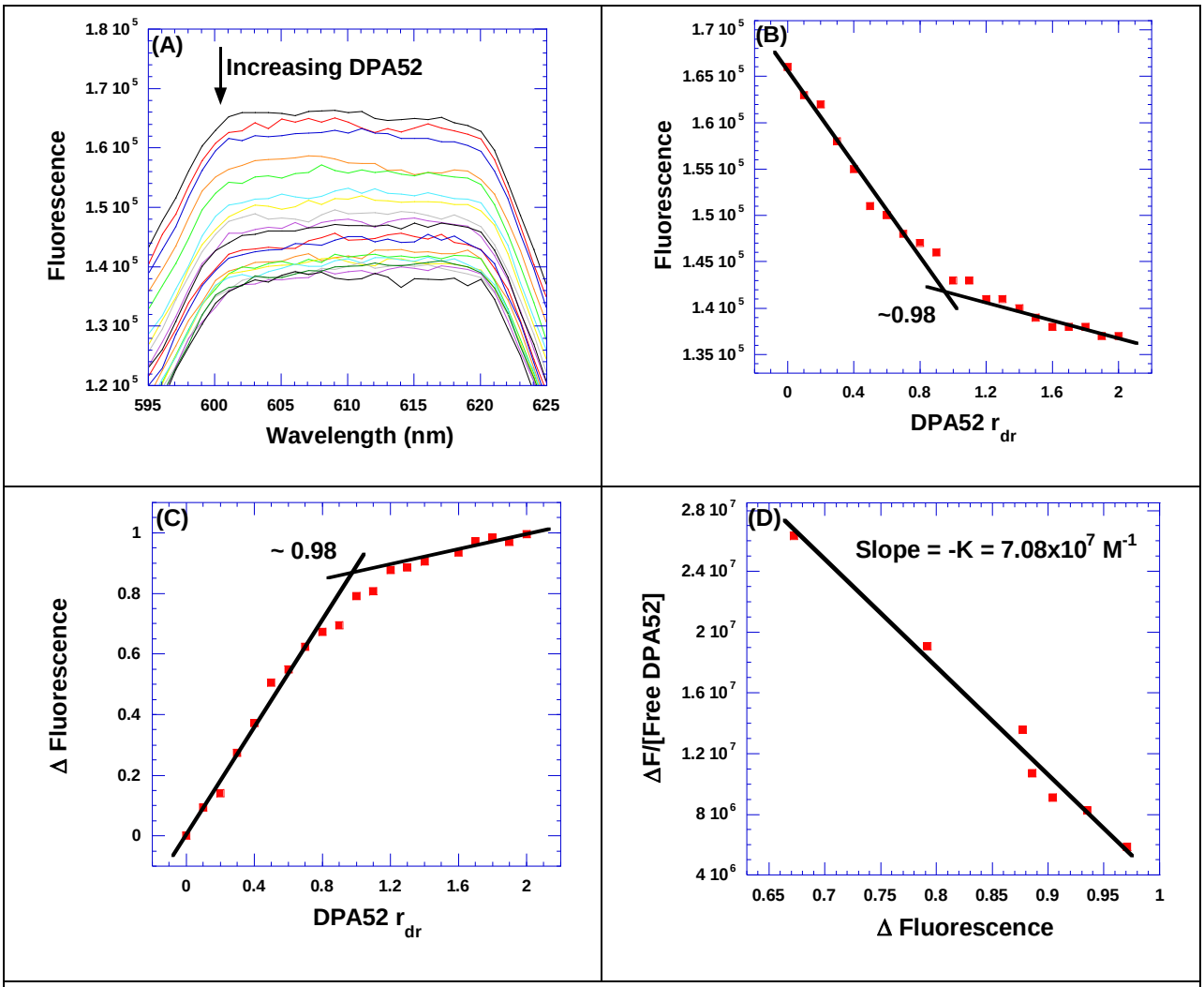

Figure S6.2. FID titration of DPA52 with HIV TAR RNA. (A) Raw fluorescence emission spectra in the presence of increasing concentration of DPA52. (B) The decrease of fluorescence intensity (at 604 nm) of HIV TAR RNA/EtBr complex with increasing concentration of DPA52 results in a saturating binding plot. (C) The plot between normalized fluorescence intensity (at 604 nm) of HIV TAR RNA-EtBr complex as a function of concentration of DPA52 results in a saturating binding plot. (D) The Scatchard plot analysis of DPA52 with HIV TAR RNA. Buffer conditions: 100 mM KCl, 10 mM SC, 0.5 mM EDTA, pH 6.8. HIV TAR RNA = 200 nM/strand. [EtBr] = 5 μM.

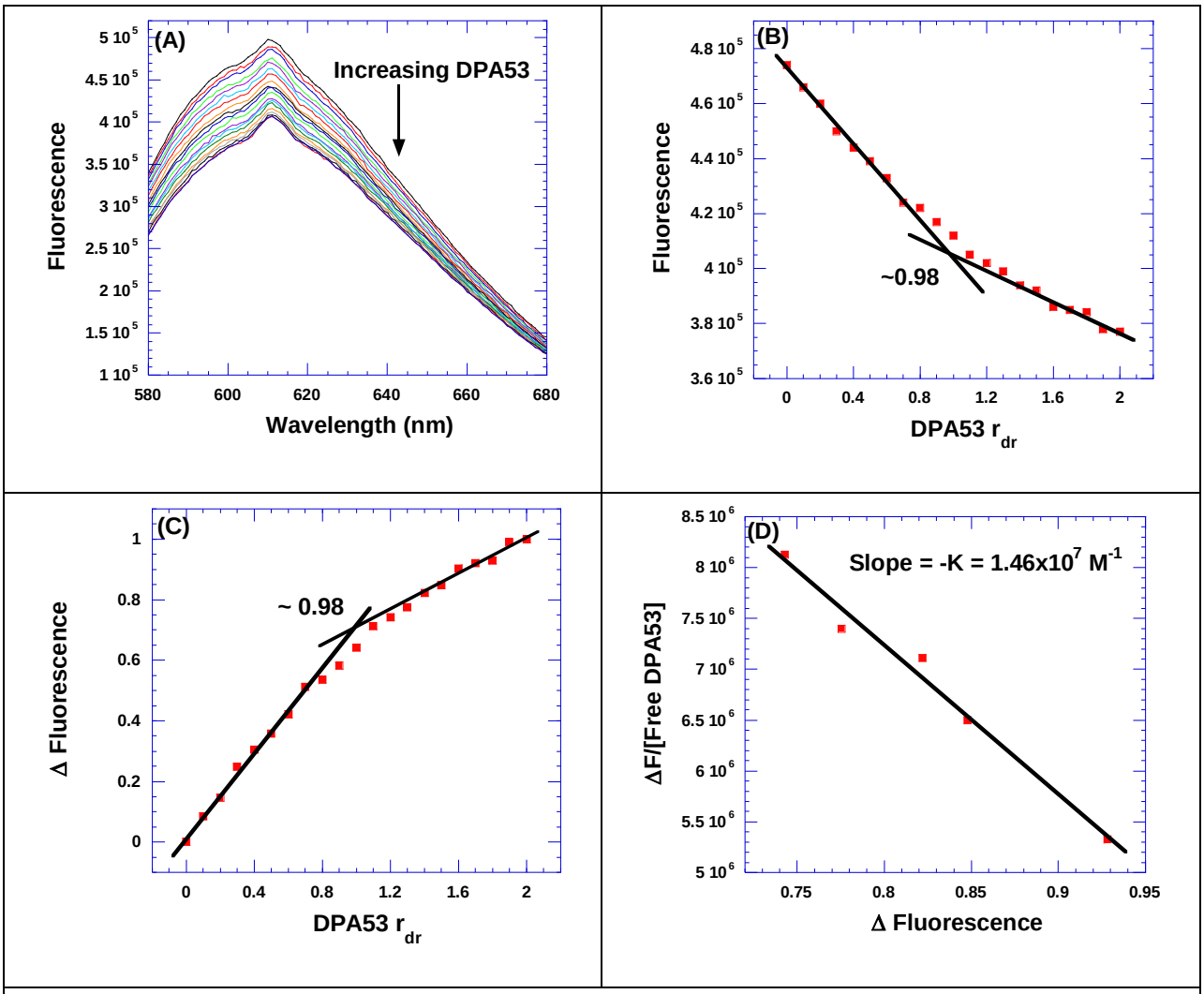

Figure S6.3. FID titration of DPA53 with HIV TAR RNA. (A) Raw fluorescence emission spectra in the presence of increasing concentration of DPA53. (B) The decrease of fluorescence intensity (at 616 nm) of HIV TAR RNA/EtBr complex with increasing concentration of DPA53 results in a saturating binding plot. (C) The plot between normalized fluorescence intensity (at 616 nm) of HIV TAR RNA-EtBr complex as a function of concentration of DPA53 results in a saturating binding plot. (D) The Scatchard plot analysis of DPA53 with HIV TAR RNA. Buffer conditions: 100 mM KCl, 10 mM SC, 0.5 mM EDTA, pH 6.8. HIV TAR RNA = 200 nM/strand. [EtBr] = 5 μM.

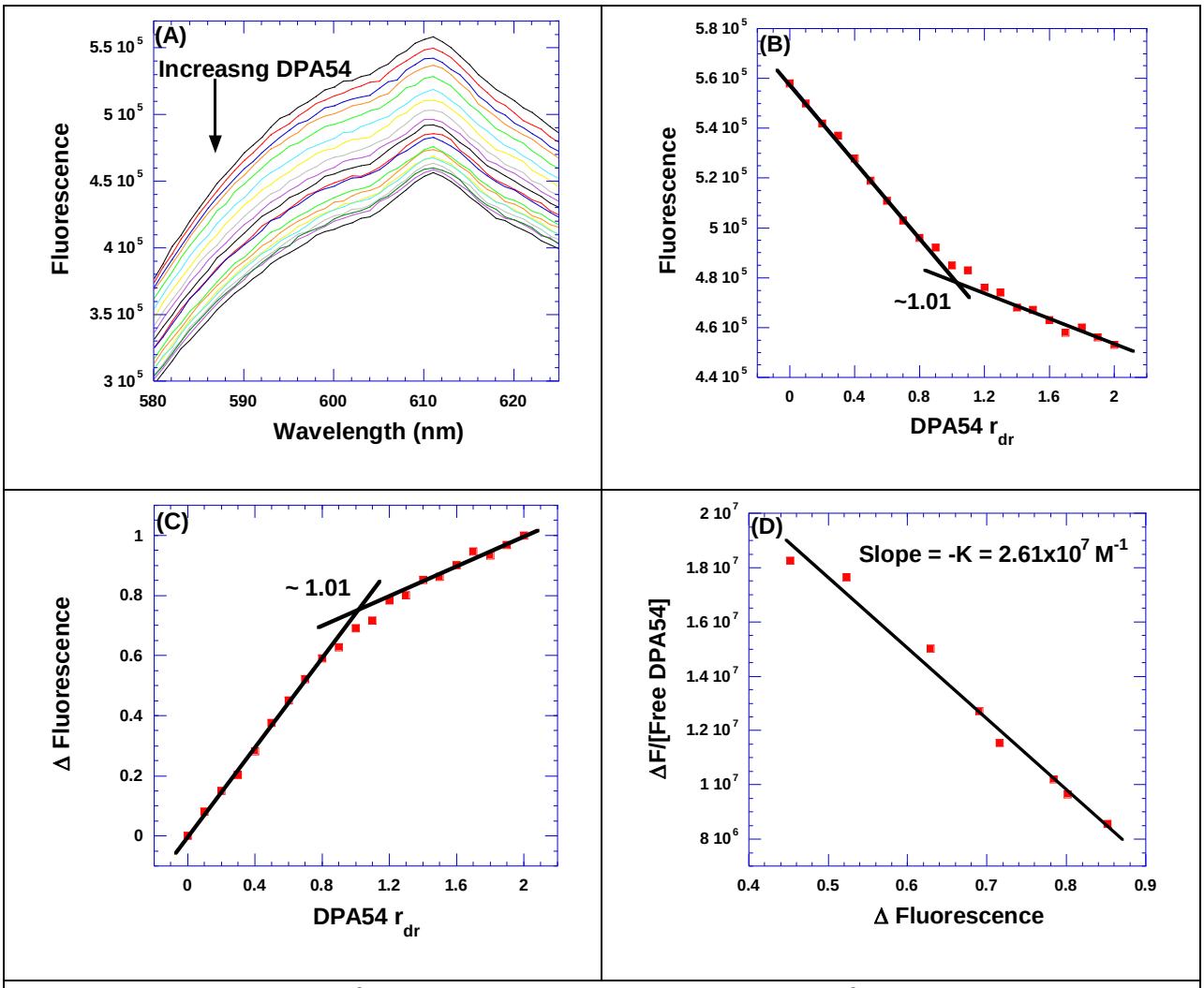

Figure S6.4. FID titration of DPA54 with HIV TAR RNA. (A) Raw fluorescence emission spectra in the presence of increasing concentration of DPA54. (B) The decrease of fluorescence intensity (at 611 nm) of HIV TAR RNA/EtBr complex with increasing concentration of DPA54 results in a saturating binding plot. (C) The plot between normalized fluorescence intensity (at 611 nm) of HIV TAR RNA-EtBr complex as a function of concentration of DPA54 results in a saturating binding plot. (D) The Scatchard plot analysis of DPA54 with HIV TAR RNA. Buffer conditions: 100 mM KCl, 10 mM SC, 0.5 mM EDTA, pH 6.8. HIV TAR RNA = 200 nM/strand. [EtBr] = 5 μM.

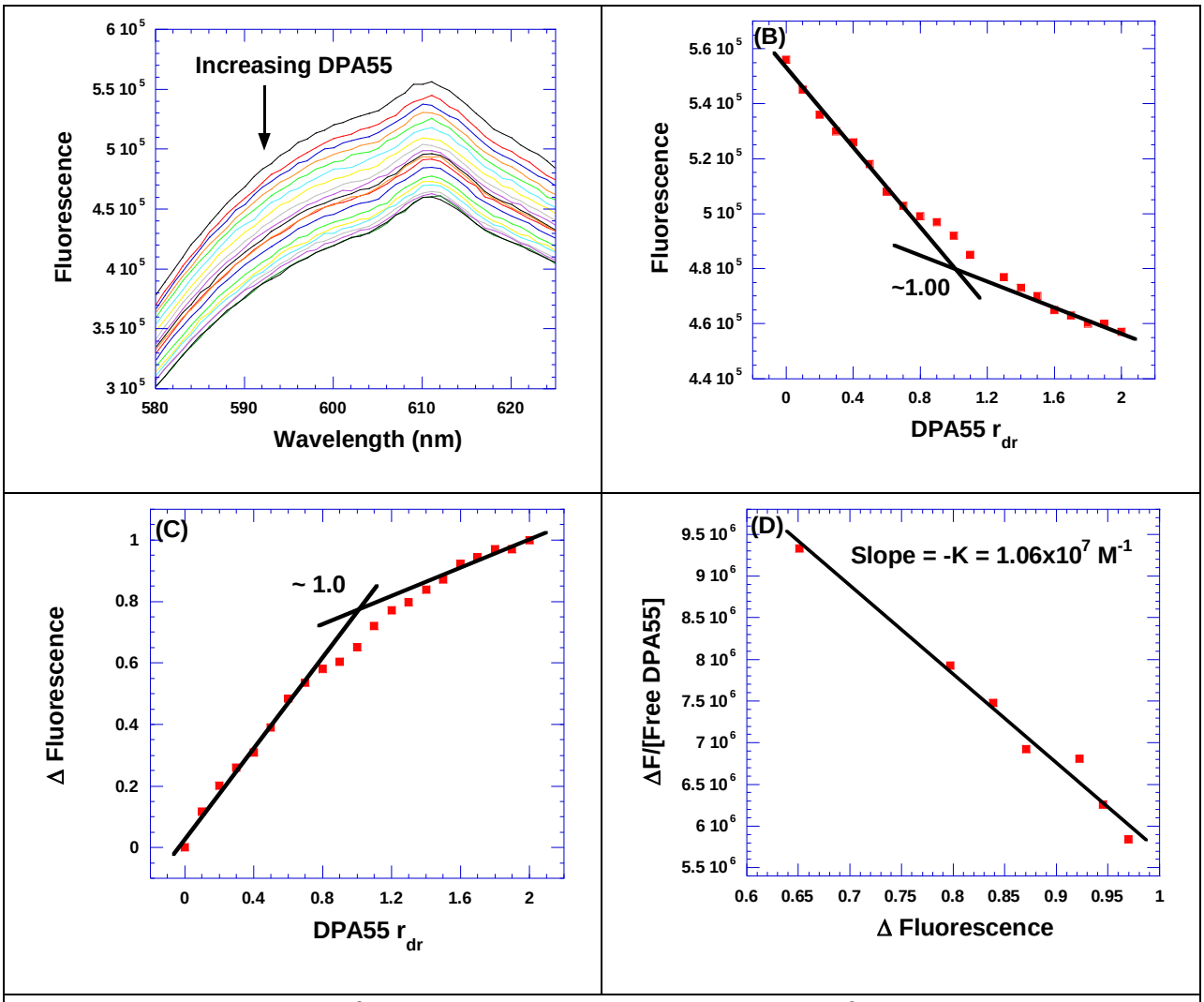

Figure S6.5. FID titration of DPA55 with HIV TAR RNA. (A) Raw fluorescence emission spectra in the presence of increasing concentration of DPA55. (B) The decrease of fluorescence intensity (at 611 nm) of HIV TAR RNA/EtBr complex with increasing concentration of DPA55 results in a saturating binding plot. (C) The plot between normalized fluorescence intensity (at 611 nm) of HIV TAR RNA-EtBr complex as a function of concentration of DPA55 results in a saturating binding plot. (D) The Scatchard plot analysis of DPA55 with HIV TAR RNA. Buffer conditions: 100 mM KCl, 10 mM SC, 0.5 mM EDTA, pH 6.8. HIV TAR RNA = 200 nM/strand. [EtBr] = 5 μM.

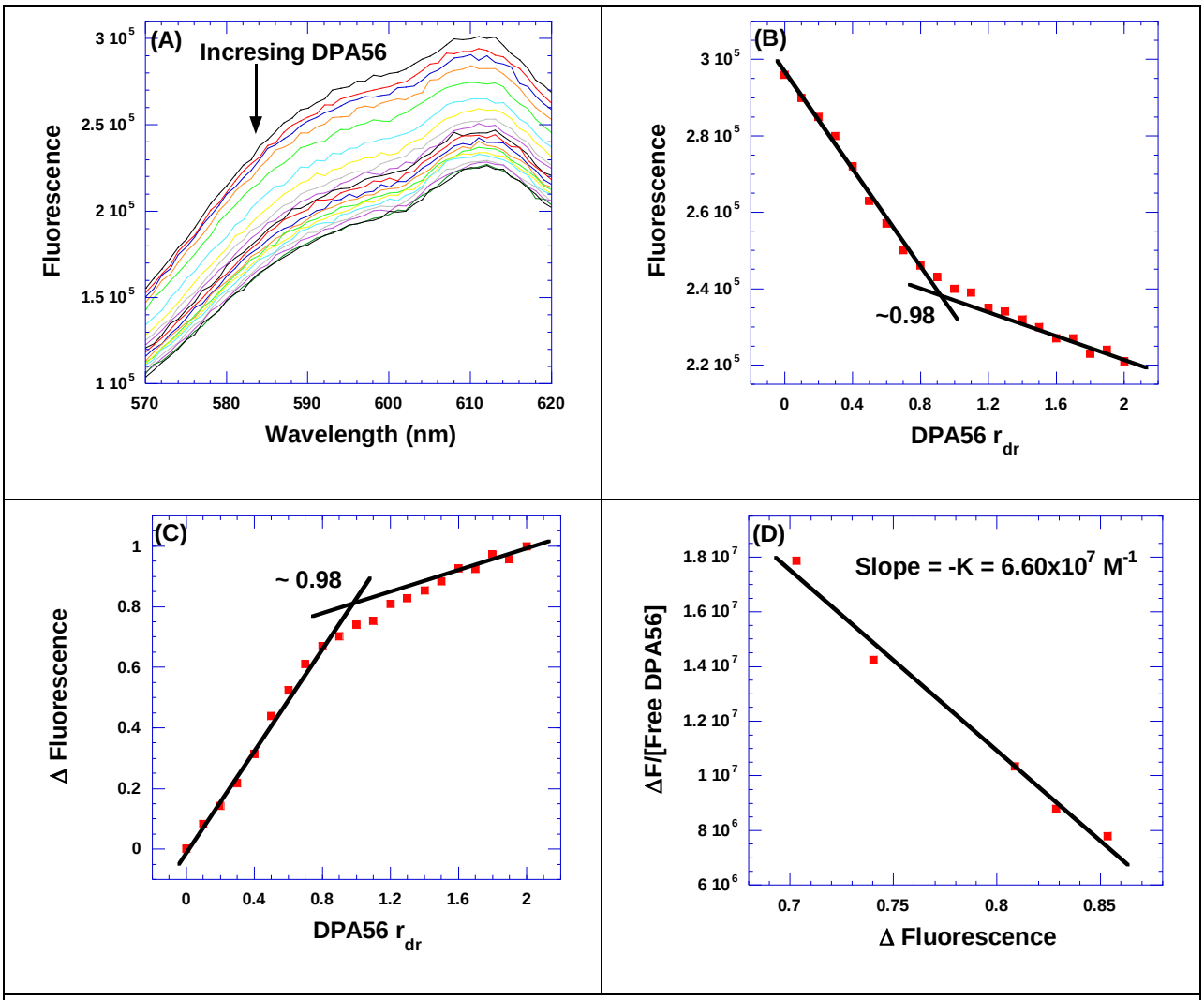

Figure S6.6. FID titration of DPA56 with HIV TAR RNA. (A) Raw fluorescence emission spectra in the presence of increasing concentration of DPA56. (B) The decrease of fluorescence intensity (at 614 nm) of HIV TAR RNA/EtBr complex with increasing concentration of DPA56 results in a saturating binding plot. (C) The plot between normalized fluorescence intensity (at 614 nm) of HIV TAR RNA-EtBr complex as a function of concentration of DPA56 results in a saturating binding plot. (D) The Scatchard plot analysis of DPA56 with HIV TAR RNA. Buffer conditions: 100 mM KCl, 10 mM SC, 0.5 mM EDTA, pH 6.8. HIV TAR RNA = 200 nM/strand. [EtBr] = 5 μM.

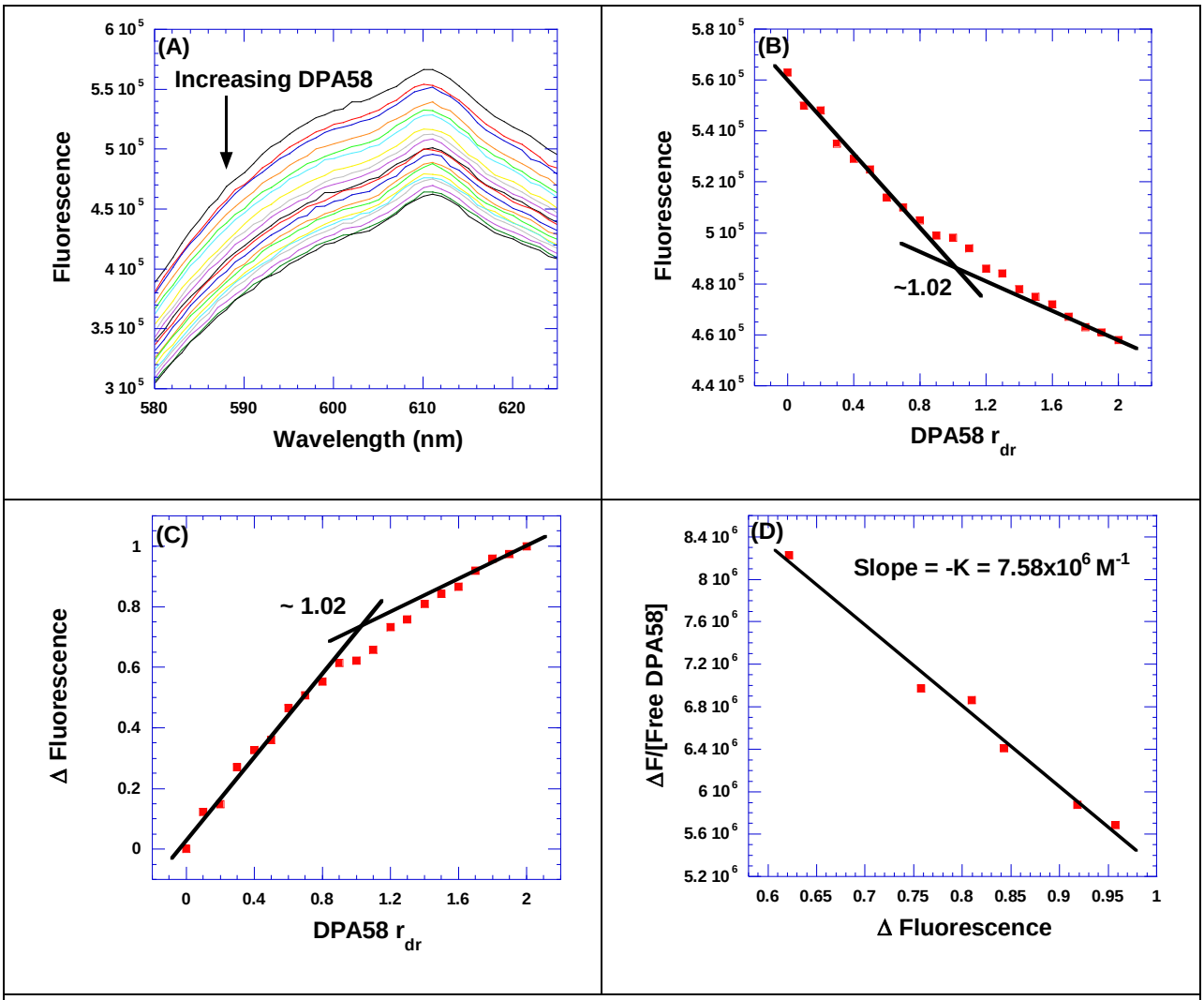

Figure S6.7. FID titration of DPA58 with HIV TAR RNA. (A) Raw fluorescence emission spectra in the presence of increasing concentration of DPA58. (B) The decrease of fluorescence intensity (at 612 nm) of HIV TAR RNA/EtBr complex with increasing concentration of DPA58 results in a saturating binding plot. (C) The plot between normalized fluorescence intensity (at 612 nm) of HIV TAR RNA-EtBr complex as a function of concentration of DPA58 results in a saturating binding plot. (D) The Scatchard plot analysis of DPA58 with HIV TAR RNA. Buffer conditions: 100 mM KCl, 10 mM SC, 0.5 mM EDTA, pH 6.8. HIV TAR RNA = 200 nM/strand. [EtBr] = 5 μM.

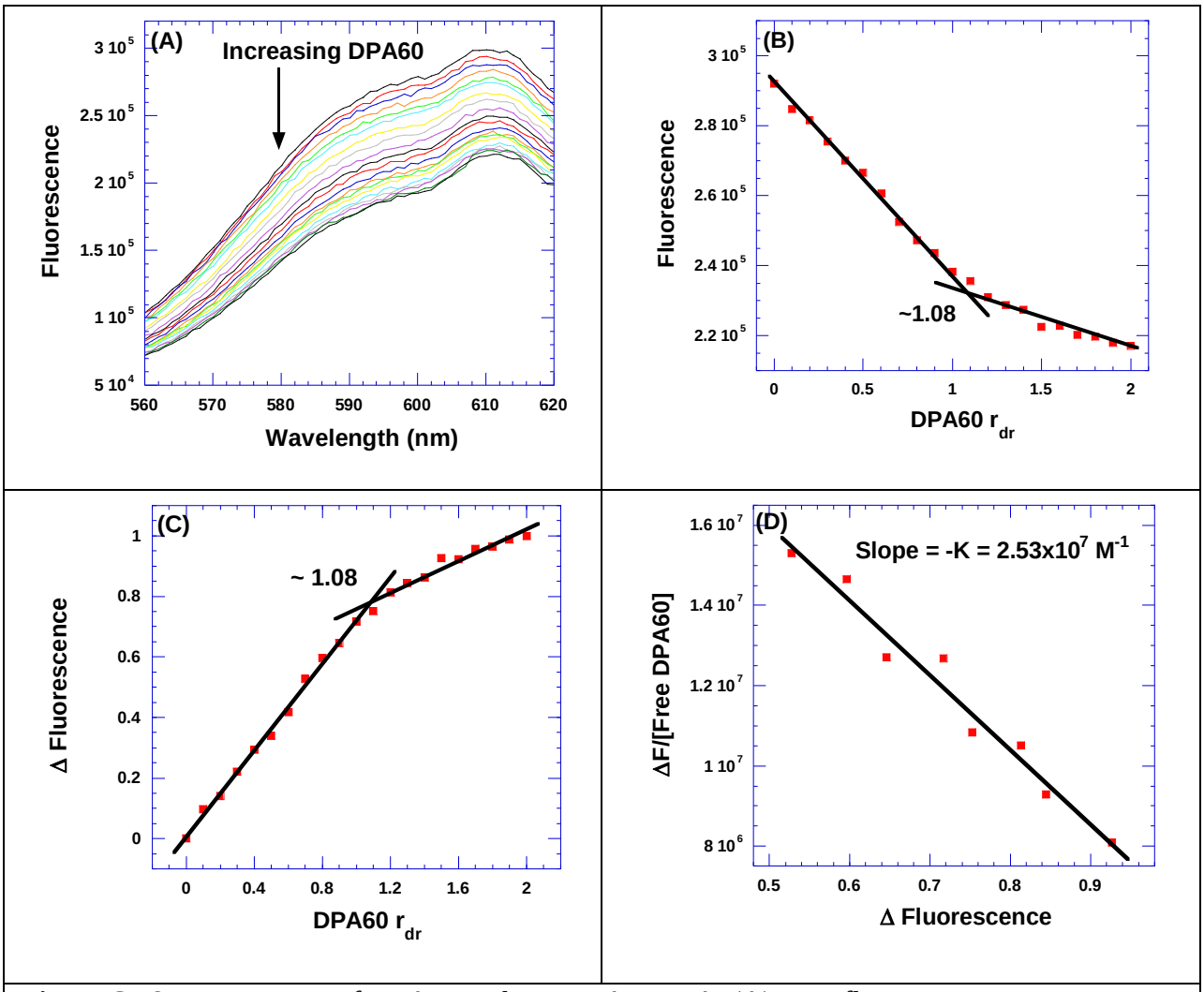

Figure S6.8. FID titration of DPA60 with HIV TAR RNA. (A) Raw fluorescence emission spectra in the presence of increasing concentration of DPA60. (B) The decrease of fluorescence intensity (at 615 nm) of HIV TAR RNA/EtBr complex with increasing concentration of DPA60 results in a saturating binding plot. (C) The plot between normalized fluorescence intensity (at 615 nm) of HIV TAR RNA-EtBr complex as a function of concentration of DPA60 results in a saturating binding plot. (D) The Scatchard plot analysis of DPA60 with HIV TAR RNA. Buffer conditions: 100 mM KCl, 10 mM SC, 0.5 mM EDTA, pH 6.8. HIV TAR RNA = 200 nM/strand. [EtBr] = 5 μM.

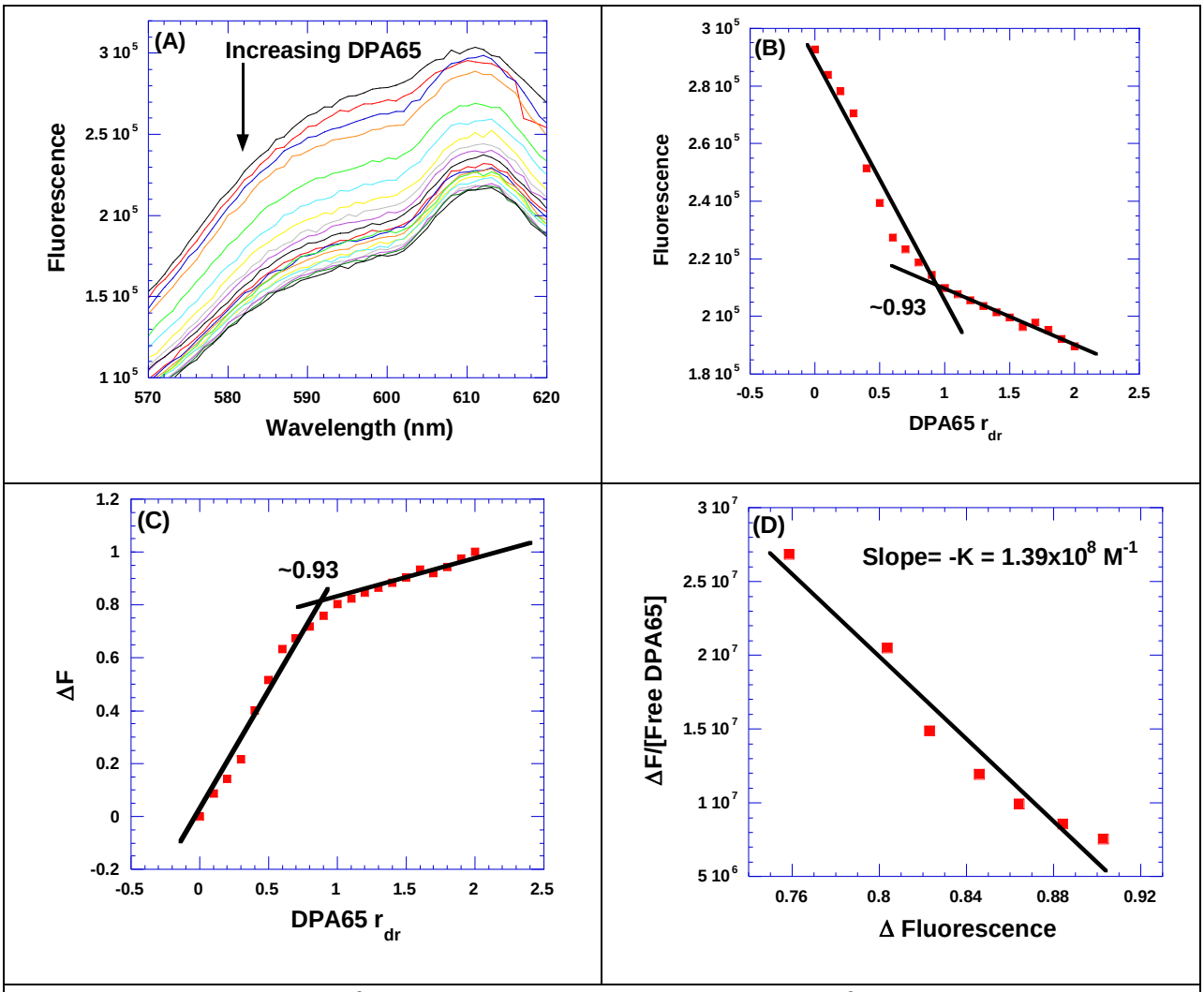

Figure S6.9. FID titration of DPA65 with HIV TAR RNA. (A) Raw fluorescence emission spectra in the presence of increasing concentration of DPA65. (B) The decrease of fluorescence intensity (at 605 nm) of HIV TAR RNA/EtBr complex with increasing concentration of DPA65 results in a saturating binding plot. (C) The plot between normalized fluorescence intensity (at 605 nm) of HIV TAR RNA-EtBr complex as a function of concentration of DPA65 results in a saturating binding plot. (D) The Scatchard plot analysis of DPA65 with HIV TAR RNA. Buffer conditions: 100 mM KCl, 10 mM SC, 0.5 mM EDTA, pH 6.8. HIV TAR RNA = 200 nM/strand. [EtBr] = 5 μM.

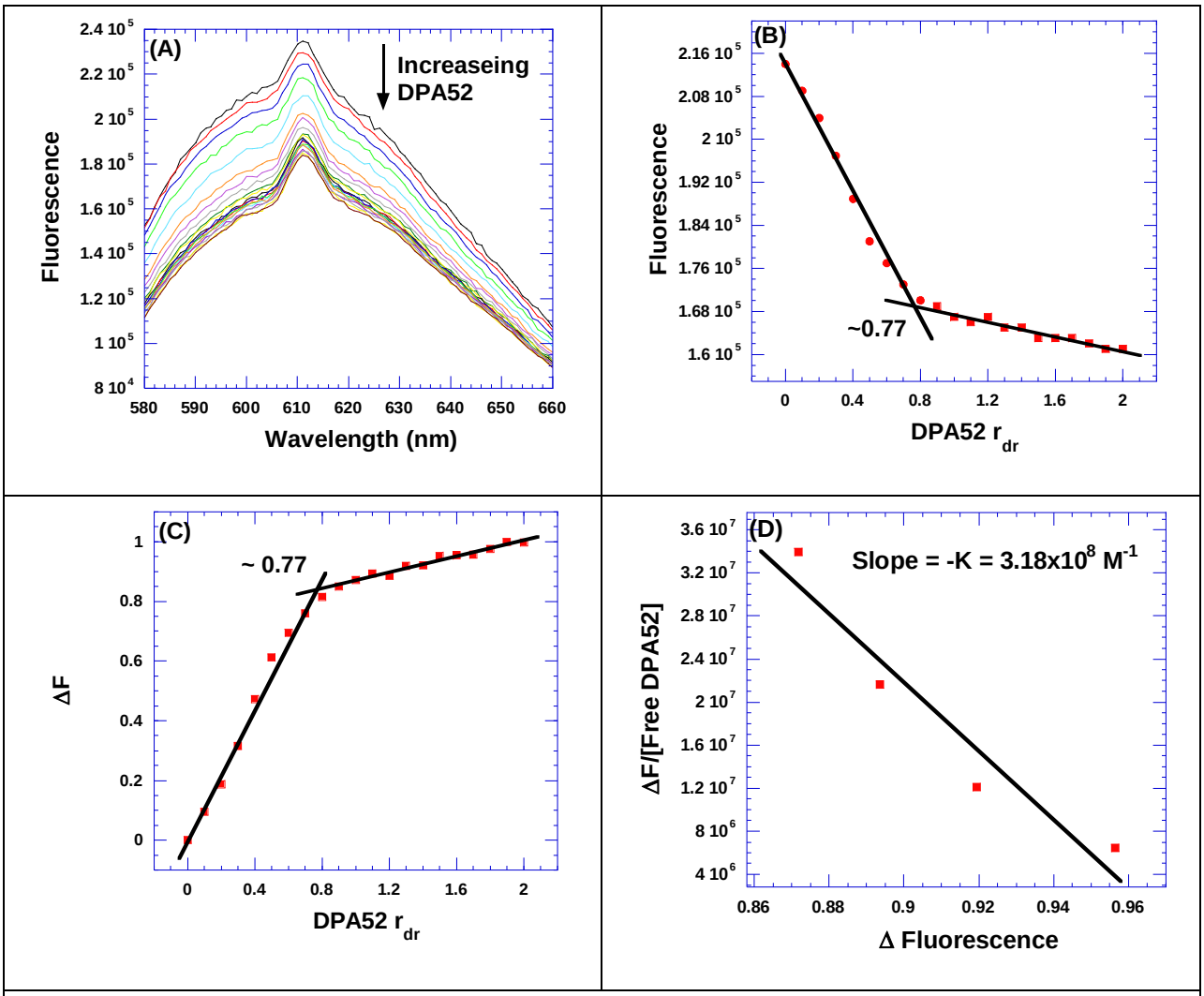

Figure S6.10. FID titration of DPA52 with HIV TAR RNA. (A) Raw fluorescence emission spectra in the presence of increasing concentration of DPA52. (B) The decrease of fluorescence intensity (at 604 nm) of HIV TAR RNA/EtBr complex with increasing concentration of DPA52 results in a saturating binding plot. (C) The plot between normalized fluorescence intensity (at 604 nm) of HIV TAR RNA-EtBr complex as a function of concentration of DPA52 results in a saturating binding plot. (D) The Scatchard plot analysis of DPA52 with HIV TAR RNA. Buffer conditions: 50 mM KCl, 10 mM SC, 0.5 mM EDTA, pH 6.8. HIV TAR RNA = 200 nM/strand. [EtBr] = 5 μM.

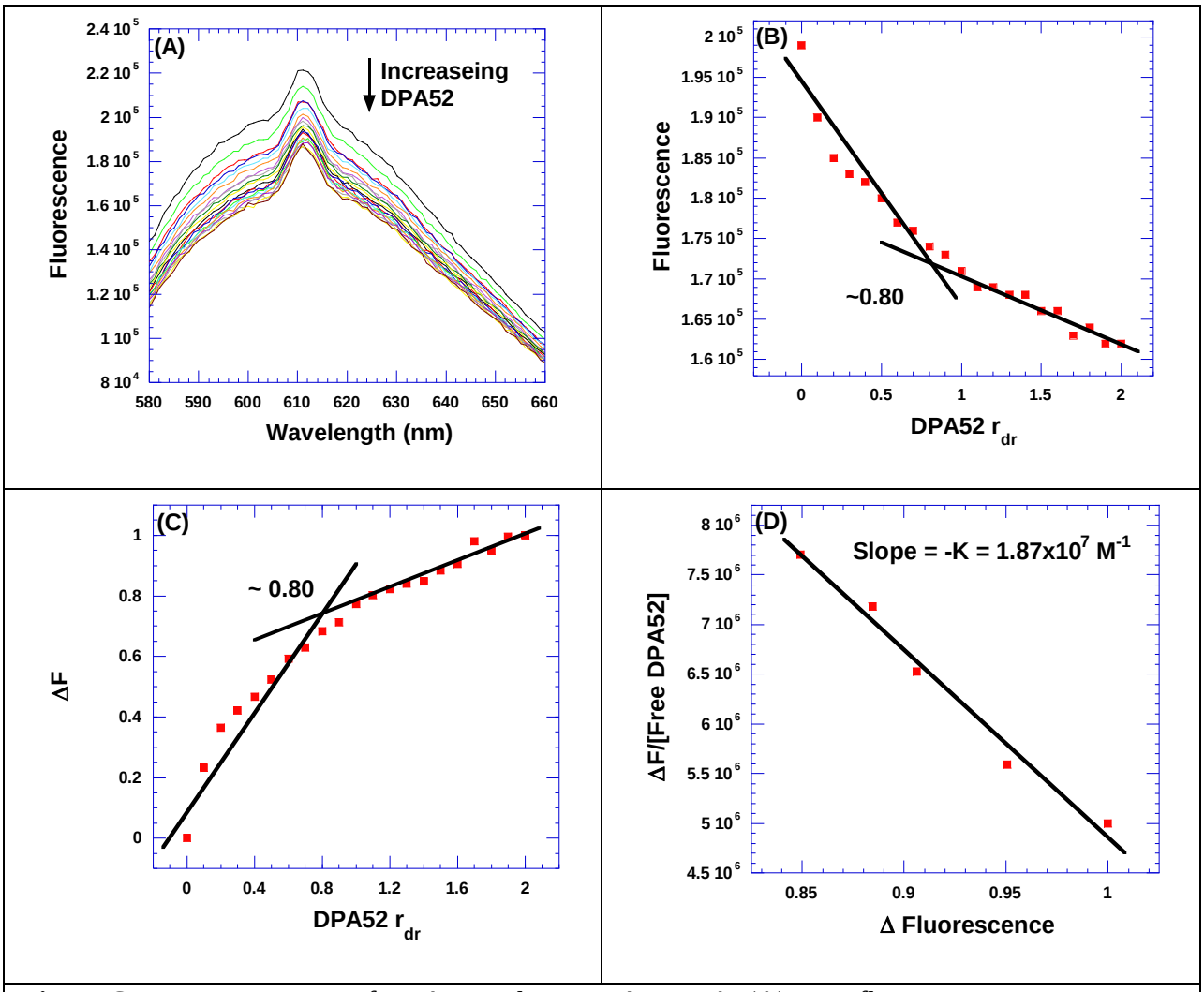

Figure S6.11. FID titration of DPA52 with HIV TAR RNA. (A) Raw fluorescence emission spectra in the presence of increasing concentration of DPA52. (B) The decrease of fluorescence intensity (at 604 nm) of HIV TAR RNA/EtBr complex with increasing concentration of DPA52 results in a saturating binding plot. (C) The plot between normalized fluorescence intensity (at 604 nm) of HIV TAR RNA-EtBr complex as a function of concentration of DPA52 results in a saturating binding plot. (D) The Scatchard plot analysis of DPA52 with HIV TAR RNA. Buffer conditions: 150 mM KCl, 10 mM SC, 0.5 mM EDTA, pH 6.8. HIV TAR RNA = 200 nM/strand. [EtBr] = 5 μM.

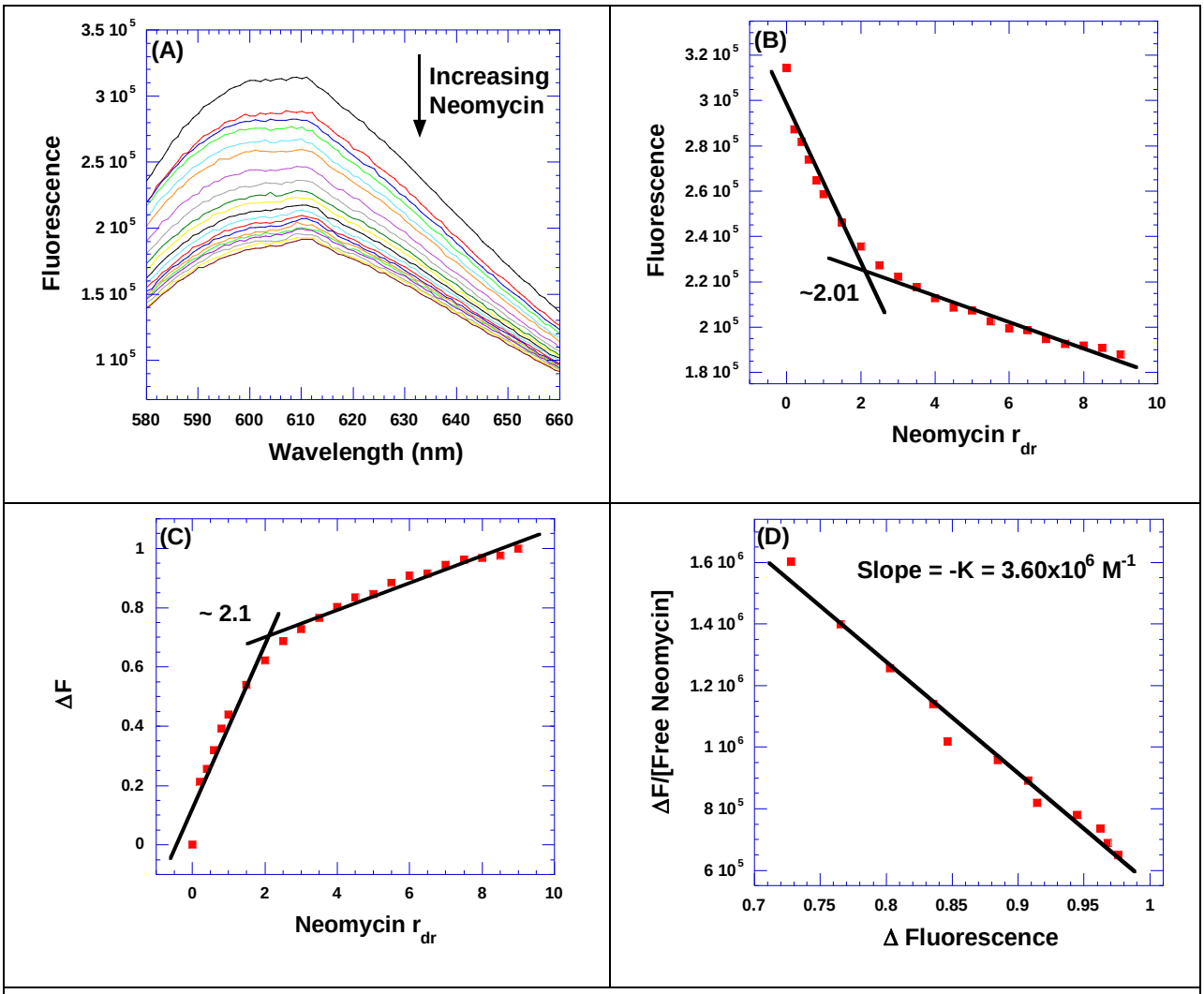

Figure S6.12. FID titration of neomycin with HIV TAR RNA. (A) Raw fluorescence emission spectra in the presence of increasing concentration of neomycin. (B) The decrease of fluorescence intensity (at 611 nm) of HIV TAR RNA/EtBr complex with increasing concentration of neomycin results in a saturating binding plot. (C) The plot between normalized fluorescence intensity (at 611 nm) of HIV TAR RNA-EtBr complex as a function of concentration of neomycin results in a saturating binding plot. (D) The Scatchard plot analysis of neomycin with HIV TAR RNA. Buffer conditions: 100 mM KCl, 10 mM SC, 0.5 mM EDTA, pH 6.8. HIV TAR RNA = 200 nM/strand. [EtBr] = 5 µM.

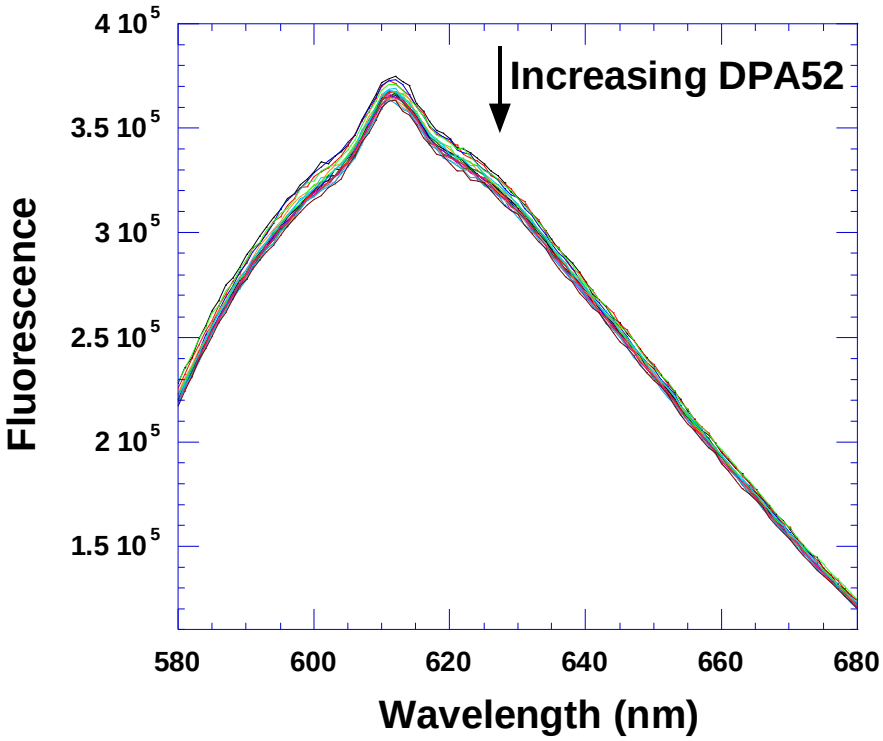

Figure S6.13. Direct titration of DPA65 in the ethidium bromide solution. Raw fluorescence emission spectrum in the presence of increasing concentration of DPA65. Buffer conditions: 100 mM KCl, 10 mM SC, 0.5 mM EDTA, pH 6.8. [EtBr] = 5 μM.